THREE-DIMENSIONAL TRIANGULATED BOUNDARY ELEMENT MESHING OF UNDERGROUND EXCAVATIONS AND VISUALIZATION OF ANALYSIS DATA

by

Brent T. Corkum

A thesis submitted in conformity with the requirements
for the degree of Doctor of Philosophy
Graduate Department of Civil Engineering
University of Toronto

ABSTRACT

THREE-DIMENSIONAL TRIANGULATED BOUNDARY ELEMENT MESHING OF UNDERGROUND EXCAVATIONS AND VISUALIZATION OF ANALYSIS DATA

Brent T. Corkum

Department of Civil Engineering, University of Toronto

Doctor of Philosophy, 1997

In the design of an underground excavation, the engineer uses analyses to quantify and understand the interaction between excavation geometry, rock mass properties and stresses. The analyses are typically complicated by the need to consider variability of each model parameter's values, three-dimensional geometric effects, and the integration of information from multi-disciplinary datasets. A major goal of this thesis is therefore to rationalize the analysis process used to represent underground excavation geometry, conduct numerical stress analyses, and visualize analysis data.

The first issue considered in this thesis is the modeling of underground excavation geometry for the purpose of performing three-dimensional boundary element stress analysis. Various geometric modeling algorithms and techniques are enhanced for the application to underground excavation geometry and the concurrent creation of a triangulated boundary element mesh. The second focus of this thesis is the visualization of underground mine datasets. In particular, a paradigm is developed that allows the efficient visualization of stress analysis data, in conjunction with other mine datasets such as seismic event locations, event density, event energy density and geotomographic velocity imaging datasets. Several examples are used in the thesis to illustrate practical application of the developed concepts.

ACKNOWLEDGMENTS

I am especially grateful to my supervisor, Prof. John H. Curran, for his vision and foresight, without which this research work would not have been possible. It is hard to believe that it all started so long ago with that trip to Montreal.

I would also like to thank my friends and colleagues, Evert Hoek, Murray Grabinsky, Joe Carvalho, and Mark Diederichs, for their countless ideas and suggestions. Without John and these others, people around the world would not be enjoying our software, and I would not have the job people dream of.

To the countless people in industry who have helped me test and perfect *Examine*^{3D}, they are the strength behind the program. Special thanks go to the people at the Noranda Research Center, who have provided much of the industrial support for this research project.

A special thanks to all my family who have helped shape my career and provided the much needed support along the way. A special thanks to Anna, who provided the necessary encouragement, and editing skills, needed to get it all done. And finally to Nan, who never gave up on me, I did it for you.

Financial support has been provided by the Noranda Group through a Noranda Bradfield Scholarship, by the University of Toronto through an Open Fellowship, and by the Ontario Government through an Ontario Graduate Scholarship.

TABLE OF CONTENTS

LIST OF FIGURES

1. INTRODUCTION

Deep within a rock mass, the state of stress is a function of the weight of overlying rock and tectonic forces. Any excavation within this rock mass induces a new state of stress surrounding the opening. Knowledge of the magnitude and orientation of stresses within this induced stress field is an essential component of excavation design. In many cases, stresses will exceed the rock mass strength, resulting in instability that can have serious consequences. As a result, numerical modeling, particularly the analysis of stresses and displacements around underground excavations, has become an increasingly important tool for the design of underground structures in both mining and civil engineering. Current numerical modeling techniques such as the Boundary Element Method (BEM), Finite Element Method (FEM), and the Finite Difference Method (FDM), have evolved to a point where they are being successfully applied to a variety of geomechanics applications. The availability of these improved methods, combined with the low cost and wide availability of personal computers and workstations, the improved computational performance of these machines, and the existence of user-friendly modeling software, have all contributed to the greatly increased use of these numerical modeling techniques for practical design.

Currently, the most widely used computer programs for analysis of stresses around underground structures are two-dimensional in nature. Thus, most of the stress analysis modeling of underground structures is done only using two-dimensional techniques. A cross-section is commonly taken at some location on the excavation geometry and plane strain assumptions are made to solve for the in-plane stresses. Although useful in certain situations, the assumptions and simplifications used in a plane strain analysis can lead to poor results if applied to certain classes of problems. In particular, a plane strain analysis assumes that there is zero strain normal to the cross-section. This idealization results in a dramatic and unrealistic simplification of the differential equations of equilibrium and compatibility for equidimensional geometries. In practical terms, it can only be used for an underground excavation whose

length is much larger than the cross-sectional dimensions (e.g. a subway tunnel), where the out of plane excavation boundaries have little influence on the stress state in the plane of the cross-section. Unfortunately, many underground structures have excavations of equidimensional shape and therefore cannot be accurately modeled using this method. These types of structures also represent a very important class of underground excavations, especially in mining.

The question then becomes: why are very few three-dimensional analyses done of underground structures? The answer is primarily because the degree of complexity that results from generating the required input for three-dimensional analysis has been overwhelming compared to that required for two-dimensional analysis. Considering the geometric complexity of many underground civil and mining engineering excavations, it is much easier to define a two-dimensional section throughout the geometry rather than to model the complete three-dimensional excavation geometry. The additional step of discretizing the geometry into a valid boundary element mesh, while simple in two-dimensions because the elements are two-dimensional line segments, becomes much more complicated and time consuming in three-dimensions. In three-dimensions, the boundary element mesh is made up of edge connected (conforming) triangular surface elements with the condition that elements should be as close to equilateral as possible to obtain good results. Therefore if one uses a three-dimensional analysis rather than a two-dimensional one, it could take days rather than minutes to model the excavation geometry, unless automated tools are available to assist the user.

Another reason for the popularity of two-dimensional programs is that it has always been difficult to quickly view and interpret the results from three-dimensional models, a relatively simple task when using two-dimensional tools. Two-dimensional techniques simply consist of contouring results on two-dimensional cutting planes. Although useful in defining the state of stress locally, this method provides little insight into the global stress distribution. This weakness in the method can cause a misinterpretation of the excavation stability since the validity of the user's results depends entirely on the location that has been selected for the calculation of stress values.

Finally, the numerical complexity is considerably reduced in a two-dimensional versus a three-dimensional analysis making this choice much more attractive. To properly establish values for model parameters, rock engineering problems have typically required a large number of parametric analyses to compensate for the lack of sufficiently accurate data available to the engineer at these sites. In the past, three-dimensional analyses were too computationally intensive and time consuming, and thus of limited practical value, especially for parametric analyses.

For all these reasons, few engineering projects in the past have had the time, the expertise, or the funds required to perform three-dimensional analyses.

Recently, research by Shah (1993) has led to dramatic improvements to the numerical algorithms used in the boundary element method used in calculating the stress analysis data. His research has also resulted in a well tuned, modular C program which efficiently implements these solution algorithms. Dr. Shah's contributions, combined with the ever improving performance of today's computers, has led to solution times that are one to two orders of magnitude faster than what was achievable a decade ago using FORTRAN on the average desktop computer. Even with these improvements in the boundary element method, the two most significant impediments to the adoption of three-dimensional stress analyses, geometric modeling and data visualization complexity, remained. Although much work has been done in the field of computer graphics (geometric modeling and data visualization), and in the mechanical engineering field (mesh generation), very little has been done until now to apply this work to the three-dimensional stress analysis of underground excavations. An excellent opportunity to apply the recent advancements in computer graphics, meshing capabilities, and numerical analysis can be found in mining today.

During and following excavation, in association with the redistribution of stress around the new openings, seismic events occur within the rock mass. Many mines have in place monitoring equipment which can accurately locate these events in space, and provide information on their magnitude and properties. Mines use this information to identify rockburst prone regions, for the purpose of mine safety

and the definition of future mining patterns. Since many of these events occur because of stress redistribution, they can provide information on the state of stress within the rock mass and can be used in conjunction with the stress analysis results for correlation purposes. As well, active and passive tomography imaging can be used to generate volumetric P-wave velocity data within the rock mass. This velocity data can then be used to identify zones of overstress within the rock mass by interpreting the relative magnitudes of the velocity data. It is therefore very important that methods be developed to visualize seismic data in conjunction with the stress analysis results.

It is the purpose of this thesis to present a fresh, innovative, and ultimately better approach to three-dimensional visualization of both seismic and stress analysis data. Further, this thesis will present a starting point for the geometric modeling and mesh generation of the excavation geometry for the purpose of performing a boundary element stress analysis. The final outcome will produce a set of algorithms for three-dimensional analysis which, when implemented, will provide a means for the engineer to perform a quick and easy analysis of a given problem, approaching the simplicity presently found in a two-dimensional analysis.

2. *EXAMINE*^{3D} - A MODELING AND VISUALIZATION PROGRAM

Examine^{3D} is a geometric modeling, numerical analysis, and data visualization program for underground excavations in rock. The geometric modeling and data visualization components, along with the overall conceptual design of the program, are the product of this thesis. The boundary element numerical analysis component was developed by S. Shah as part of his Ph.D. thesis (Shah, 1993).

The geometric modeling component is derived from the work presented in chapter 3, while the algorithms and methodology used for the data visualization component are presented in both chapters 4 and 5. Many of the figures and results presented in this thesis were generated using *Examine*^{3D}.

In creating *Examine*^{3D}, the issue of user interface design became critical to the success of the program. Not only was it important to have a good modeling and visualization strategy, but the user of the program had to be able to efficiently and quickly build, analyze, and visualize results. The purpose of this thesis was to develop and implement techniques for the modeling and visualization of mine datasets. It was felt that the best way to achieve this goal was to develop a program that could be used to analyze real problems in industry. In order to test the modeling and visualization algorithms presented, a large user base including practicing mining and civil engineers was needed to provide feedback on the suitability of the algorithms to actual mining and civil engineering problems. In order to interest a large number of professionals to use the program (people with limited time to learn how to use it), the program had to have a high quality stable user interface, accompanied by a well written manual.

The user interface for the geometric modeler was developed using the modeling strategies and layouts found in many of the currently available commercial geometric modeling programs. Programs such as AUTOCAD™ , ALIAS™, and IDEAS™ were used to acquire a knowledge of how to best structure a geometric modeling package. Since most mining and civil engineers are familiar with AUTOCAD™, a great deal of effort was put into making the transition between the two programs fairly easy. Additionally, since ALIAS™ is acknowledged as being one of the better geometric modeling programs, effort was placed on learning and evaluating the modeling strategies this program uses.

IDEAS™ is currently one of the best engineering design tools available, incorporating modeling, numerical analysis, and graphical display of data. Many of its features and design algorithms were investigated for possible use in *Examine*^{3D}. Therefore, the user interface for *Examine*^{3D} was developed based on the current state of the art user interface design for both modeling and engineering software.

An important issue in the development of a graphically-based modeling and visualization program is the hardware environment. The Silicon Graphics (SGI) hardware platform was chosen for its strengths in real time rendering and display of computer models, while the PC platform was chosen as the practical alternative for most civil and mining engineers. Since *Examine*^{3D} operates on both platforms, with virtually the same functionality, the only difference is the speed at which images are rendered to the display. On the Silicon Graphics Indigo, with Elan graphics, real time interaction and manipulation of the geometry and visualization data make it the best hardware system for modeling and interpreting results from complex numerical models. The speed, availability and application flexibility of Pentium based PC's make this platform more practical for the average engineer.

In order to achieve this cross platform support, the graphics package called HOOPS™, by Ithaca Software, was used. HOOPS™ is a library of computer graphics functions which allows the user to draw graphics primitives such as lines, points, and polygons, apply lighting to produce shaded images, and produce hardcopy etc., on multiple hardware platforms. *Examine*^{3D} is programmed using C with HOOPS™ library calls for displaying graphics. *Examine*^{3D} is currently over 50,000 lines of C code. On the PC, it is compiled under DOS using the Metaware C/C++ compiler and Phar Lap DOS extender for 32 bit, flat memory model, extended DOS application. The program also runs on the SGI IRIX 5.3 operating system and is compiled using the SGI C/C++ development system.

There are currently over 150 copies of *Examine*^{3D} being used in over 20 countries, by both civil engineering and mining companies. The use of the program by the engineers in these companies and the feedback from these individuals was critical to the verification and testing of the modeling and visualization techniques presented in this thesis.

3. MODELING OF EXCAVATION GEOMETRY

There are generally two reasons for modeling the three-dimensional geometry of underground excavations. First of all, models can be used by mining engineers, civil engineers and geologists to understand the three-dimensional nature of the excavations. The models are generally built using computer aided design (CAD) packages such as AUTOCAD™ and use surface building primitives such as polygons or surface patches. The most common surface being modeled is the interface between underground openings and the rock mass. To visualize the geometry of the openings, it is easiest to view them using a surface mesh of the rock-excavation interface. In effect, the rock is removed and the openings become the solid. Geologic features are also commonly modeled and these include discontinuities such as faults and joints, dikes, material boundaries, and the ore body extents. In all cases, it is generally the interface between these structures that is modeled for the visualization process.

The second reason for the three-dimensional geometric modeling of underground excavations is so that a mesh can be developed for use in a numerical analysis. Although the model can also be used to visualize the mine geometry, the process of defining a mesh for use in a numerical analysis usually entails some simplification of the mine geometry. The rationale for this stems from the degree of complexity (number of elements) that current stress analysis techniques can manage. As a result, the geometry used for analysis might not be suitable for other purposes (e.g. mine layout). Although the geometry is generally simpler, this does not mean that the modeling of this geometry is easier. On the contrary, restrictions in the format that the geometry must be in for the purpose of doing the stress analysis make the modeling process more difficult. The most difficult restriction, which arises from the direct boundary element stress analysis approach adopted by Shah (1993), is that the geometry be composed of planar, conforming (edge connected) triangular elements, and the triangular elements be as close to equilateral as possible. This restriction, although cumbersome for the purpose of modeling, has its numerical advantages in that the number of degrees of freedom are substantially less than nonconforming elements. This produces a smaller number of computations, reduced storage

requirements and faster solution times. This also allows for the analysis of more complex problems since the users will have more elements at their disposal. In addition, accuracy close to the boundary is improved.

Unfortunately, the difficulty of modeling complicated excavation geometry with these restrictions is not trivial. This chapter presents the issues involved with the modeling of planar, triangular, conforming boundary element surface meshes. A set of methods and algorithms is also provided as an initial attempt at dealing with this very difficult problem. These methods and algorithms will provide the necessary groundwork for further study into the modeling of mine geometry under these restrictive conditions.

3.1 Details of the Boundary Element Mesh Geometry

The type of boundary element being used in the analysis governs the type of mesh and its method of construction. Three-dimensional boundary elements can either be flat sided or curved, and are generally triangles or quadrilaterals. The boundary element mesh itself can either be conforming or nonconforming. In addition, a conforming mesh requires that every element edge be shared by only one other element. The formulation of the mesh also ensures a continuity of displacement along the element edge. The degrees of freedom are located at the vertices or nodes of the element, and each node is shared by all elements attached to it. The nonconforming mesh does not have the edge connection restriction and there is no continuity in displacement between elements.

From a modeling point of view, the nonconforming element is much more attractive. The flexibility of not having to worry about edge connectivity at stope or drift intersections is a tremendous advantage. It is much easier to model the intersection of two objects (i.e. stopes, drifts) when it is not necessary to consider connecting elements from one object to the other. Since elements can be broken down without regard to the connectivity of adjoining elements, the process of mesh refinement is simpler in the case of nonconforming meshes.

There is an advantage though, in using the conforming mesh, related to the nodal sharing formulation. Since the nonconforming element does not have shared nodes, the number of degrees of freedom for most practical applications is larger. In fact, for most models currently using conforming triangular elements, the number of elements is usually double the number of nodes. If each one of these triangular elements was formulated as a constant nonconforming element with one node located at the center of the element, then there would be twice the number of degrees of freedom for the same mesh. Computation time to solve such a system of equations is greatly increased and the amount of memory required to store the matrix is increased by a factor of four. The issue of accuracy must also be considered. The conforming triangular element has three nodes, yielding a more accurate linear displacement profile across the element. The constant nonconforming element has a less accurate constant displacement profile. Shah (1993) demonstrated that one could expect a more accurate result using the higher order elements and that the conforming elements are less computationally intensive, less memory intensive, and yield better results for equivalent degrees of freedom.

After defining and comparing the conforming and nonconforming elements, the problem now is to determine which element is the more feasible choice. Taking into consideration the above discussion, the triangular conforming element seems to be the ideal choice for performing the analysis. A triangular element has a simpler formulation with an ability, as a simple geometric primitive, to more easily model almost any three-dimensional surface. Unfortunately, the complexity of modeling three-dimensional objects, in particular underground excavations, is greatly increased by the use of a conforming element. The challenge is whether it is possible to build a fast, easy-to-use surface modeler, capable of building a conforming boundary element surface mesh to model underground structures. One objective of this thesis is to answer this challenge by providing the ground work for conformal mesh building procedures. The following sections will present a set of algorithms for generating conforming, triangle based meshes of underground structures. Many of these algorithms are based on current CAD and geometric modeling techniques, with modification for the purpose of application to underground structures.

3.2 The Complexity of Mine Geometry

To fully appreciate the difficult task of constructing a three-dimensional, edge connected, well formed triangular surface mesh of most underground excavations, one need only view a set of mine plans. The mine plans are a series of two-dimensional longitudinal, cross-sectional, and level sections detailing the current mine openings. These plans are used by all facets of the mining operation (geology, mine planning, rock mechanics etc.) for determining spatial distribution of excavations and geology. It is from these plans that any three-dimensional model of the underground openings must be constructed. Figure 3.1 and Figure 3.2 are the 14th and 15th level plans at the Placer Dome Campbell mine, which is stored in AUTOCAD™ DWG format. The shaded regions represent the stopes which would extend between levels, while the rest of the tunnels are access drifts form the main shaft. These plans represent

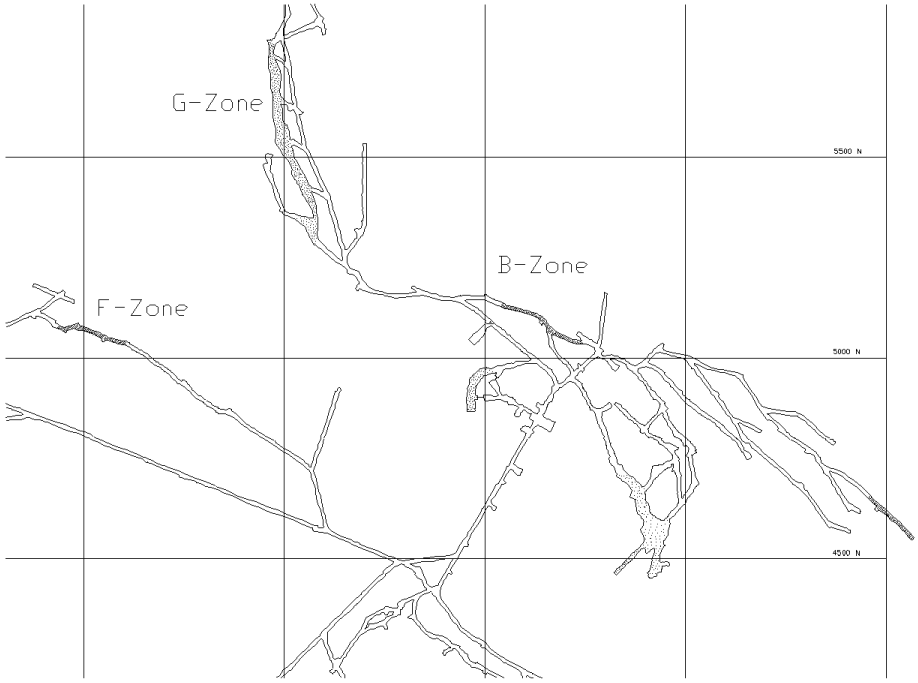

Figure 3.1 Drift and Stope Geometry on Level 14 of the Placer Dome Campbell Mine

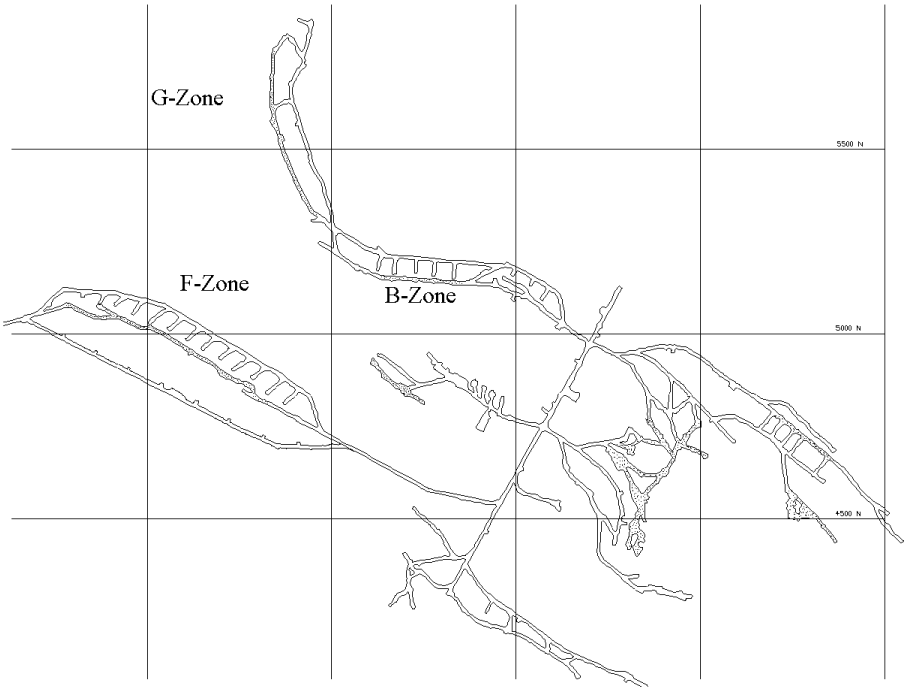

Figure 3.2 Drift and stope geometry on level 15 of the Placer Dome Campbell mine

the mine geometry on two adjacent sections. It is important to note how dissimilar the sections are. This illustrates why the task of generating the three-dimensional representation can be quite difficult. Although longitudinal sections and cross-sections through certain ore zones sometimes give an indication of the stope geometry between levels, this is mine specific and not always available.

The three-dimensional surface model created from the sections in Figure 3.1, Figure 3.2, and other sections can be seen in Figure 5.18. Analyzing the geometry of the stopes is further complicated, because depending on the mining method, the geometry of the stopes between levels can be quite regular (blasthole stopes) or quite irregular (cut and fill mining). This is influenced by the geometry of the orebody, the type of ore, and the amount of acceptable dilution. To make matters worse, the stopes between levels are commonly geometrically discontinuous and overlapping (Figure 3.3). This makes connecting stopes between different levels quite difficult. Depending on the age of the mine, the geometry of older openings on upper levels will be recorded on blue prints. This makes the process of

modeling even more difficult since the blue prints must first be digitized to extract the stope geometry for use in generation of the surface model.

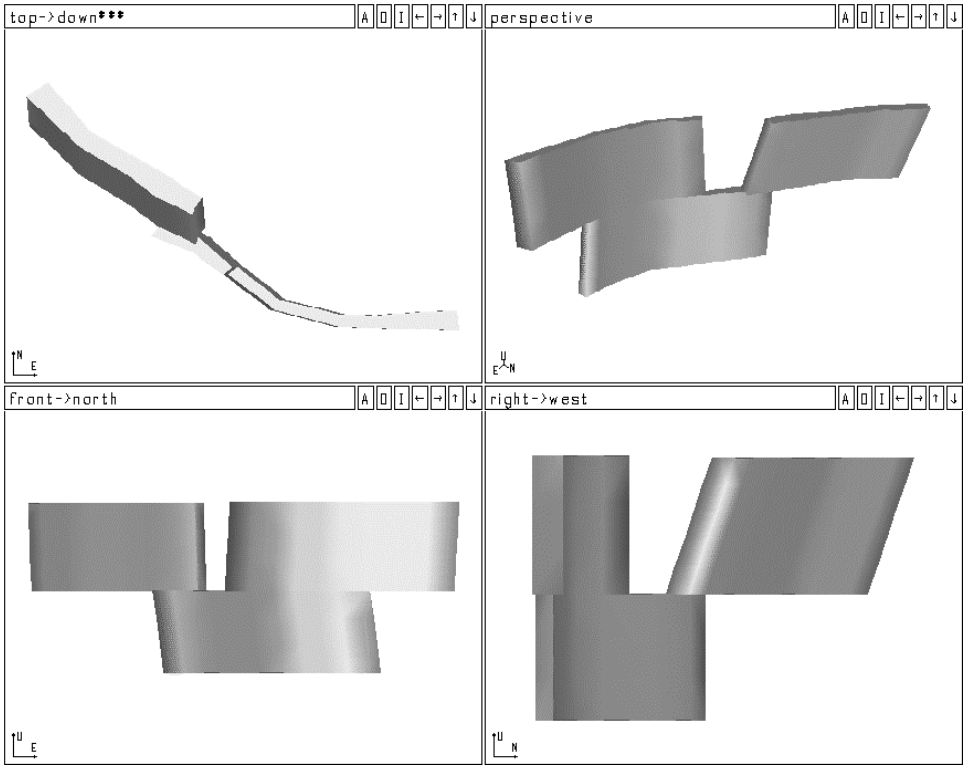

Figure 3.3 Discontinuous and overlapping blasthole stopes

3.3 The Coordinate System

An important practical consideration in the modeling process is the choice of the global cartesian xyz coordinate system such that it simplifies the entry of geometry data from other sources. Most ground control and rock mechanics engineers deal with coordinate systems with two of the axes directions aligned to the compass directions north, south, east or west and the third axis being up or down. Unfortunately there is no common standard which defines a global coordinate system convention for mine data (i.e. xyz = north, up, east). As a result, coordinate data from different mines can have completely different global coordinate system conventions. To make things even more difficult, divisions within the same mine, such as ground control and geology, might store spatial information

using different global coordinate systems. As an example, one department might define a xyz coordinate in a northing, up, easting frame of reference while another might use northing, easting, down as the directions of the xyz global coordinate system axes. So any system which must import and export geometric data must be flexible in managing different coordinate systems and must be able to present stress analysis results in easily understandable frames of reference. Therefore all directional information in *Examine*^{3D} by default is presented in a (north, up, east) coordinate system. Conversion between other coordinate systems is simply done by specifying the physical directions associated with a xyz coordinate which is being imported or exported.

3.4 Mesh Generation Techniques for Underground Excavation Geometry

This section presents the three major techniques used in generating a three-dimensional boundary element surface mesh of an underground excavation in rock. These techniques are extrusion, skinning, and facing. Each is discussed in detail below.

3.4.1 Extrusions

One of the simplest methods for creating a three-dimensional polygonalized surface is the extrusion of a two-dimensional polyline. This technique can be found in most of today's popular CAD and geometric modeling packages such as AUTOCAD™, ALIAS™, and IDEAS™. To create the surface, a polyline is usually extruded some distance in a direction normal to the plane of the polyline. The cylinder is a prime example of a surface which is created by such a process. In mining, many of the excavations can be modeled by the extrusion process. For example, shafts, drifts, crosscuts, and blasthole stopes are just a few types of structures which can easily be modeled using this process. As well, many underground civil engineering structures, such as subway tunnels and hydroelectric power caverns, can be modeled by extrusion.

A generalized form of an extrusion can be created by taking a three-dimensional polyline, termed the extrusion contour, and sweeping it along some extrusion path. The path is defined by another

three-dimensional polyline which corresponds to some point on or near the extrusion contour. CAD, computer graphics, and computer vision literature generally refer to this technique as generalized cylinders, generalized extrusions or generalized sweeps. Generalized cylinders were first introduced by Binford and Agin (1973) for the purpose of modeling three-dimensional shapes as part of a hand-eye robotics project at Stanford University in the early seventies. In this case, the extrusion contour was represented by circles, and the extrusion path was some analytical function. Nevatia and Binford (1977) further extended the idea for the purpose of object recognition. Their cross-sections were planar polygons while the path was a three-dimensional polyline. Shani and Ballard (1984) used B-splines to represent both the extrusion contour and the path. In mining applications, generalized extrusions can best be applied in modeling ramped access tunnels.

The implementation of generalized extrusions for the purpose of modeling underground access tunnels is straightforward. Most tunnel geometry is usually available from mine plans, which may already be in some electronic form, i.e. AUTOCAD™, or in hardcopy blue print form, which can then be digitized. Regardless of the format, a polyline which approximates the contour of the tunnel can easily be generated. The next step in the process is to produce the polyline path that the tunnel takes. The point on the extrusion contour that corresponds to the extrusion path is noted, and the extrusion contour is swept along the extrusion path. Figure 3.4 shows the cross-section and path polylines for a ramped underground access tunnel.

The only difficulty with this approach is the possibility of self-intersection. If the data defining the path or the extrusion contour are in error, it is conceivable that the resulting generalized cylinder intersects itself. If this is not taken into account, and the geometry is used in the numerical analysis, numerical convergence of the boundary element analysis is unlikely. If this is allowed to happen, there is a good chance that the user may lose confidence in the modeling system. As a result, additional logic for determining whether invalid element intersections exist has to be added to the modeling system before the geometry is used in any analysis.

In the case of a polyline vertex where there are two tangent vectors according to the two adjoining line segments the average tangent vector is calculated, and the extrusion contour is oriented according to this direction. Many applications of generalized cylinders allow for in-plane rotation or twisting of the extrusion contour as it is swept along the path. In the case of tunnels, in-plane rotation of the extrusion contour is restricted. This restriction ensures that the floor of a tunnel always remains

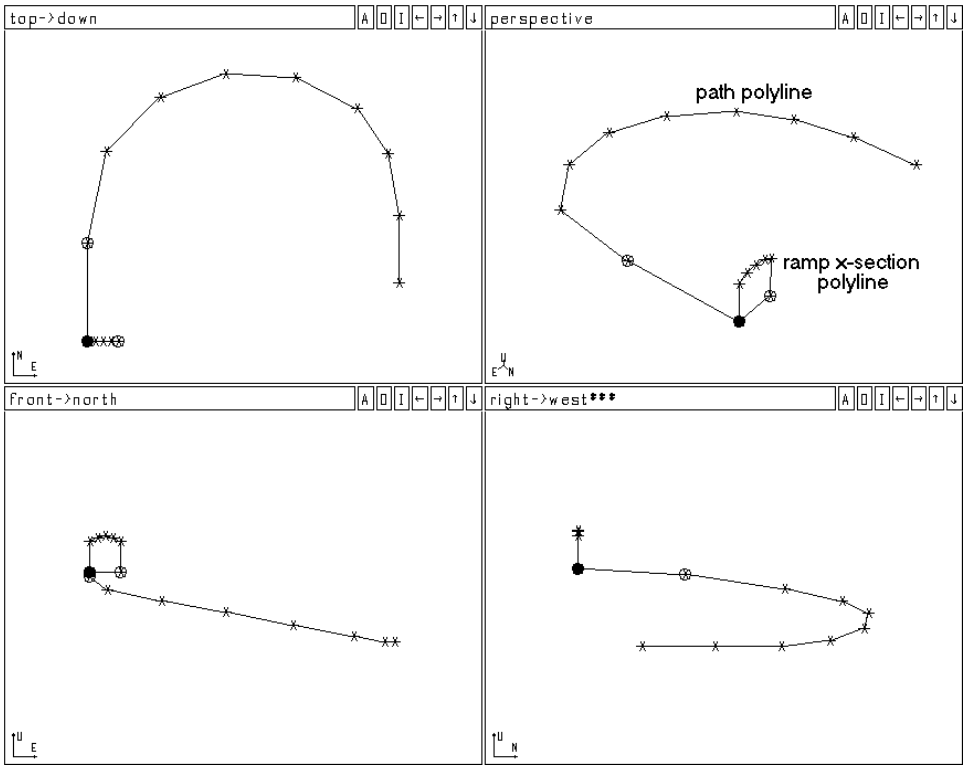

Figure 3.4 Generalized extrusion of a ramped access tunnel

down. The next step of the process creates a surface mesh of the tunnel by connecting adjacent extrusion contours. All extrusion contours are discretized according to some final mesh density parameter, with each contour having the same number of discretizations. Adjacent contours are then triangulated by connecting adjacent discretization points, or nodes, as shown in Figure 3.5, which is the surface mesh created using generalized extrusion of the polylines in Figure 3.4. The discretization of both the

extrusion contour and the path are done such that the aspect ratios of the resulting elements are not more than 3:1. This restriction in aspect ratio helps to ensure the numerical accuracy of the numerical analysis.

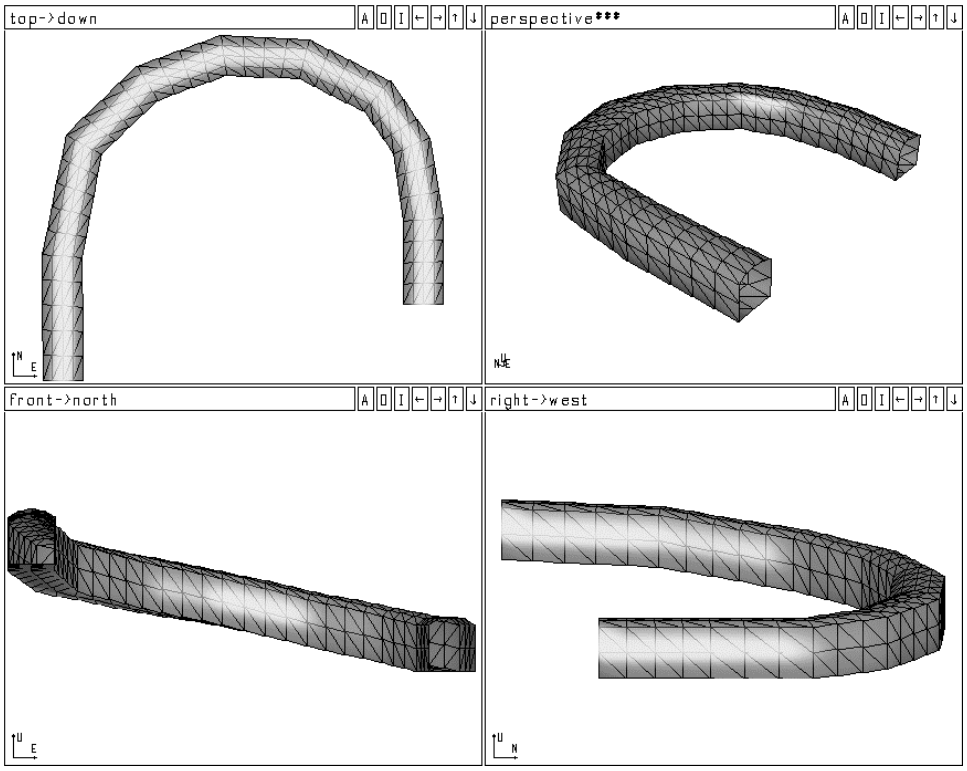

Figure 3.5 Surface mesh created from a generalized extrusion

3.4.2 Skinning

In mining and civil engineering, the format by which excavation geometry is stored generally consists of two-dimensional serial cross-sectional contours. These two-dimensional contours are commonly in some electronic format such as the AUTOCAD DXF format or an equivalent computer-aided design (CAD) drawing exchange format. In some cases, geometry is presented as paper blue prints, in which case there is a digitization process to convert the data to a digital format. AUTOCAD DXF files are the most common form in which the geometry is presented to the numerical

modeler. The geometric primitives making up these cross-sections are generally two-dimensional or three-dimensional closed polylines, consisting of hundreds of individual line segments. These polylines represent the outline of the mined geometry on a single section.

The problem is to reconstruct the surface of the excavation using this sectional information. Since this problem also occurs in many other branches of science and engineering, there is a wealth of information resulting from research into this reconstruction process. For example, in the medical field, numerous sections or slices are created by imaging techniques such as computed axial tomography (CAT), nuclear magnetic resonance (NMR) , and ultrasound. In microscopy, thin sections at different depths are recorded and the cross-sectional images are used to reconstruct the three-dimensional structure. In CAD, the three-dimensional construction of machine parts using cross-sectional data is commonly performed. However, the reconstruction process in the above fields is for the sole purpose of visualizing the three-dimensional object that is represented by the two-dimensional contours. For our purposes, it is not only necessary to visualize the three-dimensional geometry but, more importantly, to be able to utilize the resulting three-dimensional surface reconstruction in a boundary element stress analysis. The three-dimensional reconstruction must be composed of triangles which are completely edge connected and have aspect ratios which do not cause numerical instability in the analysis phase, requiring that the elements be as close to equilateral as possible.

The term skinning is used to describe the process of taking a series of polylines or curves, which define the cross-sectional shape of the object at various locations, and wrapping a layer of polygons or surface patches around the contours to create the surface mesh of the object. The process for generating this skin can be broken down into several subproblems as was done by Meyers et al.(1992) with some modification due to the boundary element mesh restrictions. The first problem is simplification of the contours. As can be seen by Figure 3.1, the contours generally model the actual physical geometry of an excavation, resulting in contours that can be quite complex. If one were to skin these contours, the number of elements would greatly exceed the limitations of memory and storage required for the

boundary element stress analysis on most of today's personal computers and workstations. Consequently, these contours must be simplified to a level of complexity that will best model the actual geometry, yet will still yield useful stress analysis results. The more one simplifies the geometry, the fewer elements will be required. When there are fewer elements, the analysis will run faster but the results will be less accurate. A trade-off is being made between speed and accuracy. The decision concerning the level of simplification of the geometry is best left to the engineer who has to determine the time constraints for a project and the importance of the accuracy of the results. The current skinning algorithm is a manual process where the user must create new contours from the actual contours by redigitizing them to the level of detail required for the specific analysis.

The second problem of skinning is one of correspondence. Correspondence is the term used to describe the sequence in which a series of skin contours attach to each other. In the case of mining or civil engineering structures which are defined by level plans or sections, this information is readily available from the drawings. More important is the problem of how the contours actually connect to each other. The procedure for connecting the contours, referred to as tiling by Meyers et al. (1992), defines the best topological adjacency relationship between the contours. The process determines how adjacent contours are attached, and the triangulation of the space between the two contours. The tiling problem has been the subject of most of the previous work on creating surfaces from contours (Keppel 1975, Fuchs et al. 1977, Christiansen and Sederberg 1978, Ekoule 1991). Using graph theory and a metric for distinguishing good surfaces from bad, an automatic connection between two contours can be made. Unfortunately, there are certain pathological cases which cause problems depending on the metric used to determine the optimal surface (Meyers et al. 1992).

To resolve the problem of tiling, a more straightforward but robust algorithm was adopted for determining the connection between two adjacent polyline contours. During the simplification process, the user is required to redigitize the mine sections in order to define the connection between two contours defining the same excavation. Each polyline defining an excavation must have the same number of

vertices and the ordering of these vertices must be such that vertex one attaches to vertex one of the adjacent polyline, vertex two attaches to vertex two etc. The tiling procedure is then a simple process of connecting common edges between the two adjacent polylines using two triangular elements as in Figure 3.6. If two adjacent contours are far enough apart as to cause the creation of high aspect ratio elements, intermediate polylines are generated by interpolating between the two. If the elements created are too large causing inaccurate stress analysis results, adjacent polylines are first discretized to some density to create the desired mesh density.

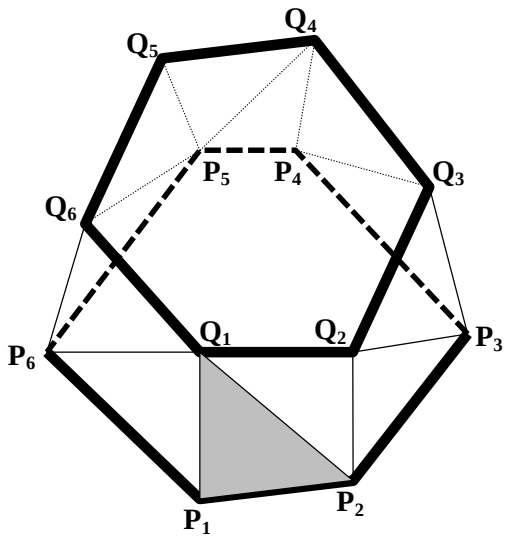

Figure 3.6 Tiling between two adjacent polylines

Figure 3.7 is an example of a series of adjacent polylines extracted from the cross-section plans at the Mines Gaspe, Quebec, defining the E-32 stope. Notice the two distinct sets of polylines representing two different parts of the stope. These two sets of polylines are skinned separately to produce the geometry in Figure 3.8. Notice that the two skins are not closed at the ends and also that the two skins intersect. The next section discusses the technique used for closing the ends of skin and extrusion geometry and defining skin intersection geometry.

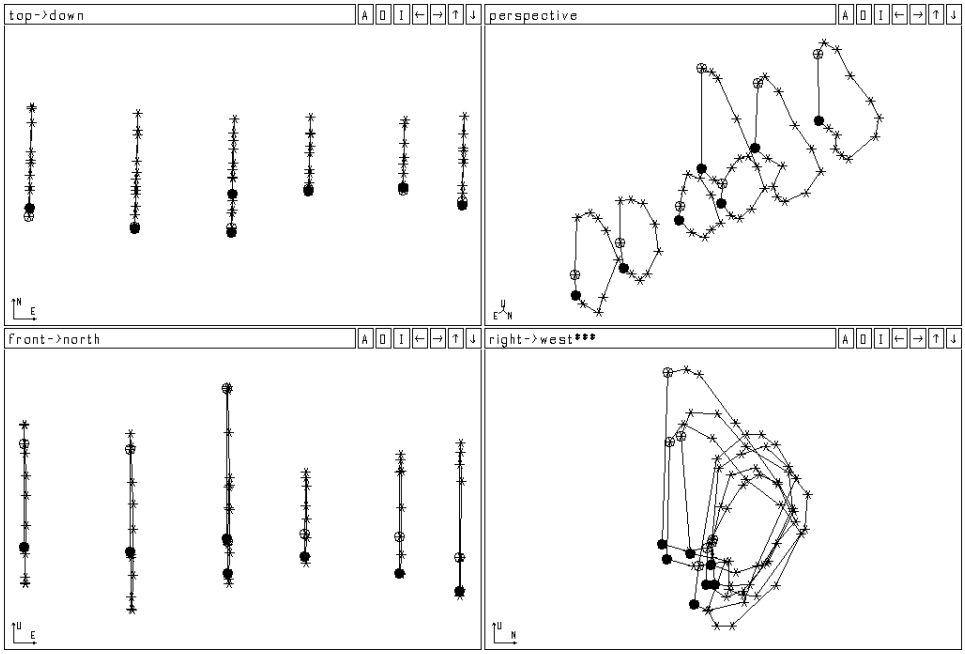

Figure 3.7 A series of skin polylines for Mines Gaspe E-32 stope

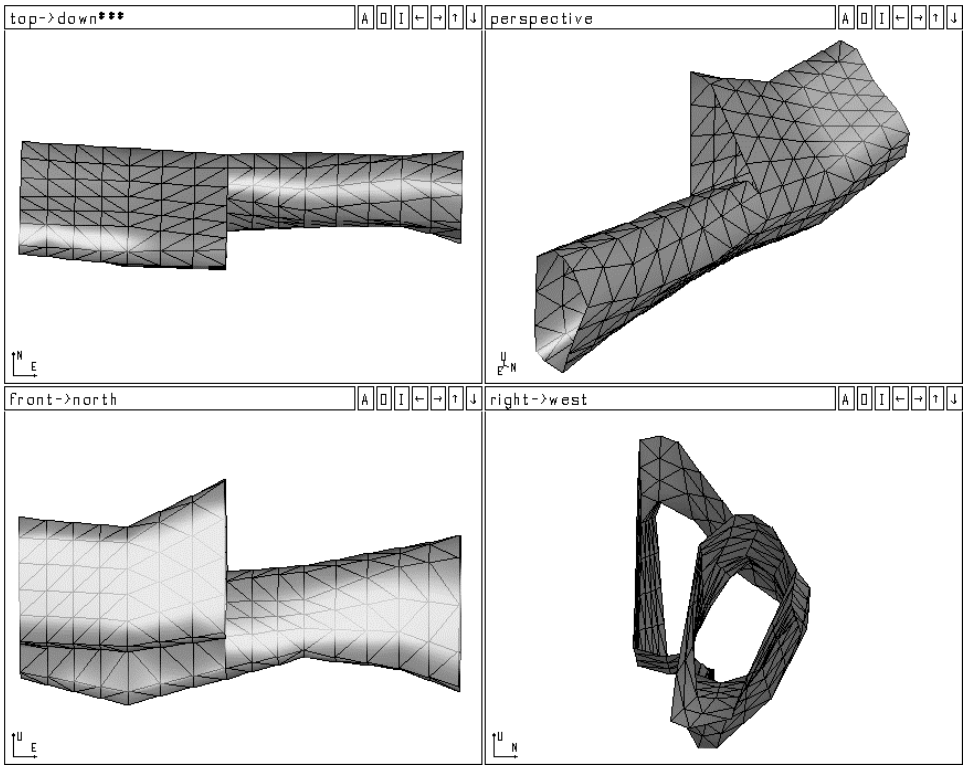

Figure 3.8 Skinned surface mesh of the Mines Gaspe E-32 stope

3.4.3 Facing

As seen in the previous sections, the process of extrusion and skinning creates a surface which is either defined by the skin polylines or the extrusion contour. In creating this surface geometry, no attention is paid to the ends of the skin or extrusion. Figures 3.5 and 3.8 illustrate this point, since both ends of the generalized extrusion in Figure 3.5 are not closed and the ends of the skins in Figure 3.8 are also open. As seen from Figure 3.8, at the point where the intersection of the two skins occur, the geometry is quite complex. A valid boundary element mesh must be completely closed, so a technique termed facing has been developed for the purpose of handling these end caps and intersection planes (faces).

Facing is the technique used for meshing the two different types of faces associated with skinning and extrusion surfaces. The first type of face, termed end facing, is associated with the ends of a skin or extrusion surface and is described by a single polyline which defines the perimeter of the hole

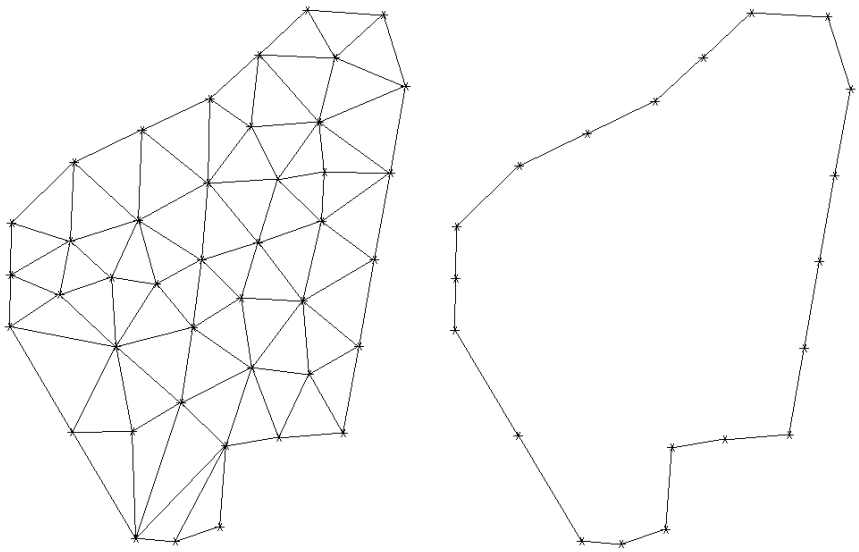

Figure 3.9 Face (left) and face polyline (right) for end facing

in the mesh. Figure 3.9 illustrates the face polyline and the end face for the west end of the Mines Gaspe E-32 stope in Figure 3.8. The second type of face, termed intersection facing, is associated with the

intersection of multiple skin and extrusion surfaces. Figure 3.10 illustrates the two face polylines and the intersection face for the intersection of the two E-32 stope excavations in Figure 3.8. It is basically a method used to attach or chain together the two skins. It is also the most difficult facet of the surface modeling to implement due to the complexity of the geometry where multiple skins intersect. It is also very important that the triangles used to patch between the skins be fairly equilateral.

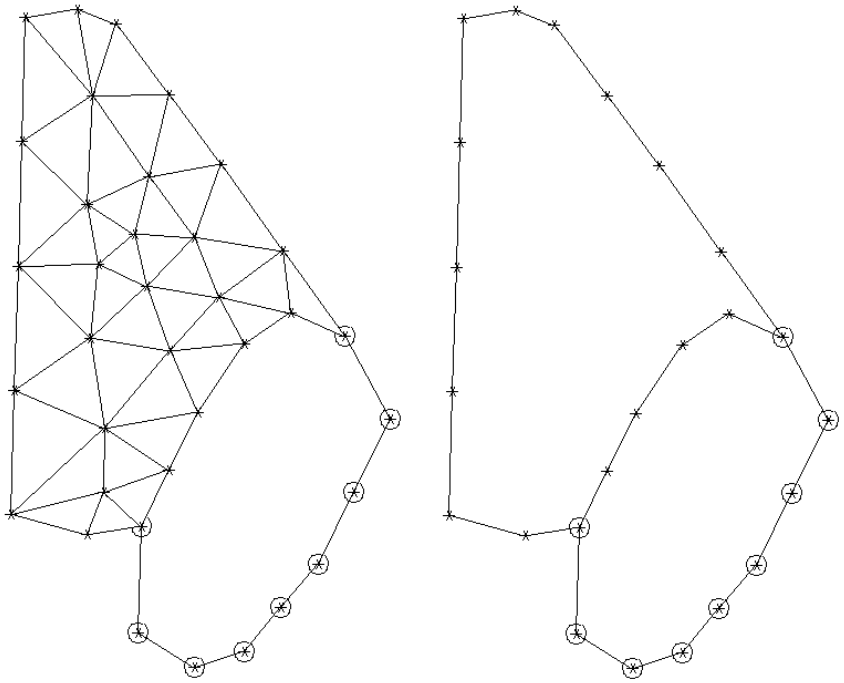

Figure 3.10 Face (left) and face polylines (right) for intersection facing

The algorithms used for facing are based on the technology developed for automatic mesh generation in a two-dimensional finite element program (PHASES) developed for applications in rock engineering by Hoek, Carvalho and Corkum (1992). The automatic generation of two-dimensional triangular finite elements and the automatic three-dimensional generation of triangular boundary elements on a plane are very similar in application. In both cases, a bounded two-dimensional region is filled with edge connected triangular elements under the condition that the elements be as close to equilateral as possible.

At the end of each skin and extrusion there is a boundary polyline. In the case of an end face, it is this polyline which defines the bounded plane in which elements must be generated. In the case of an intersection face, the boundary polyline from two or more skins define the bounded plane. The boundary polylines for intersection faces should lie within the same plane. In the case of intersection faces with multiple boundary polylines, one set of polylines describes the end of the skin geometry to one side of the face plane and the remaining polylines describe the end of the skin geometry on the other side of the face plane. The areas which are outside the region of the intersection of these two sets of boundary polylines define the region which needs to be meshed (see Figure 3.11).

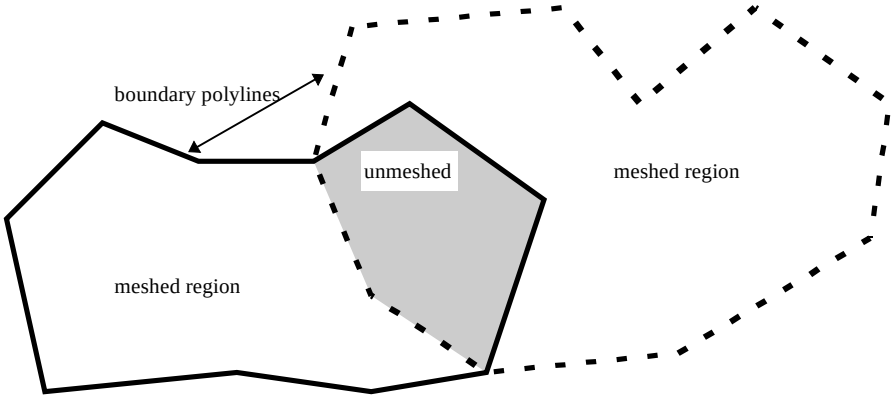

Figure 3.11 Intersection face geometry

There are many techniques available for the automatic meshing of a bounded region (see Cavendish, 1974; Simpson, 1979). One of the most powerful techniques employs Delaunay Triangulation, a method of triangulating a set of points within a closed region. An important property of the two-dimensional Delaunay Triangulation is that its triangles are as close to equilateral as possible for the given set of nodes (Sibson, 1978). This makes it well suited for use in creating a boundary element mesh of triangular elements. Consequently, ill-conditioned and thin triangles are avoided whenever possible. There has been much work done on the implementation of Delaunay Triangulation for automatic finite element mesh generation. The actual Delaunay Triangulation algorithm will not be

covered here, however the reader is referred to Cavendish et al., 1985 for an in-depth discussion on its implementation.

There are three distinct steps in creating a mesh using Delaunay Triangulation. The first step is to create a set of nodes within the region to be meshed. The second is to use Delaunay Triangulation to operate on this set of points. The third is to improve the mesh by a process called smoothing.

Two of the more popular methods for creating this set of points for the first step are grid and quadtree insertion. The grid insertion technique, used by Cavendish (1974), inserts a series of points within a region by first overlaying a regular grid and then inserting one node randomly within each grid cell. The density of the regular grid is dependent on the level of discretization on the boundary polylines. The distance between grid lines is equal to the average distance between nodes on the boundary polyline. This distance measure, *R*, is also used as a filter for node insertion. When a node is inserted randomly within a grid cell, it is first checked to ensure that it is greater than distance *R* from any other inserted or boundary node. If it is within distance *R* from another node it is discarded and another node is randomly generated within the same grid cell. This process proceeds for five iterations or until a node is found to pass this criteria. This distance criteria ensures that there are no nodes too closely spaced to each other, causing poorly shaped elements.

The second method of node insertion (quadtree) uses a quadtree subdivision algorithm for discretizing the area around the boundary polylines (Schroeder and Sheppard, 1989; Graichen et al., 1989; Ramakrishnan et al., 1992) . The modified quadtree algorithm, used by Hoek, Carvalho and Corkum in the PHASES finite element program based on the work by Graichen et al. (1989), starts by overlaying a box on top of the geometry and then subdividing the box into four equal boxes. Each box is then subdivided into four boxes until each box has zero or one boundary nodes inside it. To ensure a proper gradation, the level of sudivision for adjoining boxes cannot be greater than one level apart. Nodes are then inserted at the corners of all boxes in the quadtree.

After the nodes have been inserted, the second step is the Delaunay Triangulation of both the inserted and boundary nodes to create the boundary element mesh of the desired regions. In the process of creating the Delaunay Triangulation, the algorithm first starts by defining a convex hull that completely encompasses all the nodes, and thus ensures that no zero area triangles are created (Cavendish et al., 1985). The nodes are then inserted one by one until the triangulation is complete. All triangles that lie between the boundary polylines and the convex hull are then filtered out by determining whether the center of each triangle lies outside all of the boundary polylines, and then removing it if it does. To determine whether the center point of a triangle is outside a boundary polyline, the odd-parity rule is used (Foley et al., 1990). This rule determines if a point is inside or outside a polygon. This is done by determining the number of intersections that a ray, starting from the test point and extending infinitely in any direction, has with the polygon. If the number of intersections is an odd number, the point is inside the polygon, otherwise the point is outside the polygon.

Once the mesh has been generated, further improvements in overall mesh quality can be achieved by relocating the interior boundary element nodes (not the nodes on the boundary polylines) by a process termed smoothing. This is the third and last step in the mesh generation process. One popular method, referred to as Laplacian smoothing (Herrmann, 1976), iteratively replaces interior node P_i with:

$$P_i = \frac{1}{N_i} \sum_{j=1}^{N_i} P_j$$

where N_i is the number of nodes to which P_i is connected and P_j are the node points of the connected nodes. This process has proven useful in two-dimensional finite element mesh generation algorithms (Cavendish, 1974) and smoothes the mesh so it has better proportioned elements.

Finally, the procedure is complete and the appropriate face elements have been created using this method. The most important feature of this method is that it is totally automatic. Very little, if any, user intervention is required to create a good quality boundary element mesh within the face. Figures 3.9 and 3.10 illustrate face meshes using grid node insertion, Delaunay Triangulation, and Laplacian smoothing.

Notice that both are good quality boundary element meshes with triangles very close to equilateral, both being produced automatically without user interaction. Figure 3.12 shows the final mesh geometry of the Mines Gaspe E-32 stope. Note the faces associated with the intersection and ends of the skins created in section 3.4.2.

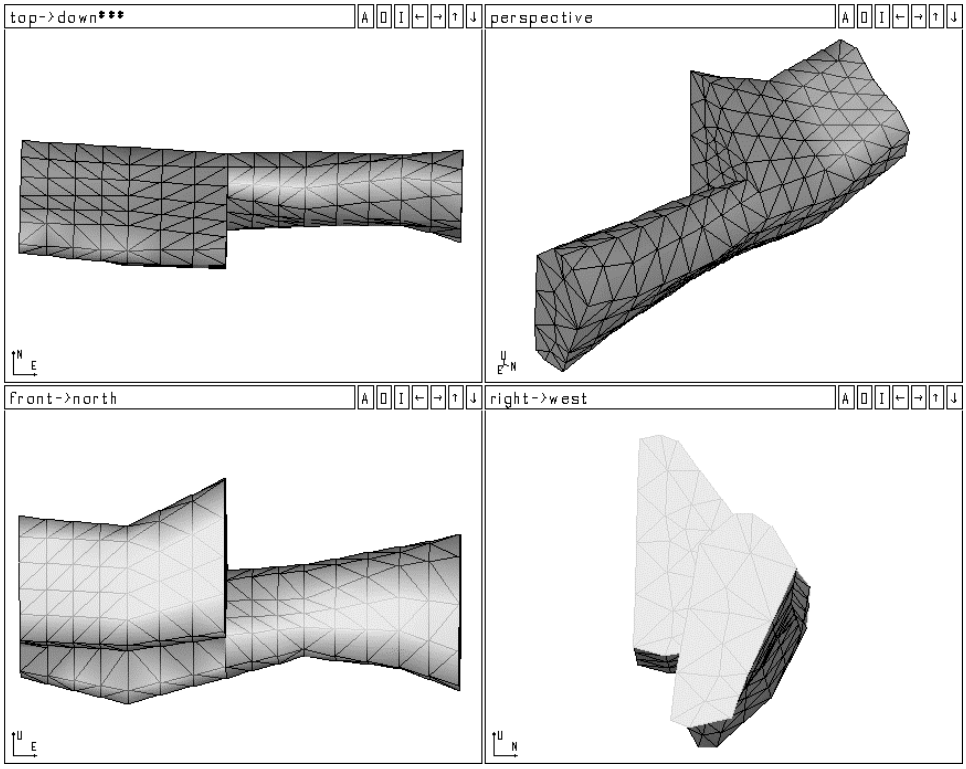

Figure 3.12 Mines Gaspe E-32 stope - final mesh geometry

3.5 Checking the geometry

An important aspect of creating the geometry is the assurance that the mesh is a valid boundary element mesh, i.e., that the geometry is closed and composed completely of edge connected triangular elements (Shah 1993). If the mesh is not valid, either the analysis will not converge to a solution, or even worse, the analysis will converge to an incorrect solution allowing for misinterpretation by the engineer. To guard against this, a set of checks have been implemented to help ensure that the mesh is valid.

The first one, termed the “leaky check”, looks for holes in the mesh and makes sure that the mesh is closed. This check is simply a matter of looping through all element edges. For each edge in the loop, this means ensuring that there is only one element sharing that same edge. Further, the numbering of the nodes on the matching edge must be opposite to the current edge.

The second check, defined as the “normal check”, makes sure that each normal vector associated with an element points into the rock mass. The node ordering and the normal to the element define which side of the element the rock lies on. The convention defined in Shah (1993) has an element with its nodes numbered in a counter-clockwise fashion as one looks at the element from outside the closed surface. If the nodes are defined in this manner, the normal to the element points into the rock mass. Once again, if the nodes and normals are incorrectly defined, no solution or an inaccurate one will result. The algorithm, which ensures that the node numbering is correct, works by first locating an element which must have a normal oriented in a certain direction. This outermost element is defined as the element which touches the northing most node and has the highest dip or slope. This element must also have a normal whose northing component is positive, ordering it in the right direction. Once this element is identified as being ordered in the correct direction and the geometry is verified as “not leaky”, the elements and nodes are guaranteed to be ordered in the right direction. Facilities have also been added to automatically reorder elements whose node numbering are found to be incorrect.

The third check, termed the “intersection check”, looks for the intersection of mesh geometries from openings in close proximity. In the process of skinning or extruding the simplified polylines associated with openings in close proximity, intersection of the boundary element meshes defining these distinct excavations can result. This intersection will also lead to no solution. To perform this check each triangular element is checked to determine whether it intersects any other element.

4. VISUALIZATION ALGORITHMS FOR MINE DATASETS

This chapter introduces many of the fundamental concepts associated with data visualization and concludes by presenting the algorithms used to generate the images which interpret mine datasets. First of all, the basic formats that rock engineering data can occur in are introduced. Many of the fundamental techniques for managing the data and the implementation of the actual visualization approach can depend entirely on the initial format of the data and how well it is presented to the visualization system (see Table 4.1). The chapter goes on to present some of the most common algorithms for visualizing scientific data. The advantages and disadvantages of these algorithms, their area of possible application and their suitability to rock engineering are discussed specifically using each in rock engineering. Many algorithms, although very powerful, are not suitable for a rock engineering visualization system and the reasons are presented in this chapter.

Method	Format
	Structured Data
Boundary Element →	Data Generated on a Uniform Grid
	Data Generated on a Rectilinear Grid
Finite Difference →	Data Generated on an Irregular Grid
Finite Element →	Unstructured Data
Recorded Data Gathered (e.g. seismic) →	Scattered Data

Table 4.1 Data format associated with analysis method

4.1 Data Formats

The three data formats most commonly found when numerically modeling underground excavations are structured, unstructured and scattered. Each format can generally be attributed to a different numerical modeling approach (i.e. boundary element, finite element, or finite difference).

In the case of the finite element and finite difference methods, the data format is determined by the method used. Both methods discretize the volume around the excavations by subdividing the region into simply-shaped elements (i.e. tetrahedrons, hexahedrons, or prisms). The stress and displacement results are then calculated at points of element intersection called nodes. Therefore, the location of the data is directly related to the method used to perform the numerical analysis. In the case of the boundary element method, stresses and displacements can be calculated at any point within the rock mass so only the surfaces of the excavations need to be discretized. As a result, the visualization system can define where the location of the stresses and displacements are to be calculated within the rock mass, providing a great deal of flexibility in visualizing the data.

As previously mentioned, it is very important to know the format and type of the data that the visualization system will be encountering. This is especially true, since the design and implementation of many of the visualization algorithms are themselves based on a certain data format, making conversion between different formats important. Seismicity is a specific dataset associated with mining. Many mines currently employ microseismic monitoring systems for measuring and locating mining-induced seismic events. These systems have become a very important tool for use in safety assessment and mine design. When considering seismic data, the random nature of the data which is spatially scattered, often is converted to a more structured format when trying to visualize certain features (i.e. energy and event densities). The following sections present an overview of the various formats in which rock engineering data could be presented to a visualization system.

4.1.1 Structured Data Format

When performing a stress analysis around underground excavations, the type of method generally determines the format of the data. The structured data format is of particular interest to this research, since it is the format of data generated from a boundary element stress analyses. Data generated from a finite difference stress analysis is also in this format.

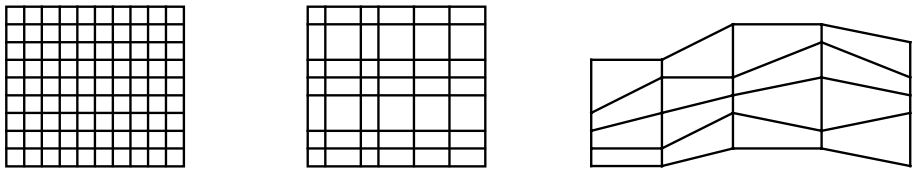

Figure 4.1 Structured data formats

There are three main types of structured data: uniform, rectilinear, and irregular grids (Gelberg et al., 1990) and examples of each can be seen in Figure 4.1. Data produced from the finite difference method is in the form of an irregular grid since this method requires volume discretization in this particular format. In the case of the boundary element method, in which case the user determines where the stresses and displacements are calculated, the most common definition is usually in the form of a uniform or rectilinear two-dimensional grid because of the ease of contouring data in this format. A natural extension of the two-dimensional grid is a three-dimensional grid which encompasses the volume of interest. Many of the more popular volume visualization algorithms use data in three-dimensional rectilinear grid form, making it the ideal choice for stress analysis data produced for use in this thesis.

With a rectilinear grid, the grid lines are orthogonal but the spacing is non-constant. The visualization system must not only store the data, but it must also store information on the different spacing. Visualization of data on a rectilinear grid is generally done using the same techniques as uniform data. Irregular data is both non-orthogonal and has variable spacing between data points. The location, along with the data value, must be stored for each node and this makes for larger storage requirements.

The uniform grid is a special case of the rectilinear grid. Its grid lines are orthogonal with data points (nodes) falling at constant interval spacing in two or three dimensional space. The spacing is equal in any one direction but need not be the same in all directions. This type of data is generally the easiest to deal with since there is low overhead with storage and data access; the physical location of each data point does not need to be stored, only the index of its location within the grid. The

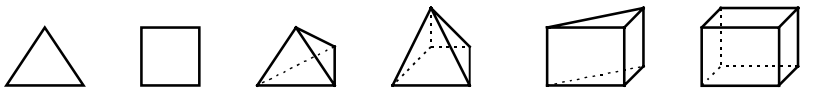

Figure 4.2 Cell types

visualization of this type of data is a straight forward process with the currently available data visualization techniques.

4.1.2 Unstructured Data Format

Data from a finite element stress analysis is generally in an unstructured format. Unstructured data is a set of connected points in two or three-dimensional space. Data points (nodes) are connected to form edges that are connected to create faces. Finally, faces are connected to form elements. The elements form the basis of the volume discretization and the subsequent location of the data points throughout the rock mass. Figure 4.2 is a sample of different two and three-dimensional elements.

4.1.3 Scattered Data Format

Scattered data lacks the connectivity associated with both structured and unstructured data. Unlike these other data formats, the spatial locations of the data occur at random locations within the volume or area of interest. Mining-induced seismicity is an example of a scattered dataset. Visualization techniques for scattered data generally determine a connectivity by two or three-dimensional Delaunay triangulation (Sibson 1978) or by using interpolation to determine values on a predefined structured or unstructured grid. Interpolation techniques for mapping random scattered data to a structured uniform grid is the direction chosen in this thesis and are presented in section 4.3.3.

4.2 Data Types

In the preceding section, the concept of data format was presented to indicate the various spatial distributions that discrete rock engineering data can occur in. Data format defines how the discrete data is located in space and its structure. The data type defines the actual quantity being calculated (stress analysis) or measured (seismicity) within the rock mass. The three most common data types in rock engineering are tensor, vector and scalar quantities. The stress tensor, which defines the state of stress at any point within the rock mass, is a 3X3 matrix of compressional and shear terms (see section 5.1.1 for a more detailed definition). . One of the principal goals of doing a stress analysis in rock engineering is to determine whether regions of overstress exist and where these regions are located. This is done by calculating the stress tensor at discrete locations within the rock mass. One of the primary objectives of this thesis is to develop a technique for quickly and accurately visualizing the stress tensor data.

Along with the stress tensor, a displacement vector can also be calculated at discrete points within the rock mass. This displacement vector yields important information on the closure distribution around the excavations.

Examples of scalar data in stress analysis include 1) one of the components of the stress tensor, 2) one of the principal stresses, 3) the strength factor which defines the degree of overstress, 4) a displacement component, or 5) the magnitude of the total displacement vector. Scalar seismic datasets include the geotomography P-wave velocity, event or energy density, and event magnitude. In rock engineering, there is no one standard tensor, vector or scalar quantity that is used in determining stability and design. So the visualization system to be developed must be flexible enough to display any component or combination of the analysis results as well as to be able to use any of these data types.

4.3 Interpolation Techniques

The interpolation of discrete data is a very important aspect of the visualization process. There are many applications of interpolation within a visualization system since data is often requested in locations other than where the analysis or measurements are performed. In the case of a stress analysis, it

is possible to go back and try to calculate results at a user prescribed location. However, using a finite element or finite difference analysis, this would not be practical since it would require remeshing to place nodal points at the desired locations. Even though a boundary element stress analysis does not require remeshing, the added computational expense of determining precise results wherever required is not practical. Instead of calculating every required value, interpolation is used to create two-dimensional contours on a three-dimensional cutting plane to resample structured or unstructured grids, to calculate results at a point within a cell and to resample scattered data to create a structured dataset. It is also used in the creation of iso-valued surfaces and the generation of intermediate cutting planes within a three-dimensional uniform grid of data. Depending on the application, the method of interpolation can be quite different. In the case of creating contours, simple two-dimensional bi-linear interpolation techniques are used while iso-valued surfaces require three-dimensional tri-linear interpolation. The resampling of scattered data onto uniform grids uses a completely different set of interpolation functions to achieve acceptable results. The following sections present an overview of the different methods.

4.3.1 Two-dimensional Bi-linear Interpolation

In the case of two-dimensional uniform or rectilinear grid data, the simplest interpolation technique for calculating values within the grid is bi-linear interpolation. Figure 4.3 illustrates how bi-linear interpolation is used to calculate the value of an arbitrary point within a grid cell. The calculation of values at points within the cell are based entirely on the values at the four grid points. The bi-linear interpolation function is linear across the cell edges but is quadratic within the cell, thus producing smooth internal contours. This interpolation method is particularly useful when generating contours on a two or three-dimensional cutting plane. In the case of a two-dimensional cutting plane, the data values at pixels internal to the grid cell are first interpolated and then are colored depending on the relative position of their value within a contour range bar. A contour range bar is a colored scale which maps the value to a color for graphical display of the data (see Figure 5.1 in the next chapter for an

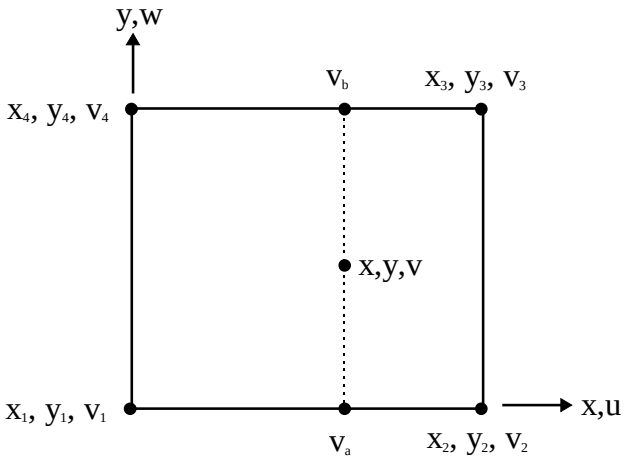

$$u = \frac{x - x_1}{x_2 - x_1}; w = \frac{y - y_1}{y_2 - y_1}$$

$$v_a = (1-u)v_1 + uv_2$$
$$v_b = (1-u)v_4 + uv_3$$
$$v = (1-w)v_a + wv_b$$

Figure 4.3 Bi-linear interpolation over a grid cell

example of a contoured cutting plane and contour range bar). In the case of a triangulated region, used in the case of the surface boundary elements or with a two-dimensional finite element analysis, a bi-linear interpolant can be constructed over each triangle. Figure 4.4 illustrates the method for constructing a bi-linear interpolating function for a triangle.

For both gridded and triangulated volume discretizations, higher order and higher continuity can

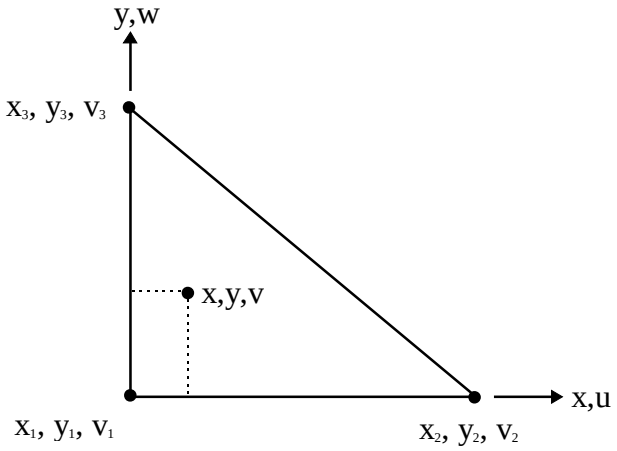

$$u = \frac{x - x_1}{x_2 - x_1}; w = \frac{y - y_1}{y_3 - y_1}$$

$$v = (1-u-w)v_1 + uv_2 + wv_3$$

Figure 4.4 Barycentric interpolation over a triangle

be achieved by using a bi-cubic interpolating function. Partial derivatives are required at each of the

nodes using this function. These derivatives can be estimated from the surrounding data using a finite difference approach or they can be calculated directly from the underlying function when the values at the nodes are computed.

4.3.2 Three-dimensional Tri-linear Interpolation

The single most utilized interpolation method is the tri-linear interpolation method. The reason for its widespread use is because the structured grid data format is the basis of the three-dimensional volume visualization algorithms used to generate the graphical display of the data. To calculate a data value within this three-dimensional grid, tri-linear interpolation is performed within the grid cell that the sample point falls in. It should be noted that higher order interpolation methods are possible, but the added computational complexity slows down the rendering of the graphical display of the data. This detracts from the benefits of the interactive visualization process. It is debatable whether or not improved accuracy results from these higher order interpolation functions.

Tri-linear interpolation is simply a three-dimensional extension of the bi-linear interpolation within a two-dimensional grid cell, as presented in Figure 4.3. The equations for tri-linear interpolation are based on the picture of a generic cube (Figure 4.5). The diagonal corner locations of the cube are x_1,y_1,z_1 and x_2,y_2,z_2 respectively. The location of the sample point within the cube is x,y,z. Three

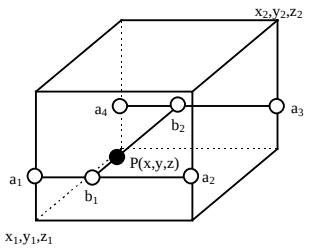

Figure 4.5 Tri-linear interpolation (after Gelberg et al., 1990)

interpolations are performed: (1) along the four vertical edges to form two lines and four values (a_1,a_2,a_3,a_4); (2) along the two lines to form a single line and two values (b_1,b_2); and (3) along the line to form a value P(x,y,z). The following are the equations used to perform the interpolation:

$$u_1 = (x-x_1)/(x_2-x_1); \qquad u_2 = (x_2-x)/(x_2-x_1)$$
$$v_1 = (y-y_1)/(y_2-y_1); \qquad v_2 = (y_2-y)/(y_2-y_1)$$
$$w_1 = (z-z_1)/(z_2-z_1); \qquad w_2 = (z_2-z)/(z_2-z_1)$$

$$a_1 = v_1*P(x_1,y_2,z_1) + v_2*P(x_1,y_1,z_1)$$
$$a_2 = v_1*P(x_2,y_2,z_1) + v_2*P(x_2,y_1,z_1)$$
$$a_3 = v_1*P(x_2,y_2,z_2) + v_2*P(x_2,y_1,z_2)$$
$$a_4 = v_1*P(x_1,y_2,z_2) + v_2*P(x_1,y_1,z_2)$$

$$b_1 = u_1*a_1 + u_2*a_2$$
$$b_2 = u_1*a_4 + u_2*a_3$$

$$P(x,y,z) = w_1*b_1 + w_2*b_2$$

4.3.3 Scattered Data Interpolation

For scattered data typically found in seismic event datasets, data must be first mapped to a format that can be manipulated by the visualization system. The most effective algorithms for visualizing data require that the data be in a structured grid format and that the visualization system already manages stress analysis data in this format. Therefore, the scattered data is mapped to a structured uniform grid. In order to map the scattered data to the grid structure, values at the grid vertices must be calculated using interpolation. Each method presented here performs the interpolation by first constructing a functional representation of the data. This is done by using different basis functions and then calculating the value at the new location using this function. The first method developed to interpolate data to a uniform grid used inverse distance weighting of the data. This scheme has become known as the Shepard method (Shepard, 1968) and can be written in the form:

$$F(P) = \frac{\sum_{i=1}^{N} \frac{F_i}{\|P - P_i\|^2}}{\sum_{i=1}^{N} \frac{1}{\|P - P_i\|^2}}$$

where P is the location of the point to be interpolated, F(P) is the interpolated value, P_i the location of the scattered data, F_i are the scattered data values, and $\|P-P_i\|^2$ represents the distance from P to P_i. The main deficiencies of this method are, 1) the local extrema are typically located at the data points and this results in poor shape properties, and 2) undue influence of points which are far away. To eliminate these deficiencies, Franke and Nielson (1980) developed the modified quadratic Shepard's method. Their method modifies the weight function $\|P-P_i\|$ to localize the approximation and replaces F_i with a suitable local approximation $Q_i(P)$. This method has the form:

$$Q(P) = \frac{\sum_{i=1}^{N} \frac{Q_i(P)}{\rho_i^2(P)}}{\sum_{i=1}^{N} \frac{1}{\rho_i^2(P)}} \quad ; \quad \frac{1}{\rho_i(P)} = \frac{(R_w - \|P - P_i\|)_+}{R_w \|P - P_i\|}$$

where R_w is the limiting distance for the weighting function. Thus, for a data point whose distance from the interpolation point is greater than R_w , the weight is zero. $Q_i(P)$ are quadratic polynomials obtained from a least squares fit and constrained to take the value of F_i at P_i. A more in-depth discussion of this method can be found in Nielson (1993).

Two other methods which produce very effective interpolations and visualizations of scattered data are the Hardy's multiquadric method (Hardy, 1990) and the thin-plate spline method (Duchon, 1975). Both belong to a class of methods which have become known as radial basis function methods. These methods are very elegant from a mathematical point of view. The name is derived from the fact that the basis functions are constructed from a function of one variable h(s). Also, the basis function associated with each point is of the form $h_i(P) = h_i(\|P-P_i\|^2)$, where $\|P-P_i\|^2$ is the distance from (x,y) to the ith data point (x_i,y_i). The form of the approximating function is:

$$F(P) = \sum_{i=1}^{N} a_i h_i(P) + \sum_{i=1}^{M} b_i q_i(P)$$

where $q_i(P)$ is a basis for the polynomials of degree < m which allows for polynomial precision. The coefficients a_i and b_i are calculated by solving the following system of (N+M) equations

$$\sum_{j=1}^{N} a_j h_j(P_i) + \sum_{j=1}^{M} b_j q_j(P_i) = f_i \;\; ; \; i = 1,\ldots,N$$

$$\sum_{i=1}^{N} a_i q_j(P_i) = 0 \;\; ; \;\; j = 1,\ldots,M$$

The Hardy multiquadric method is a function of the form:

$$F(P) = \sum_{i=1}^{N} a_i \sqrt{\|P - P_i\|^2 + c}$$

where $c > 0$ and the coefficients a_i are computed by solving the NxN linear system of equations $F(P_i)=f_i$ for i=1,...,N. The value of c can be any real number, with an optimum choice depending almost entirely on the function values f_i (Carlson and Foley, 1990). Foley (1990) gives the simple approach to determining c as being the area of a bounding rectangle multiplied by some constant ranging between 0.1 and 1. If the function is varying rapidly, Carlson and Foley (1990) also suggest using a value of c ranging from 1e-4 to 1e-6. If there are a large number of data points, c should again be small so as not to cause an ill-conditioned matrix.

The thin-plate splines method has the form:

$$F(P) = \sum_{i=1}^{N} \left\{ a_i \|P - P_i\|^2 \log(\|P - P_i\|) \right\} + b_1 + b_2 x + b_3 y$$

with the (N+3) unknown coefficients a_i and b_i being solved for using the N equations $F(P_i)=f_i$ and the three equations:

$$\sum_{i=1}^{N} b_i = 0 \;\; ; \;\; \sum_{i=1}^{N} b_i x_i = 0 \;\; ; \;\; \sum_{i=1}^{N} b_i y_i = 0$$

Thin-plate spline is derived because the interpolant minimizes the integral of the square of the second derivative, which measures the strain energy in a clamped elastic plate.

The disadvantage of using both the Hardy multiquadric and thin-plate spline methods is the need to store and solve a NxN matrix for each interpolated point. If the solution is performed in memory, using standard row reduction techniques, only a few hundred data points may be used. To solve this problem, iterative out of core solvers can be used (Shah 1993), or a localization of the problem as in Franke (1982).

Since these three methods (inverse distance, Hardy multiquadric, and thin-plate spline) depend on the Euclidean distance, they are all easily generalized to three-dimensional data.

4.4 Scientific Visualization of Three-dimensional Volumes

In many branches of science and engineering, the researcher is confronted with the task of interpreting complex three-dimensional datasets of numbers and/or symbols. Scientific visualization helps us extract meaningful information from these complex and often voluminous datasets through the use of interactive computer graphics and imaging. This is done by creating a representation of the data, visible object or image. It is this representation that can give researchers valuable insight into their dataset, allowing them to make interpretations.

Volume visualization is a method for creating these computer graphics images from the three-dimensional volumetric data. The field of volume visualization can be traced back to the late 1970's when medical researchers (Harris, 1978; Herman, 1979) made the first attempts at visualizing interior systems (volumes) using tomographic data. However only since the late 1980's, with important breakthroughs in algorithms and the availability of fast, low cost computer graphics hardware, has scientific visualization emerged as a discipline. Visualization is currently the subject of considerable research and development activity and it is significantly changing the way engineers and scientists do their work. The following sections present a taxonomy of important three-dimensional volume visualization techniques and their applicability to the visualization of mine datasets.

4.4.1 Discrete Shaded Contouring

The contouring of results on a two-dimensional cutting plane is one of the simplest and most utilized methods for visualizing the data from a three-dimensional stress analysis. This cutting plane is defined by the engineer before the analysis, usually in the form of a uniform grid of sample points. Unfortunately, this process pre-determines the area where the results will be of most value. This requires the engineer to execute the analysis again if analysis data is required at a different location. This can result in a long and tedious visualization and interpretation phase of the overall analysis.

By using the concept of defining a three-dimensional volume of interest and calculating results on a uniform three-dimensional grid within this volume, it is possible to define a series of cutting planes which span this volume. The advantage of this method is that the definition of the cutting plane on which data is required moves from a pre-processing requirement to a post-processing data interpretation function. This provides the engineer with all the possible data in one step, allowing for very quick and easy interpretation of stress analysis results. Another important advantage of defining a contoured cutting plane is that it allows the engineer to sweep the cutting plane through the volume, yielding information on how the stress state is changing in three-dimensions.

The process of creating the volumetric cutting planes is quite simple. A three-dimensional uniform grid of values can be envisioned as a series of stacked two-dimensional data planes. Linear interpolation is used to create a cutting plane that lies between any two planes of data. Once a two-dimensional grid of data has been interpolated, discrete shaded contouring of the data is performed.

To create the contours, two techniques have been utilized. The first method takes a two-dimensional grid cell, de-composes it into two triangles and then subdivides each triangle into a series of polygons. Each polygon represents a distinct contour interval. The subdivision algorithm uses linear interpolation along the triangle edges to first calculate the locations of contour intersection and then proceeds to traverse the edge of the triangle to close the contour interval polygon. Coherence between adjoining grid cells of equal contour interval is used to reduce the overall number of polygons.

The advantage of this method is that the viewing transforms and rendering algorithms found in many computer graphics systems can be used for quickly and interactively displaying the planes in three-dimensions.

Another technique which operates at the graphics system level uses color index interpolation when rendering a polygon. Some graphics systems (e.g. HOOPS™) allow for definition of color indices at polygon vertices which, when used in conjunction with a color map, permit the generation of false-colored contoured polygons. This method interpolates the value of the index at a particular pixel associated with a point on a projected polygon and coloring the pixel accordingly. The advantages are that it produces nicely curved contours and requires less memory for storage of the cutting plane polygons. In the case of contouring results on the surface of excavations, this method does not require any storage which makes it even more attractive. However, this method does require certain access to the graphics subsystem which is not always possible, as was found in earlier versions of HOOPS™.

4.4.2 Marching Cubes

The marching cubes algorithm belongs to a family of surface-based techniques which apply a surface detection method to calculate the iso-valued surface, $f(x,y,z)$=constant, defined by some threshold value. The technique was developed by Lorenson and Cline (1987) for visualization of medical data generated from computed tomography (CT), magnetic resonance (MR), and single-photon emission computed tomography (SPECT). The format of the data consists of a uniform 3D grid of density values. Each grid cell is cubical in shape and is termed a volume element or voxel (Figure 4.6).

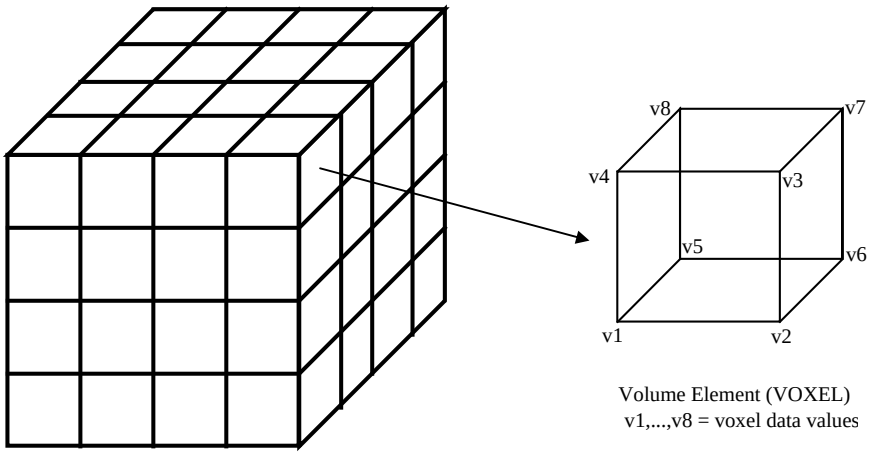

Figure 4.6 Uniform Gridded Data

The marching cubes algorithm uses a divide and conquer solution strategy by solving for the intersection of the iso-valued surface with a voxel, then "marching" to another voxel ("cube") and calculating the proportion of the surface in that voxel. Thus, the solution for the intersection is calculated on a voxel by voxel basis, without data from adjoining voxels being used for the intersection calculation. To find the surface intersection within the voxel, each of the eight vertices is first classified depending on whether the vertex is inside or outside the surface. If the vertex is outside the surface, then its value is greater than or equal to the surface value, while if it's inside the surface then its value is less than the surface value (see Figure 4.7).

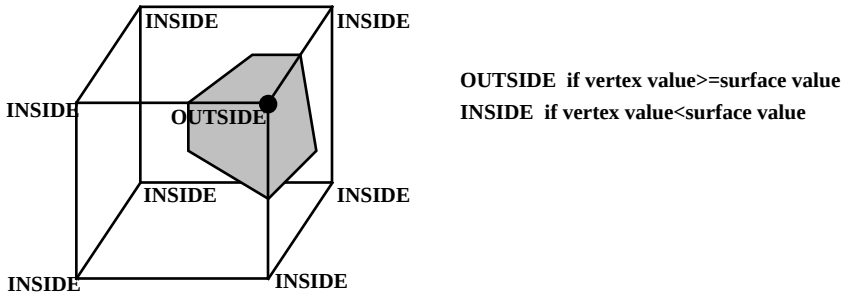

Figure 4.7 Classification of cube vertices

The next step is to calculate the index for each cube based on the binary classification of each vertex. An eight bit value is constructed, each bit representing a vertex, and each bit having the value of either 1 or 0 depending on whether the vertex is outside or inside the surface. Thus, the eight bit value can range from 0 to 255, 0 if all vertices are inside and 255 if all vertices are outside. Figure 4.8 illustrates the calculation of an index for the surface-cube intersection in Figure 4.7.

Using the cube index, a table of triangle edges is accessed to yield all the edge intersections for the given cube configuration. With eight vertices, there are $2^8 = 256$ ways a surface can intersect the

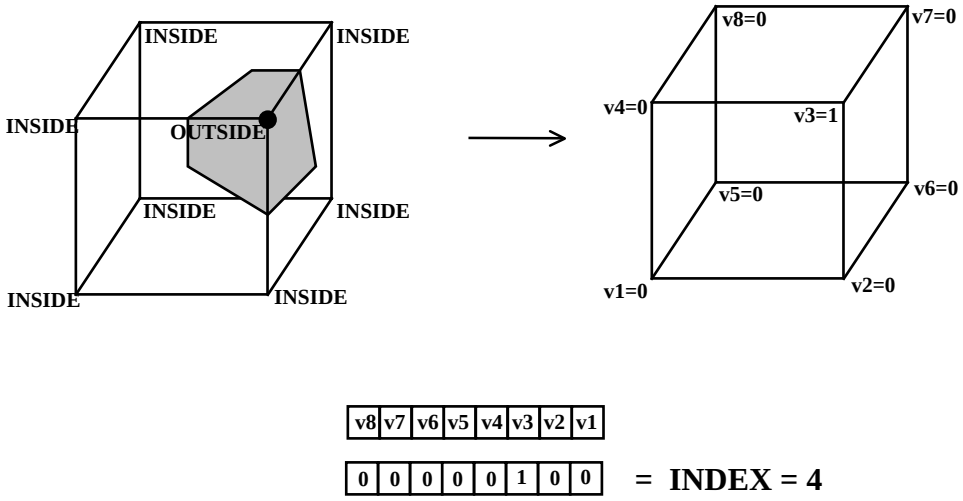

Figure 4.8 Calculation of a cube index

cube. The problem quickly reduces to only 128 cases by noting that the complementary case of an index value, calculated by changing all inside values to outside and vice versa, yield the same surface. Rotational symmetry further reduces the problem from 128 to just 14 possible cases of surface intersection (see Figure 4.9). For each of the 14 cases, a list of triangle edges is created, and the triangle edge table is formed. Using the index, a list of all triangle edges and vertices is formed, noting that all vertices fall on a cube edge. The vertex locations are then linearly interpolated along each of the relevant cube edges.

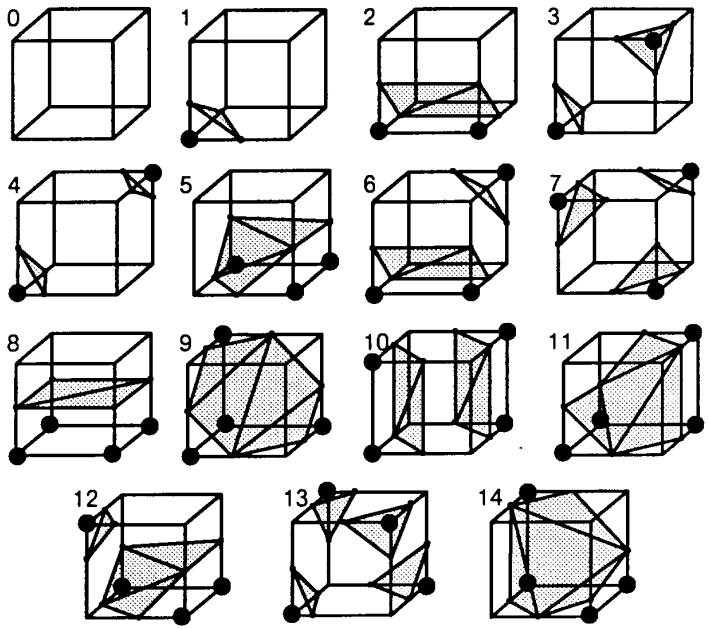

Figure 4.9 Triangulated Cubes (after Lorensen 1990)

The final step in the marching cubes algorithm calculates the unit normal of the iso-valued surface at each triangle vertex. This normal is used for rendering purposes, in particular, Gouraud-shaded images (Foley et al., 1990) rely on the existence of this normal. Rendering of the isosurface is still possible without this normal, using the flat shading model, but the calculation of this normal is computationally simple, and the use of Gouraud shading produces more realistic images. The calculation of surface normals at triangle vertices takes into account the fact that a surface of constant value has zero gradient along the surface tangential direction. As a result, the gradient vector is normal to the surface. Consequently, the calculation of the surface normal can be accomplished by calculating the gradient vector at the location in question. A simple method for calculating the gradients uses central differences to first calculate the gradient vectors at the cell vertices, then linearly interpolating along the cell edges to calculate the gradient vector at a triangle vertex. The gradient at each cell vertex can also be computed directly from the numerical analysis and linearly interpolated to the triangle vertices.

Another technique for calculating normals inserts each triangle into a mesh structure during the marching cubes procedure. This mesh structure contains connectivity information which can be used to

calculate vertex normals by averaging adjoining triangle normals. A benefit of using this mesh structure is the reduction in stored data since there is no duplication of common triangle vertices. This fact can be extremely important for large models on personal computers.

Unfortunately, the use of geometric primitives to fit measured or calculated data is seldom entirely successful. The marching cubes algorithm has the difficulty of resolving ambiguities at saddle points (see Figure 4.10) and this can result in incorrect tilings. Although work has been done to try and solve this ambiguity problem (Wilhelms and Van Gelder 1990) the issue has not been completely solved. The marching cubes algorithm, as with all surface-based techniques, requires binary classification of the

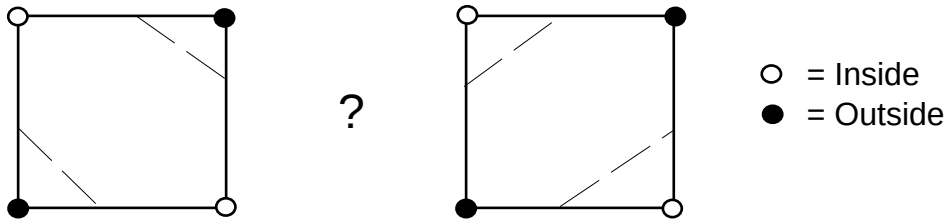

Figure 4.10 Saddle Point Ambiguity

data; either a surface passes through the voxel or it does not. In the presence of small or poorly defined features, error-free binary classification is often impossible. This results in visual artifacts in the final rendered image, specifically spurious surfaces and erroneous holes in the generated surface. Fortunately, the stress analysis and seismic datasets presented in this thesis are generally well defined, thus reducing the impact of these visual artifacts. Unlike medical imaging, where exact rendering of the data is crucial, the amount of acceptable error in the final rendered image is much more flexible in rock engineering. In most cases, the general trends of the data are of primary interest and the exact details are of less importance. This stems from the degree of confidence and accuracy either in the stress analysis input data (i.e. far field stresses, material properties), or in the case of seismic data, the technology used for gathering and interpreting the data.

An important consideration is the absence of data within the underground excavations. To account for this, modification of the algorithm to handle holes was made. The determination of grid

points within excavations is done prior to the analysis phase in order to speed up the stress analysis and to guarantee interpretation of valid results. The information of which grid points are inside excavations is readily available to the visualization system. The modification of the marching cubes algorithm entails using linear extrapolation to determine fictitious values at voxel corners just inside the excavations. This was done in just the voxels that intersected excavation boundaries (voxels with corners both inside and outside excavations). Once values are extrapolated at the interior cell vertices, the determination of the isosurface within these voxels proceeds as normal. The result of this extrapolation process is an isosurface that best illustrates the results close to the excavation surface. Voxels that are entirely within the excavation are flaged as such, and removed from the isosurface generation process, increasing the speed of the method.

The marching cubes algorithm has many advantages which make it particularly suitable for the visualization of mine datasets. In particular, the use of simple polygon geometric primitives allows for compact storage and efficient display. Currently, most three-dimensional graphics systems are engineered around the efficient display of polygons with some systems using special hardware to assist in rendering these polygons. This allows for interactive display and manipulation of the geometry, an extremely important quality in the visualization system, and is one of the main reasons for adopting the marching cubes algorithm in *Examine*^{3D} as the best method for visualizing and interpreting mine datasets.

4.4.3 Dividing Cubes

The dividing cubes algorithm, as with the marching cubes algorithm, belongs to the family of s*urface-based* techniques. While the marching cubes algorithm uses triangle primitives to reconstruct an iso-valued surface, the dividing cubes algorithm uses points with normals. The marching cubes algorithm is designed to be used with smaller datasets where the number of triangles generated is somewhat less than the number of pixels occupied by the image. Conversely, the dividing cubes algorithm is applicable for larger datasets, where the number of triangles approaches the number of

pixels. Since the stress analysis and seismic datasets are almost always small, this method has little application. The reader is referred to Lorensen (1990) and Cline (1988) for the details of the dividing cubes algorithm and its applications.

4.4.4 Direct Volume Rendering (DVR) Techniques

As previously mentioned, surface-based techniques have problems with surface detection when the data contains poorly defined or fuzzy features. Direct volume rendering (DVR) techniques get around this problem by eliminating the need for binary classification of the data. DVR techniques are a family of techniques which display the sampled data directly without first fitting geometric primitives to it. They assign color and opacity to each voxel, then form images by blending the semi-transparent, colored voxels that project onto the same pixel. Artifacts are reduced by negating the need for thresholding during classification.

Researchers at Pixar, Inc. seem to have been the first to apply direct volume rendering to scientific and medical volumetric data. Drebin et al. (1988) present a method which assumes that the measured data consists of several different materials and computes the occupancy fractions of each material in each voxel. Using these fractions and the color and opacity control parameters for each material, the calculation of color and opacity is performed for each voxel. Each slice of voxels is then projected on to the image plane and blended together with the projection formed by previous slices.

Levoy's algorithm (1988, 1989, 1990) is similar to the approach of Drebin et al. but computes colors and opacities directly from the scalar value of each voxel and renders the three-dimensional volume grid in image order using ray tracing (Foley et al., 1990). Image order methods scan the display screen to determine, for each pixel, the voxels (grid cells) which affect it.

Conversely, object order techniques, where the list of voxels is traversed to determine which pixels are affected, are also quite common. Westover (1989, 1990) has proposed a method which

operates entirely in object order by transforming each voxel to image space, performing shading to determine color and opacity, and blending the two-dimensional footprint into the image array.

The major drawback associated with DVR methods is the tremendous computational expense. The essential requirement for a user to quickly and interactively visualize a stress analysis or seismic dataset can not be stressed enough. Although this ability is possible with surface based techniques, the same cannot be said of DVR techniques on today's PC platforms.

Another point in favor of surface-based techniques is that most graphics systems can easily handle the rendering of polygons, with some systems providing assistance with specialized hardware. This provides the necessary speed and interaction required for a visualization system. In fact, the graphics system HOOPS™, used for the visualization system of this thesis, is based entirely on polygonal graphic primitives, with little support at the pixel level. This makes the addition of DVR methods quite difficult.

The final consideration is that surface techniques work very well in the visualization of stress and seismic datasets. In both cases, there is no fuzziness to the data, features are generally well defined and the binary classification of the data is not a problem. For these reasons, DVR techniques are not currently employed in the visualization of datasets presented in this thesis and will not be covered in further detail. The reader is refereed to the above references for more information on the implementation of DVR methods.

4.4.5 Trajectory Ribbons

Trajectory ribbons are a convenient method for visualizing the flow of stress around underground openings and are used to gain insight into the spatial change in principal stress direction due to the excavations. This method was formulated by the author as a technique for providing the mining and civil engineers the ability to understand the effect that any underground opening could have on the complete

stress field. The engineer can then quickly understand the effect that any new opening would have on the stress field and be able to design accordingly.

The basis of this method lies in the visualization of vector fields associated with steady state fluid flow (Helman and Hesselink, 1990; Globus et al., 1991; Kenwright and Mallinson, 1992; Hulquist 1992) . In the case of stress analysis datasets, a stress tensor is computed at every point on a uniform grid. This tensor has up to three principal stresses and three principal stress directions. Each principal stress and its direction is orthogonal to the other principal stresses. Therefore, at each grid point, three vectors define the directions and magnitudes of the three principal stresses. By focusing on the major principal stress vector, a discretely sampled vector field *F*, which represents a continually varying major principal stress vector, can be visualized by computing and displaying the integral curves through the field. For any cell, the trajectory ribbon (parameterized by t) can be represented as $\mathbf{X}(t)=\{x(t),y(t),z(t)\}$ which is the solution to the first order differential equation:

$$\frac{dX}{dt} = F(X(t))$$

with the initial condition $X_o=X(t_o)$.

To solve this equation, a fourth order Runge-Kutta method with adaptive step size (Δt) control (Press et al., 1989; Hornbeck, 1975) is used within each grid cell. Each of the six distinct components of the stress tensor at the eight corners of the grid are used to tri-linearly interpolate a new tensor at any location within the cell (section 4.3.2). An eigenvector/eigenvalue analysis is then done on the interpolated stress tensor to calculate the major principal stress vector.

Alternatively, the principal stress vector at each of the eight corners can be used to interpolate a new vector within a grid cell. This method is much faster since only three components of the vector are interpolated and no eigenvector/eigenvalue analysis needs be performed. Both methods produce acceptable results in most situations but studies by the author indicate that under conditions of high stress gradient, interpolation of the stress tensor yields better results than using the principal stress vector

approach. This is especially true in regions close to excavations, where the stress gradient is high and there is a great deal of rotation in the principal stresses.

The process of creating the trajectory ribbon starts by first defining the initial seed point within the rock mass. The Runge-Kutta method is then used to determine a new point along the integral curve. This new point is connected to the initial point by a ribbon. The orientation of the ribbon at each interval is such that the normal to the ribbon represents the direction of the minor principal stress and the direction associated with the in plane width is the direction of the intermediate principal stress (Figure 4.11). The color of the ribbon corresponds to the magnitude of the major principal stress. The width of the ribbon is a constant and the ribbon fragment is split into two planar triangles. Since this method proceeds stepwise, it is a straight-forward process to pass from one cell to an adjoining cell. This process continues until the ribbon intersects the bounds of the entire grid. Two examples of trajectory ribbons and their application can be found in section 5.1.1.2, Figure 5.9 and Figure 5.10.

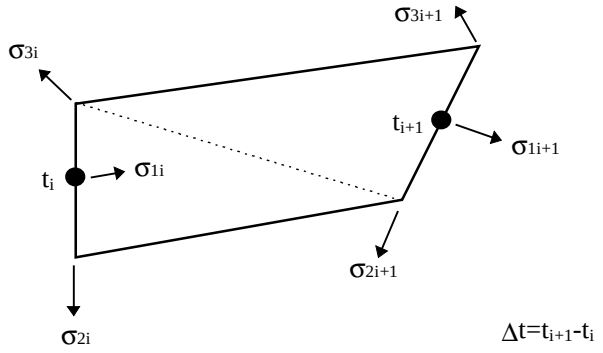

Figure 4.11 Trajectory ribbon fragment

Concurrently and independently, research by Delmarcelle and Hesselink (1992) resulted in a very similar visualization technique called hyperstreamlines. Although the method is similar in determining the integral curve through the principal stress vector field, it uses a different method for actually displaying the results. Instead of a ribbon, the technique uses a trajectory tube with an elliptical in

cross-section, with the orientation and length of the major and minor axes of the ellipse corresponding to the magnitude and direction of the intermediate and minor principal stresses. This method has the advantage that relative magnitudes of the intermediate and minor stresses can also be visualized, unlike trajectory ribbons. The advantage of the ribbons is that they are simpler for the interpretation of stress flow in the vicinity of a complex system of excavations. For this reason the ribbons have been maintained as the visualization technique for illustrating stress flow.

5. VISUALIZATION OF MINE DATASETS

This chapter presents an overview of rock engineering datasets of importance in the design of underground excavations in rock. The author presents, in particular, datasets which result from the numerical modeling of stresses and displacements around these excavations as well as the corresponding seismic activity which results from these excavations.

This chapter will also deal with the techniques that, when used in numerous case studies, provided the best results for the interpretation of stress analysis and microseismic data. The emphasis will be on the advantages and disadvantages of each method, along with a guide for helping the practicing engineer choose when to employ each technique.

5.1 Three-dimensional Stress Analysis Datasets

The three-dimensional stress analysis around an underground excavation yields information on the stress state, strain and displacements at certain points within the rock mass. Using the direct boundary element program developed by Shah (1993), stress and displacement information can be accurately calculated at any user prescribed location. This is unlike the finite element method where the mesh defines where displacements and stresses are calculated. For locations other than those used in the formulation of the element, i.e. nodes and gauss points, the values must be interpolated.

Another important consideration is the type of constitutive relations used for the rock in the analysis. Unlike an elastic analysis, a plasticity analysis yields information on the yielding and progressive failure of the rock. The difficulty with a plasticity analysis is to accurately calculate the rock's constitutive parameters. Without a sound knowledge of these parameters, the results of such an analysis may be questionable.

For the purpose of this thesis, only elastic stress analysis datasets generated from the boundary element method, and in particular those from the implementation of Shah (1993), will be considered. As

a result, subsequent sections on stress analysis data will only deal with the datasets which can be produced by a three-dimensional elastic stress analysis.

5.1.1 Stress Data

At each point, the stress state consists of a stress tensor defined as a 3X3 matrix of compressional and shear stresses aligned with some global coordinate system. Generally, the convention in rock engineering is such that the stresses are defined in terms of a x,y,z cartesian coordinate system with compressional stresses being positive. In matrix form they may be written as:

$$\sigma_{ij} = \begin{bmatrix} \sigma_{xx} & \sigma_{xy} & \sigma_{xz} \\ \sigma_{yx} & \sigma_{yy} & \sigma_{yz} \\ \sigma_{zx} & \sigma_{zy} & \sigma_{zz} \end{bmatrix}$$

As a result of equilibrium requirements, the matrix is symmetric and $\sigma_{ij}=\sigma_{ji}$. The eigenvalues and eigenvectors of this matrix correspond to principal stresses and their corresponding directions. The principal stress space, by definition, is one in which there are not any off diagonal shear stress terms and the diagonal terms represent the minimum intermediate and maximum stresses. The maximum shear stress can be calculated using the equation:

$$\tau_{\max} = \frac{\sigma_1 - \sigma_3}{2}$$

where τ_{max} is the maximum shear stress, σ_1 is the maximum or major principal stress and σ_3 is the minimum or minor principal stress. A more extensive review on stress tensors can be found in Brady and Brown (1985), or Frederick and Chang (1965).

5.1.1.1 Visualization of Scalar Stress Data

The visualization of stress tensor data has historically taken the form of displaying one of the scalar components of the stress tensor, principal stresses, or maximum shear stress by contouring discrete data on a user-defined cutting plane. Figure 5.1 is an example of this type of technique.

As can be seen in Figure 5.1, this method provides a great deal of information about the

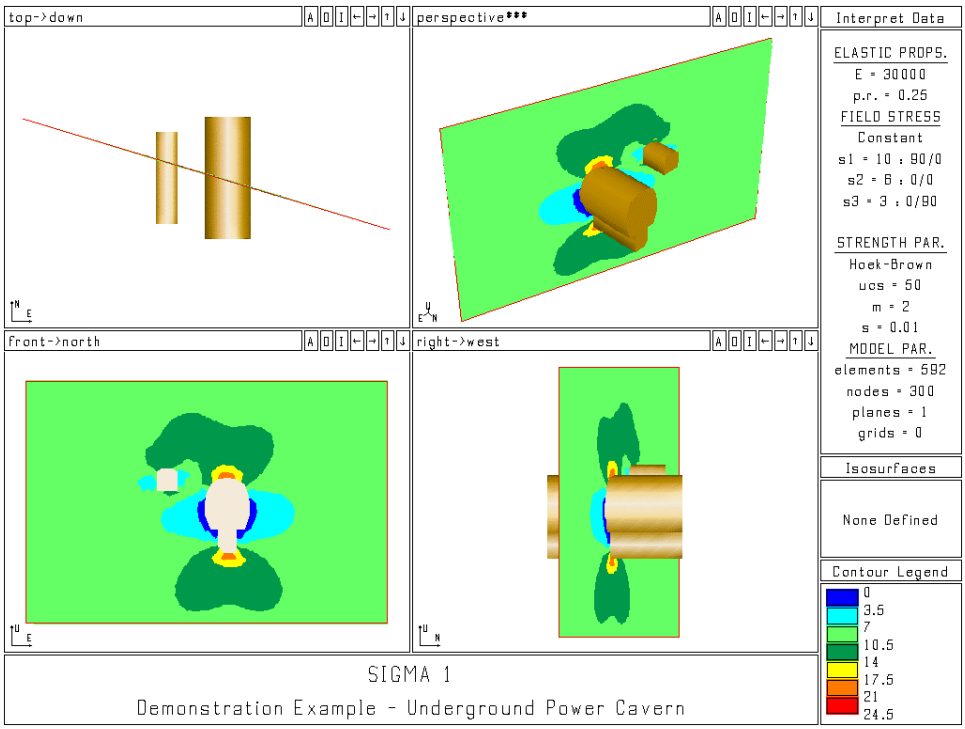

Figure 5.1 Principal stress (MPa) contoured on a cutting plane

distribution of stress locally to the cutting plane and is very easy to interpret. The ease with which the engineer can understand the data is the major reason for using this type of graphical display of data and why it is now so common in current software systems. Unfortunately, this type of display provides little insight into the global distribution of stress around the excavation. The stress state is well defined on the cutting plane, but how does the stress change away from the cutting plane? To answer this question, the engineer must either define more cutting planes and redo the analysis, or make a guess. Since redoing

the analysis can be a time consuming proposition, more often than not, the engineer ends up making an educated guess as to the stress state away from the cutting plane. Neither of these alternatives is an optimal solution.

There are two methods which have been shown to be successful in the visualization of the global

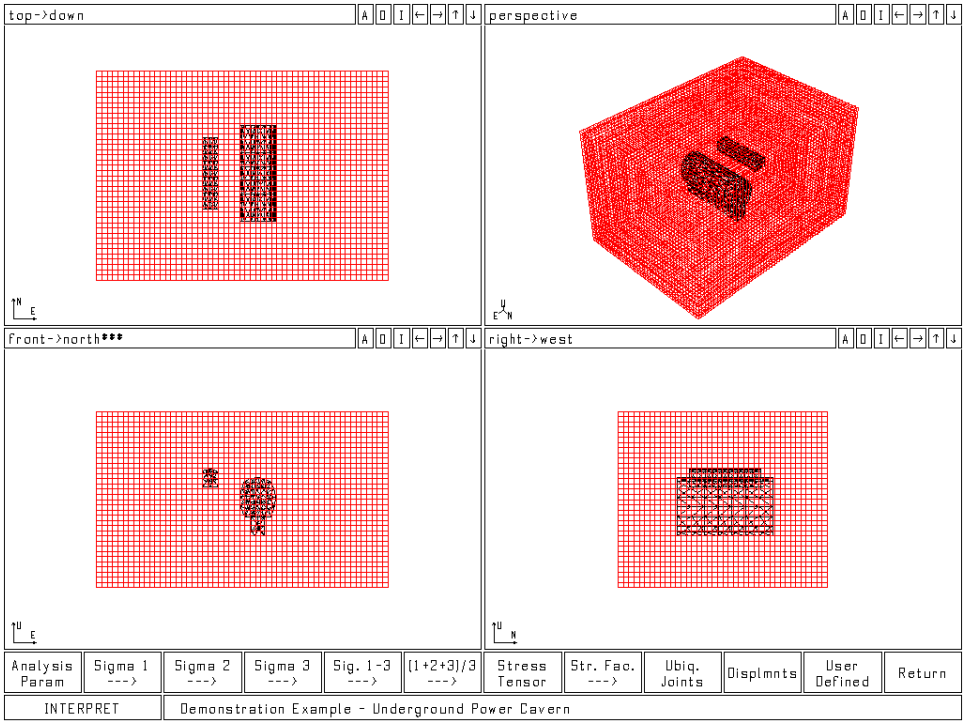

Figure 5.2 Three-dimensional grid of data

stress state. Both methods rely on the data being in structured uniform grid format (see chapter 4) rather than the two-dimensional cutting plane. The three-dimensional grid encompasses the volume of rock in which the stresses are sought as seen in Figure 5.2.

The first method, which is an extension of the two-dimensional cutting plane, works by passing a two-dimensional contoured cutting plane, in real-time, through the grid. As the cutting plane proceeds through the grid, the stress contours are updated on the plane (Figure 5.3).

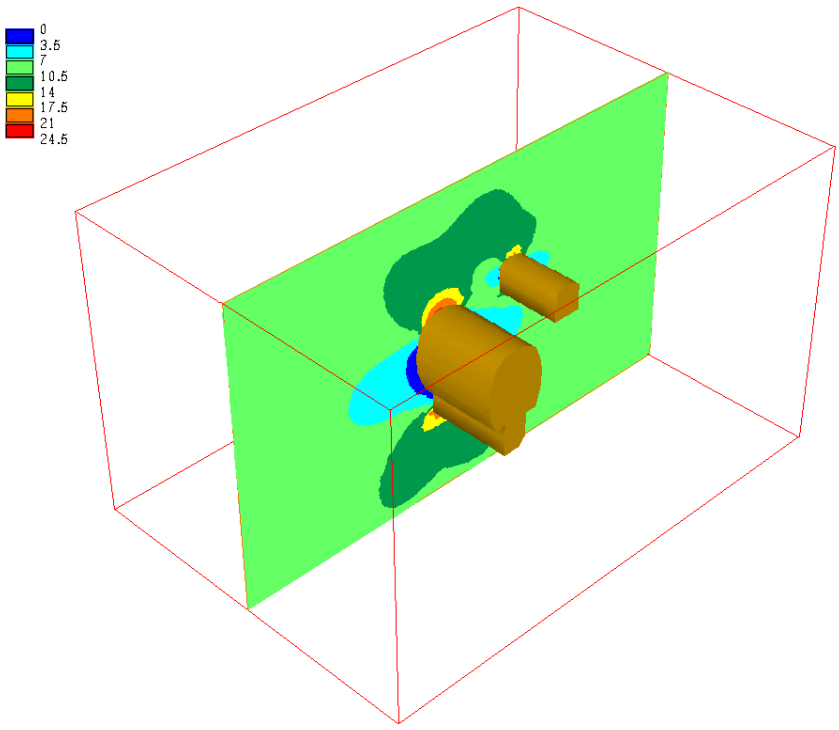

Figure 5.3 Cutting plane sweeping through a three-dimensional grid

The direction in which the plane passes can be changed giving a three-dimension perspective on how the stress state varies (Figure 5.4).

One advantage of this technique is that most engineers have experience interpreting data on two-dimensional planes and, as a consequence, have little trouble in understanding the results using this method. Another advantage is that the visualization and data interpretation phase of the analysis is a one-step process. The engineer need not go back and perform another analysis to obtain the stress state in another location, since data now exists throughout the zone of interest. More computational time is required to do the initial analysis, but this is not a serious factor in most situations since the analysis for the average mine or civil engineering structure can be performed overnight on a desktop computer. In fact, this method tends to save the amount of work the engineer has to do in the long run because the visualization process is much quicker.

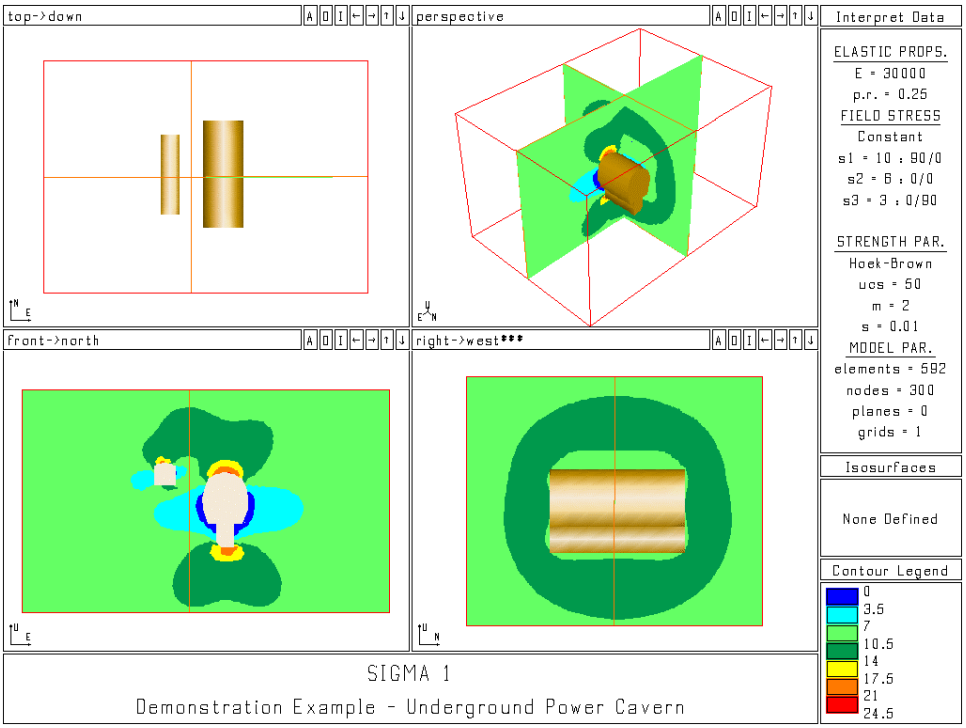

Figure 5.4 Multiple cutting planes sweeping through three-dimensional grid

The second method for volume visualization of stress data uses the marching cubes algorithm (see section 4.4.2) to generate isosurfaces of stress. These isosurfaces are the three-dimensional equivalent to a two-dimensional contour. Every point on the three-dimensional surface has one distinct value of stress. Inside this surface, the rock has a higher stress while outside the surface the stress is smaller. Figure 5.5 illustrates the use of two isosurfaces to view the global behavior of the major principal stress. From Figure 5.5, it becomes quite evident that the use of multiple isosurfaces can be quite confusing since they tend to hide the underlying geometry and conflict with each other. To help, transparency is used so that underlying geometry becomes partially visible (Figure 5.6).

Isosurfaces are inherently confusing to those who are inexperienced in looking at them. It takes time and patience to both understand and appreciate the information gained by using isosurfaces. The use of animation, the ability for the user to quickly turn and reference the model from any angle, is also extremely important. Even to the trained eye, the spatial distribution of the geometry and isosurfaces may

be hard to distinguish. This brings up a very important point concerning the presentation of results from an analysis

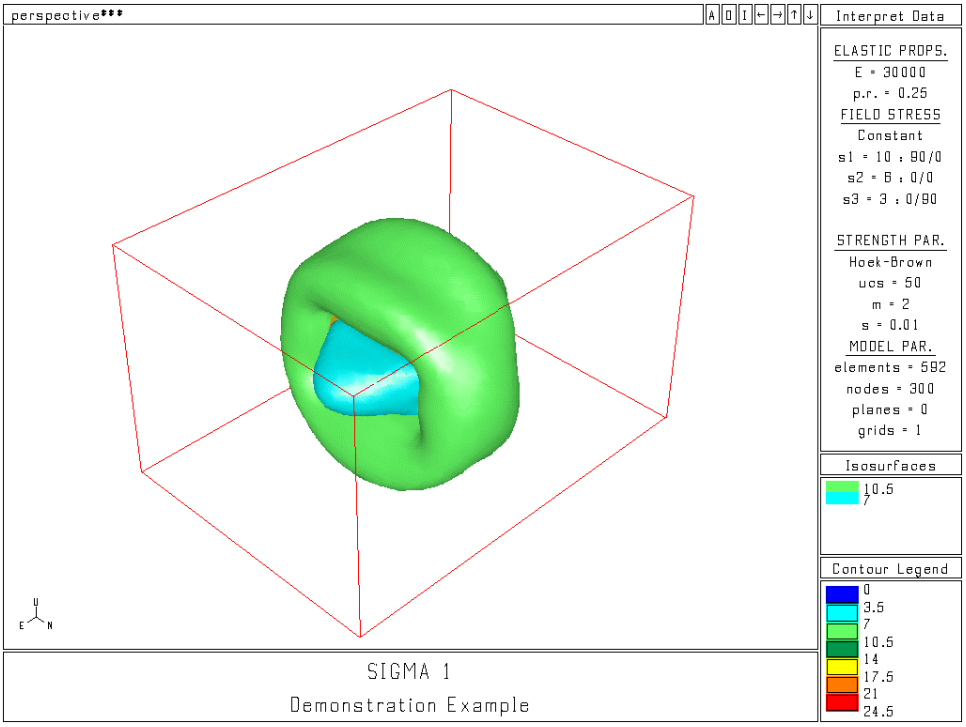

Figure 5.5 Isosurfaces of major principal stress (MPa)

Although isosurfaces are very useful to the engineer for the purpose of understanding the data, they may be confusing when placed in a report. As a result, the two-dimensional contouring techniques tend to be more accepted for this purpose.

Both contouring on a cutting plane and isosurfaces play a very important part in the visualization process. Contouring provides a great deal of information on the spatial distribution of stress locally but gives little insight into the global behavior. Isosurfaces give this global behavior but do not yield as much information locally and can be harder to interpret. As a result, a combination of both yields the best visualization process for scalar stress data.

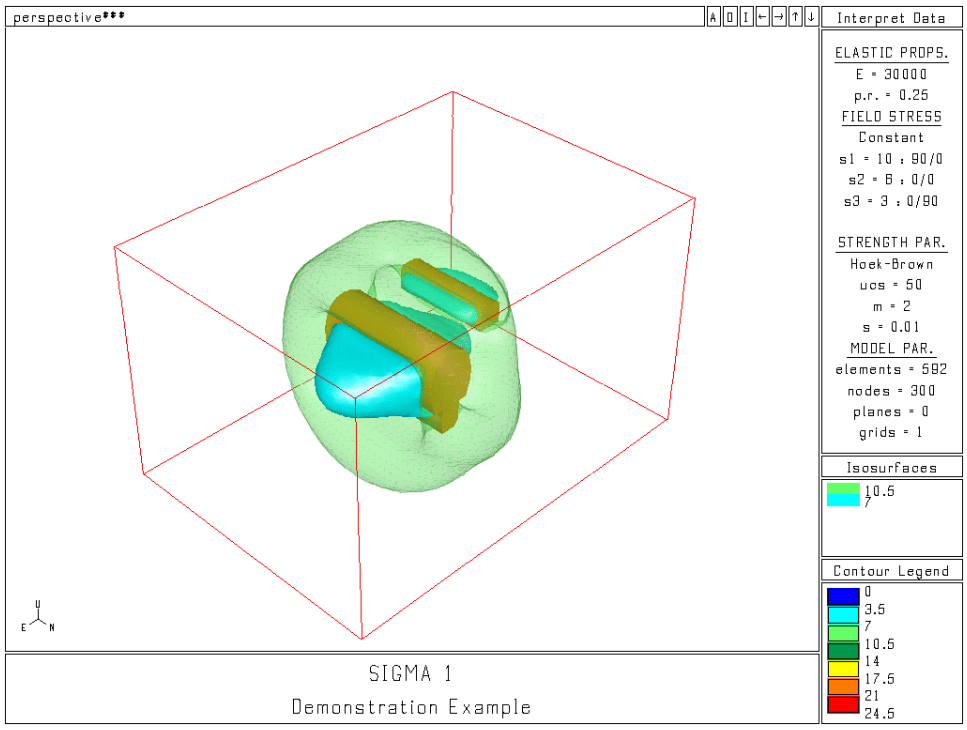

Figure 5.6 Isosurfaces of major principal stress (MPa) with transparency

The boundary element analysis performed by Shah (1993) also generates accurate values of stress at every node on the excavation surface (Figure 5.7). This information is of great importance since the engineer is generally interested in the state of stress right at the excavation/rock-mass interface for the purpose of estimating instability. As a result, the visualization of this data becomes crucial. The technique used is a simple contouring of the data on the surface of the excavation using the same method as that for a two-dimensional cutting plane. Depending on the hardware platform, either the triangle decimation contouring algorithm or the color interpolation algorithm is used. The reader is referred to chapter 4 for more information on the implementation of these algorithms.

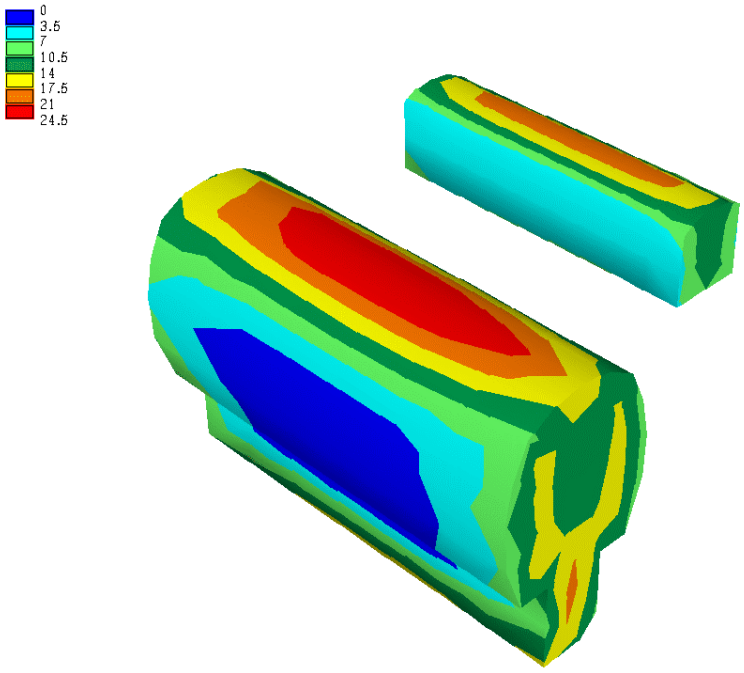

Figure 5.7 Surface major principal stress (MPa) contours

5.1.1.2 Visualization of Tensor Stress Data

The preceding section focused on the visualization of both the scalar components of the stress tensor and principal stresses. Although the visualization of the scalar components gives a great deal of information about the stress state around an excavation, a more general visualization of the spatial variability of the complete stress tensor can yield even more information. In particular, it would be beneficial to visualize the directional component of stress around the excavations.

Two methods have been adopted for exhibiting the directional variability of the stress field around underground openings. The first method uses the concept of stress trajectory ribbons to map spatial flow of stress around the excavations, while the second method uses tensor glyphs, rendered at the grid locations, to display the magnitude and direction of the principal stresses.

To visualize the spatial variability of the stresses using stress trajectory ribbons, the stress tensor calculated at every grid point is first rotated into its principal stress space by doing an eigenvector calculation. This produces three orthogonal vectors, corresponding to the three principal stresses (eigenvalues) and their directions (eigenvectors), at every grid point within the rock mass. Special cases of hydrostatic stress, which means fewer than three principal stresses, are also accounted for. If the major principal stress vector is the only component considered, the result is a vector field defined by discrete samples at the grid points. Using the analogy of the flow of fluid, where the use of streamlines map the movement of a tracer particle around some object, the flow of stress around the excavations can also be displayed. In two-dimensions, Hoek and Brown (1980) used principal stress trajectory plots to show the orientation of the principal stresses and the flow of stress around excavations (Figure 5.8). In three-dimensions, the same technique used to calculate fluid flow streamlines can be used to calculate major principal stress ribbons.

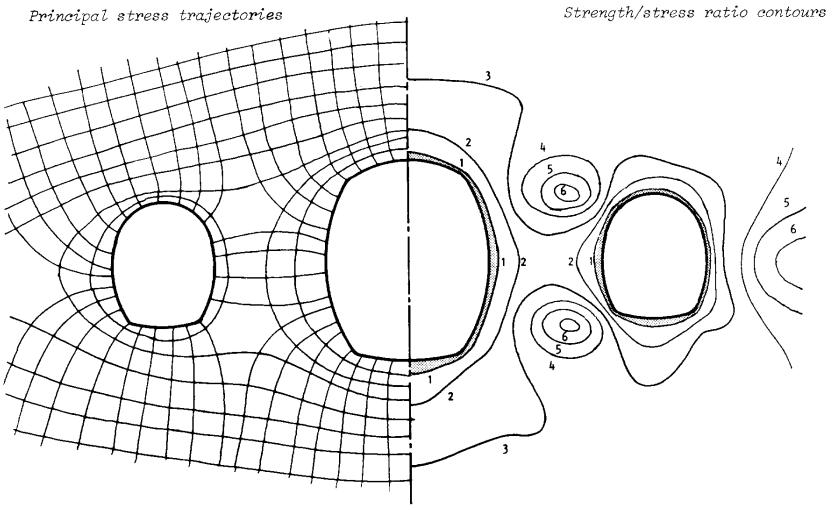

Figure 123 : Principal stress trajectories and strength/stress contours around the revised excavation layout.

Figure 5.8 Principal stress trajectories in two-dimensions (from Hoek and Brown 1980)

As described in section 4.4.5, a fourth order Runge-Kutta solution to the first order differential equation defining the major principal stress vector field is calculated using an initial seed point within the rock mass. Practically, a seed point is defined within the rock mass and from this a path (streamline or ribbon) is rendered which shows the flow of stress through the rock mass. In areas where there is no unique direction for the major principal stress (e.g. hydrostatic), the ribbon is terminated. Using a series of seed points, it becomes possible to visualize the influence of the excavations on the flow of stress in the rock mass. Figure 5.9 and Figure 5.10 illustrate the use of stress ribbons to visualize the flow of stress around underground openings.

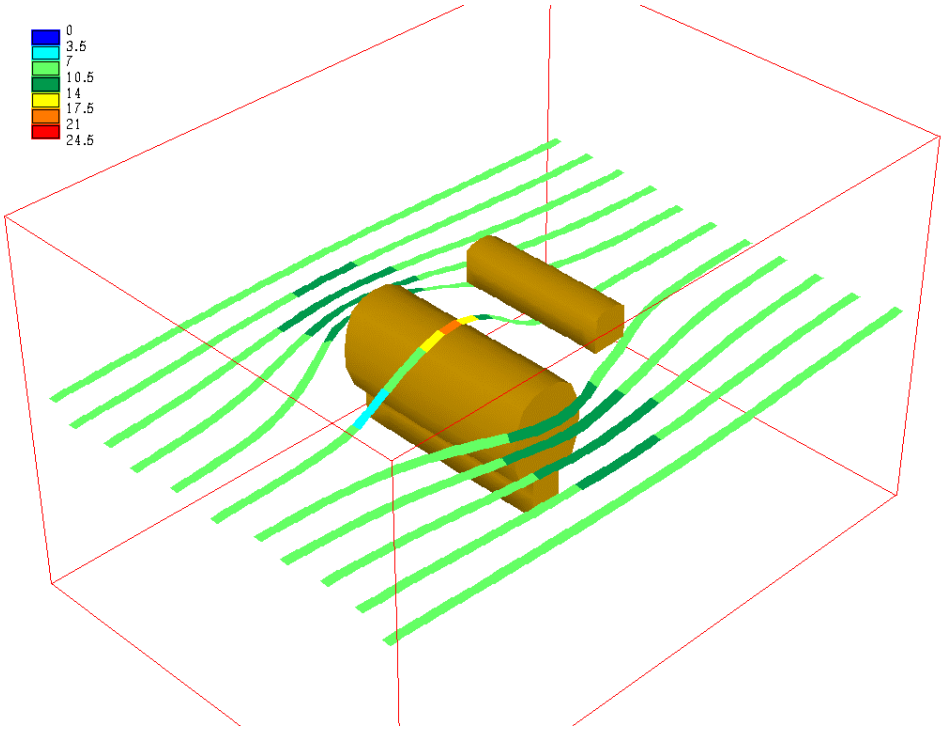

Figure 5.9 Trajectory ribbons showing stress flow around two excavations

In these figures, the seed points were defined along a discrete line segment, or "raker", at equidistant intervals. The use of a raker for defining a series of seed points has proven to yield the best results for visualization of the data using stress trajectory ribbons. Note the color and twist of the ribbons in Figure 5.9 and Figure 5.10. The color of the ribbon represents the magnitude of the major principal

stress. The twist of the ribbon is an indication of the directions of the minor and intermediate principal

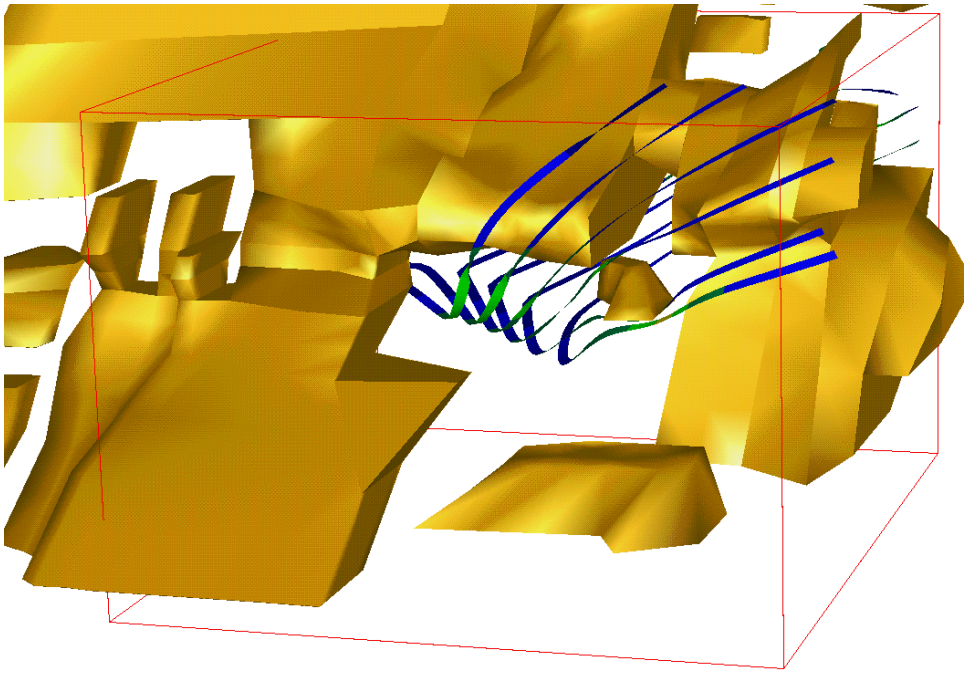

Figure 5.10 Stress (MPa) trajectory ribbons showing stress flow through a pillar

stress. In the plane of the ribbon, the path in which the ribbon propagates is the direction of the major principal stress. Perpendicular to this direction, in the direction of the ribbon width, is the direction of the intermediate principal stress. The minor principal stress direction is normal to the plane of the ribbon. This makes the visualization of the rotation of the principal stresses trivial since the twist of the ribbon is a direct indication of the stress rotation within the rock mass.

The use of stress trajectory ribbons as a visualization technique has found its application in the fundamental understanding of how the stress flows around openings and through pillars. Figure 5.9 illustrates how stress flows around the ends of the two excavations, except in the middle where it flows over the top. Only in the middle are the effects of the excavation ends minimized. Thus, the outcome of a plane strain two-dimensional analysis of a vertical slice through the middle of the excavations would yield good results. Figure 5.10 shows an important ore bearing pillar at the Falconbridge Strathcona mine in Sudbury, Ontario. During the mining of this pillar, a great deal of seismic activity and

rockbursting occurred. From the flow of the ribbons in Figure 5.10, the reason for this is quite clear; the

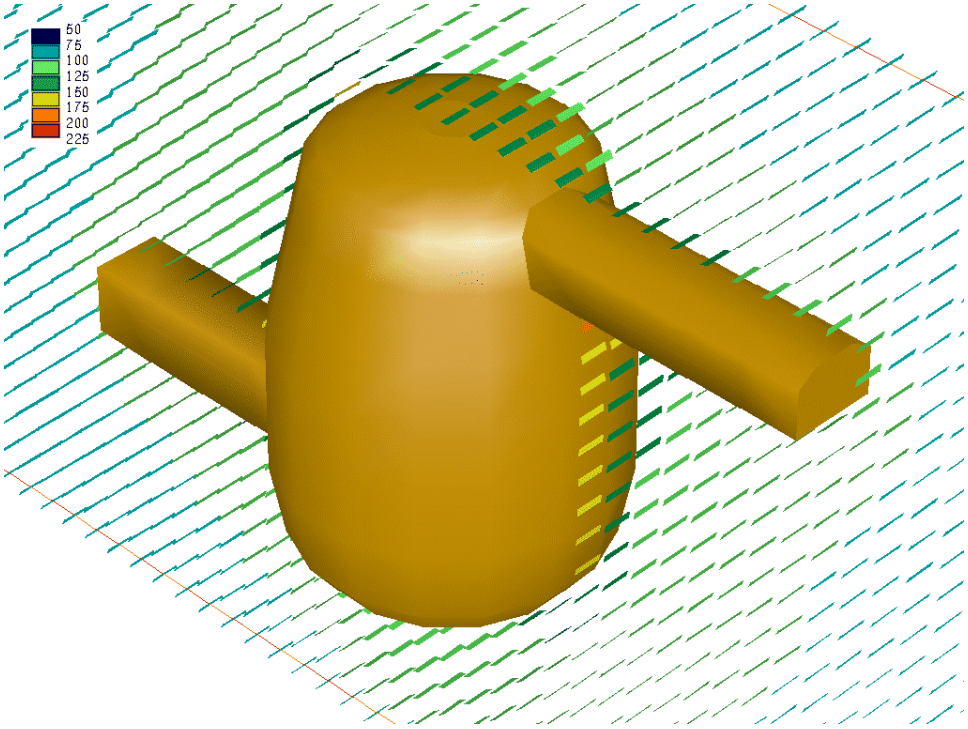

Figure 5.11 Stress tensor glyphs (plates) around the neutrino observatory cavern

pillar being mined provides a conduit for the flow of stress in this region of the mine. Consequently, the information on the flow of stress using stress trajectory ribbons can be a valuable tool for the determination of possible burst-prone ground in future mining. Further examples of the application of stress ribbons to the interpretation of stress flow around underground excavations can be found in Grabinsky (1992).

Historically, the direction of principal stresses in a region around underground openings have been viewed using glyphs. The glyphs are three-dimensional graphic symbols which convey one or more of the principal stress directions. Magnitudes of the principal stresses can also be shown by coloring the glyphs according to the color scale used for contouring. Figure 5.11 illustrates the use of tensor glyphs to visualize the direction of the principal stresses and the magnitude of the major principal stress around the underground neutrino observatory cavern in Sudbury, Ontario. In the case of Figure 5.11, the glyphs are plates oriented to the direction of the principal stresses and colored according to the

magnitude of the major principal stress. The long direction of the plate is aligned with the direction of the major principal stress, while the intermediate principal stress is aligned with the short direction and the minor principal stress direction is normal to the plate. In Figure 5.12, an arrow glyph is used instead of the plate. The arrow points in the direction of the major principal stress and the cross-section of the glyph is an ellipse whose major and minor axes are oriented in the direction of the intermediate and minor principal stress directions respectively.

The availability of different glyphs is important to the visualization process because it provides

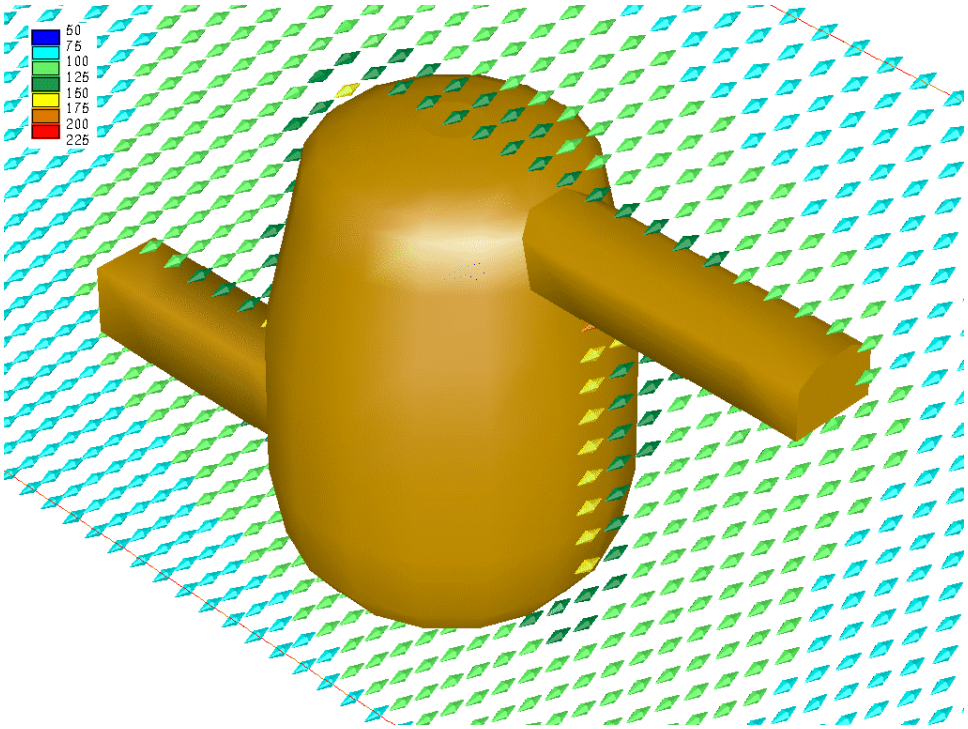

Figure 5.12 Stress tensor glyphs (arrows) around the neutrino observatory cavern

flexibility for the proper interpretation of the data by the user of the visualization system. Feedback from users has indicated that there is no unique preference in the type of glyph. The author therefore concludes that the type of glyph which yields the best interpretation of a dataset is dependent on the dataset itself and the model parameters of the particular problem being considered.

5.1.2 Displacement Data

Along with a stress tensor, a displacement vector may also be calculated at any discrete point within the rock mass. The scalar magnitude and direction of the displacement vector is of primary interest to the rock mechanics engineer. Data from insitu extensometer and closure measurements can be used to help validate the modeling results. However, it must be remembered that the displacement results presented here are based on linear elasticity. The displacements due to non-linear yielding of the rock mass are not included. These non-linear displacements in many situations can be much greater than the elastic displacements, making correlation with field data very difficult.

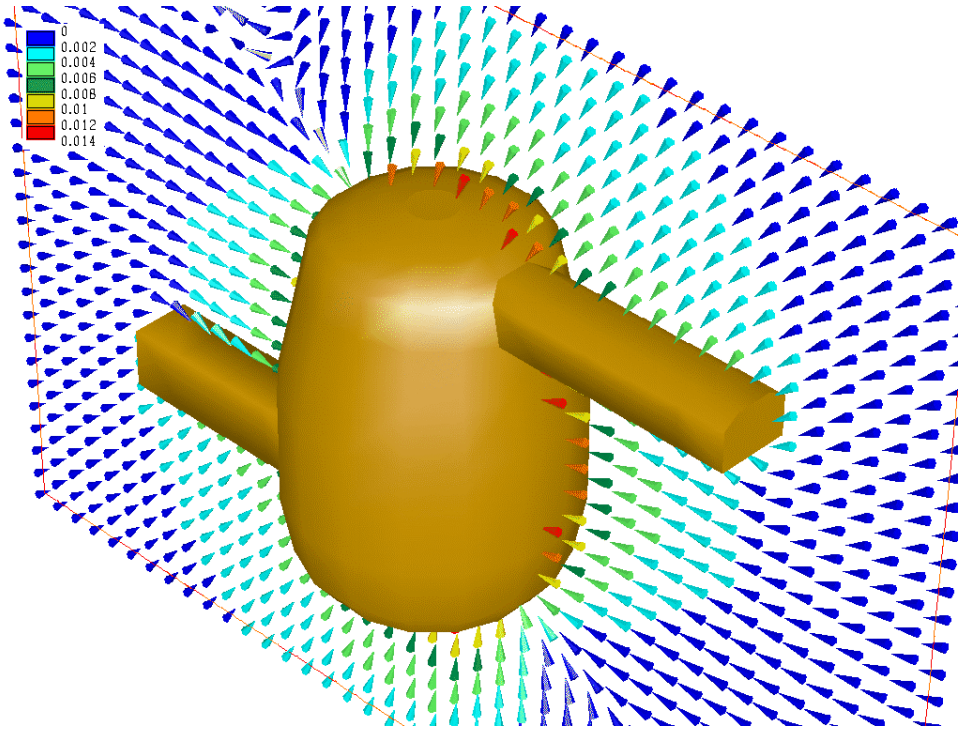

Figure 5.13 Displacement glyphs around Sudbury neutrino observatory

To visualize the scalar magnitude of total displacement or the magnitude of one of the three vector components, the techniques employed in the previous section are utilized. To look at the closure of the excavation walls, surface contours are used. Within the rock mass, cutting planes and isosurfaces

are used to examine displacement. To look at the displacement direction within the rock mass, displacement glyphs as shown in Figure 5.13 are used.

5.1.3 Strength Factor

Of utmost importance to the practicing engineer is the determination of the strength factor distribution within the rock mass. Also known as factor of safety, the definition of strength factor is simply a calculated value which measures how close the rock is to failing. The method for calculating this value is far from standardized and differs widely within the rock mechanics community. The first step in determining the strength factor is the definition of a failure criterion for the rock mass. The most common failure criterion in rock mechanics defines functions which represent the relationship between the principal stresses at failure or, more commonly, just the major and minor principal stresses. These functions also include a set of material parameters specific to the type of rock being analyzed. It is beyond the scope of this thesis to present a treatise on rock mass failure criteria (see Hoek et al. 1995); only the two most commonly used failure criteria will be defined.

The simplest and best-known failure criterion for rocks is the Mohr-Coulomb criterion. In principal stress space it is written as:

$$\sigma_{1f} = q + \sigma_3 \tan^2\left(45 + \phi/2\right)$$

σ_{1f} = major principal stress at failure
σ_3 = minor principal stress
q = unconfined compressive strength = 2c tan$(45 + \phi/2)$
c = rock mass cohesion
ϕ = rock mass friction angle

Although simple, the practical estimation of the rock mass material parameters c and ϕ can be difficult. As well, the linear relationship between σ_{1f} and σ_3 may not accurately describe the rock mass behavior, especially at low values of the minor principal stress. A more accurate and practical criterion is the empirical Hoek-Brown failure criteria defined as:

$$\sigma_{1f} = \sigma_3 + \sqrt{m\sigma_c\sigma_3 + s\sigma_c^2}$$

σ_{1f} = major principal stress at failure
m, s = material constants
σ_3 = minor principal stress
σ_c = uniaxial compressive strength of intact rock

Once the definition of the failure criterion has been established, the strength factor at a point within the rock mass can be calculated using the current stress state at that point. One of the most common methods for determining the strength factor first uses a failure criterion to determine the maximum principal stress which would fail the rock for the current insitu minimum principal stress. Then by taking the ratio between this maximum principal stress at failure and the actual insitu major principal stress, the factor of safety is calculated. This method can be written in functional form as:

$$S.F. = \frac{\sigma_{1f}}{\sigma_1}$$

$S.F.$ = strength factor
σ_{1f} = major principal stress at failure for the insitu σ_3
σ_1 = insitu major principal stress

Another method, developed by E. Hoek, J. Carvalho and M. Diederichs for use in numerical modeling programs, uses a shear strength/shear stress ratio to determine the strength factor:

$$S.F. = \frac{S_{max}}{S}$$

$S.F.$ = strength factor

S_{max} = shear stress at failure for the confining pressure $\frac{\sigma_1+\sigma_3}{2}$

S = current insitu maximum shear stress = $\frac{\sigma_1-\sigma_3}{2}$

The underlying principle of this method is that shear stress drives failure and the strength factor should represent this idea. Figure 5.14 presents the definition of S and S_{max} in graphical form.

Utilizing the above method, a scalar strength factor value is calculated at each grid point within the rock mass. The same techniques which are used to visualize scalar stress data are employed in visualizing strength factor data. Figure 5.15 shows the geometry used in the analysis of an underground powerhouse. The analysis includes the power cavern, transformer galleries, bus tunnels, and penstocks, and was done for the purpose of estimating the stability of the rock around the structure.

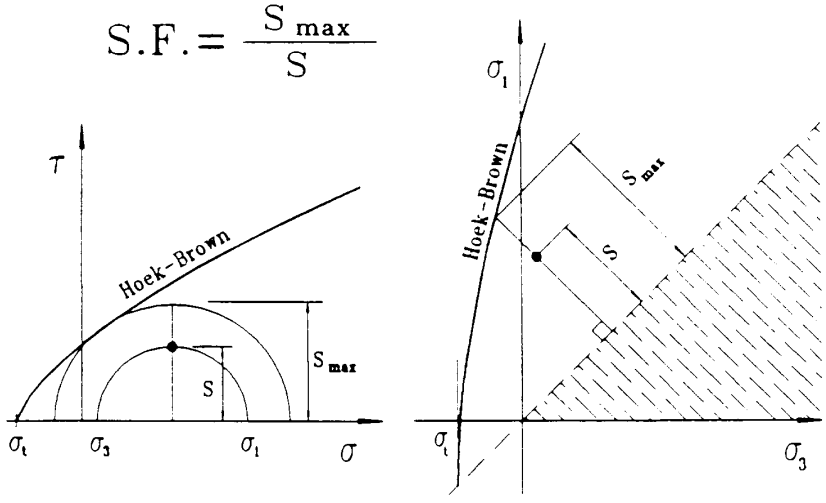

Figure 5.14 Strength factor definition

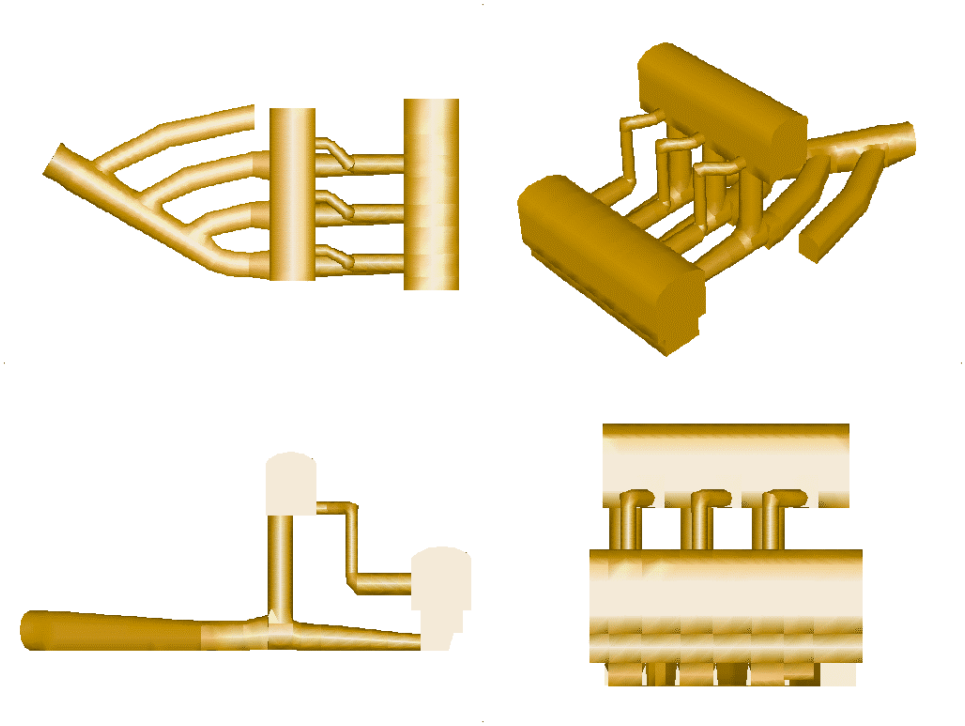

Figure 5.15 Geometry used in the analysis of an underground powerhouse

The outcome of this analysis are presented in Figure 5.16. Regions within the rock mass with strength factors less than 1.0 represent zones of possible instability. These regions are important to the rock mechanics engineer as they represent locations where support (rock bolts, shotcrete) might be needed. Using isosurfaces, the possible locations of instability are quickly determined. The use of isosurfaces is the preferable technique for interpreting strength factor data because the zones of possible instability are quickly visible.

Cutting planes, on the other hand, do not give a good indication of the total amount of instability around the entire structure. As a result, numerous cutting planes are necessary to estimate the extent of the zones of instability. This makes the process very tedious and impractical for the engineer interpreting the outcome of the analysis.

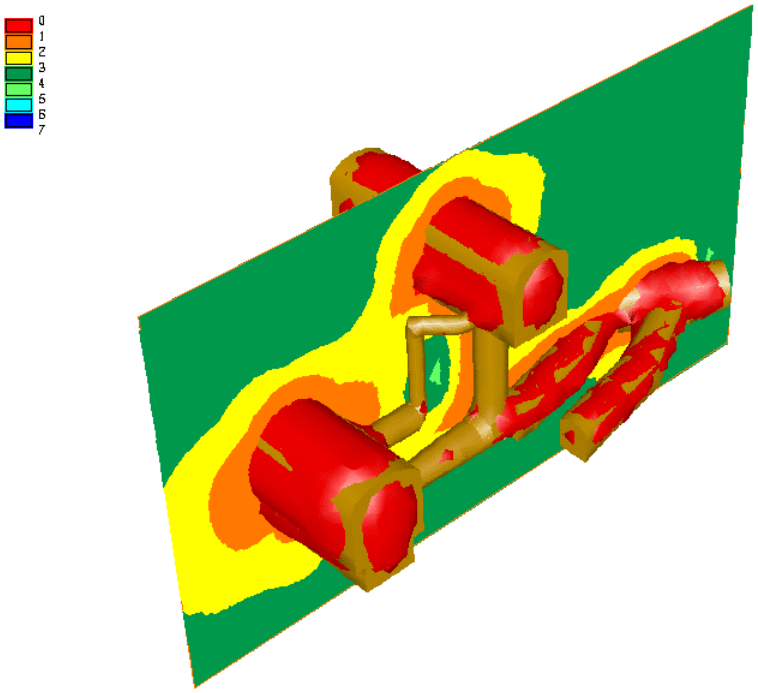

Figure 5.16 Strength factor results around an underground powerhouse

5.2 Seismic Datasets

Rockbursts and mining-induced seismicity are generally associated with deep level mining in highly stressed rock. In Canada, where mining is now being extended to greater depths, these seismic-induced events have increasingly serious social/economic consequences. A tragic incident in 1984, when four miners were killed from a Richter 3.5 rockburst at a hard rock mine in Sudbury, serves to highlight this point. In addition to safety, major losses in production can result from rockbursts in critical production areas.

In order to locate and monitor these seismic events, automatic multichannel monitoring systems are routinely used in mines around the world. Networks of sensors, installed in various locations throughout a mine, detect the arrival times of P waves generated by seismic events. Using these arrival times, the location of a microseismic event (source location) can be determined. The P-wave amplitude

is used to determine the energy magnitude of the event. The temporal and spatial distribution of the seismic events, along with the distribution of energy being released via seismicity, provide important tools for the determination of future mining patterns. As a result, the seismic data visualization and interpretation system becomes an important component in both mine planning and safety. Since stress analysis is also becoming an increasingly important tool for mine planning, combining the seismic and stress analysis visualization and interpretation systems could prove to be a very powerful tool for the mining engineer.

5.2.1 Event Locations

The visualization of the spatial distribution of microseismic events is very important, as stated in the previous section. To visualize the spatial distribution of discrete events, it is simply a matter of displaying the source locations with the stress analysis geometry and/or geometry obtained from another source (i.e., CAD data from mine planning). The use of stope geometry is important in understanding the spatial distribution of events due to mining. The temporal visualization of the microseismicity as the ore body is being mined will also augment the data interpretation process. Figure 5.17 represents the mined stopes at the Placer Dome Campbell mine in Red Lake, Ontario. The reader may note the general complexity of the stope geometry, which is quite typical of many Canadian hard rock mines. The complexity of the geometry can make the visualization and interpretation of microseismic event distribution very difficult. Current systems for displaying event locations operate by overlying the events onto two-dimensional digitized level plans in some CAD system. An example of this can be found in Young et al. (1989). While this yields acceptable results for quickly determining the general areas of high seismicity, the true spatial distribution of the events with regard to all the openings is difficult. Additionally, the correlation of seismic data with the results of the stress analysis data is not straight forward.

Figure 5.18 displays a segment of the microseismic activity monitored during a seven year period while portions of the G-Zone were being mined. Using the visualization and data interpretation features of *Examine*^{3D}, researchers at Queen's University have been successful in determining a good correlation between the monitored microseismic data and the results of a stress analysis of the 2151-6E stope at Campbell mine (Bawden and Todd,1993). The results of this study have provided confidence in the data produced by the *Examine*^{3D} stress analysis and in the use of *Examine*^{3D} as a stress analysis tool which will help in predicting future stope behavior.

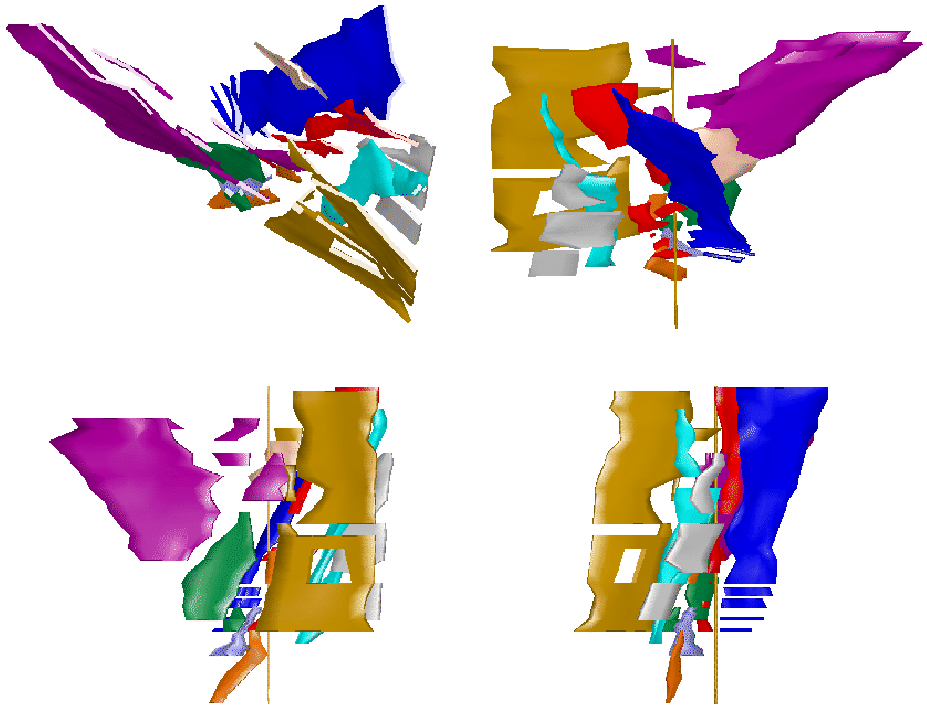

Figure 5.17 Stope geometry of the Placer Dome Campbell mine

Figure 5.19 is another example of the three-dimensional display of microseismic event locations located at the Falconbridge Lockerby mine in Sudbury. In this example, drift, shaft and ore pass geometry were incorporated from the Autocad™ mine geometry database for use in the visualization process. The actual stopes were taken from an *Examine*^{3D} stress analysis model. As seen in Figure 5.19,

the majority of the events occur in a pillar between the upper two stopes. The visualization of the temporal and spatial distribution pattern of the events provides important information for the determination of how the ore in this pillar might be mined. If a large number of events are currently occurring in the pillar, it is an indication that the rock is overstressed, and that rockbursting could accompany mining in this region.

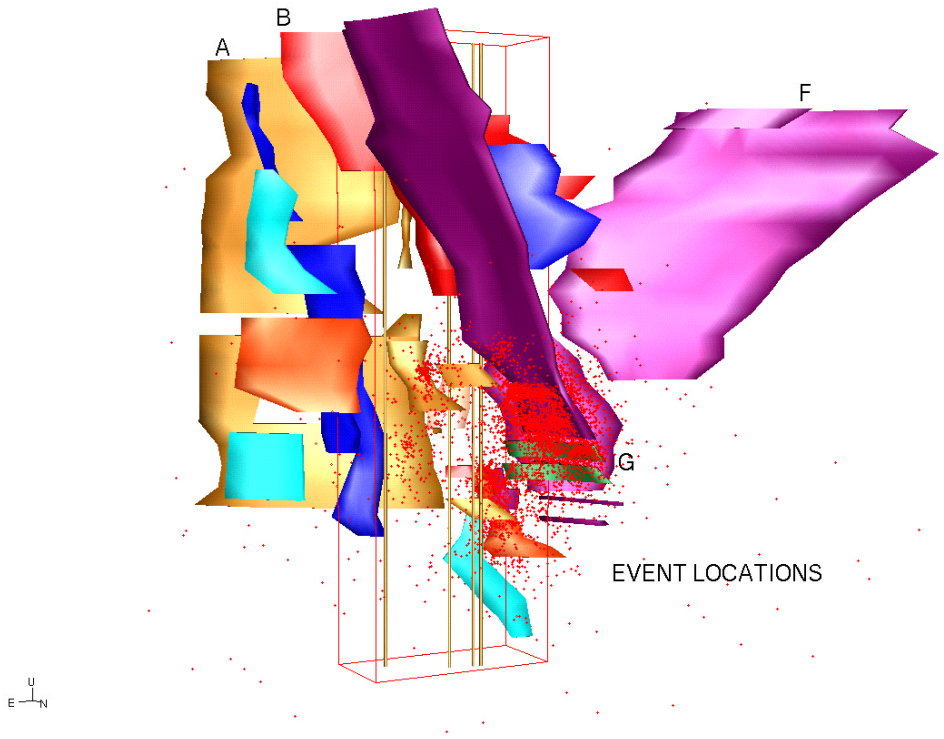

Figure 5.18 Microseismic event locations near the G-Zone at the Campbell mine

If current mining in the region around the pillar does not produce events within the pillar, it could mean that the rock has failed, resulting in a destressed zone within the pillar. It is unlikely that mining in this region would result in rockbursting. Field observation in this area could help in determining whether this is actually the case. Therefore, the pattern of propagation of the seismically active zones produces important information on yielded and overstressed regions within the rock mass.

Figure 5.20 shows part of Atomic Energy of Canada's Underground Research Laboratory (URL) in Lac du Bonnet, Manitoba. The URL is a major research facility for the investigation of safe, permanent nuclear waste disposal. An experiment at this facility was conducted whereby a 3m diameter circular tunnel was excavated horizontally in a granite batholith. The purpose was to monitor the rock mass behavior that would occur from excavation, operation and closure of a nuclear fuel waste disposal vault. (Lang et al., 1986; Read et al., 1993). A microseismic system was installed to measure the full waveform of any seismic events produced by excavation of the tunnel.

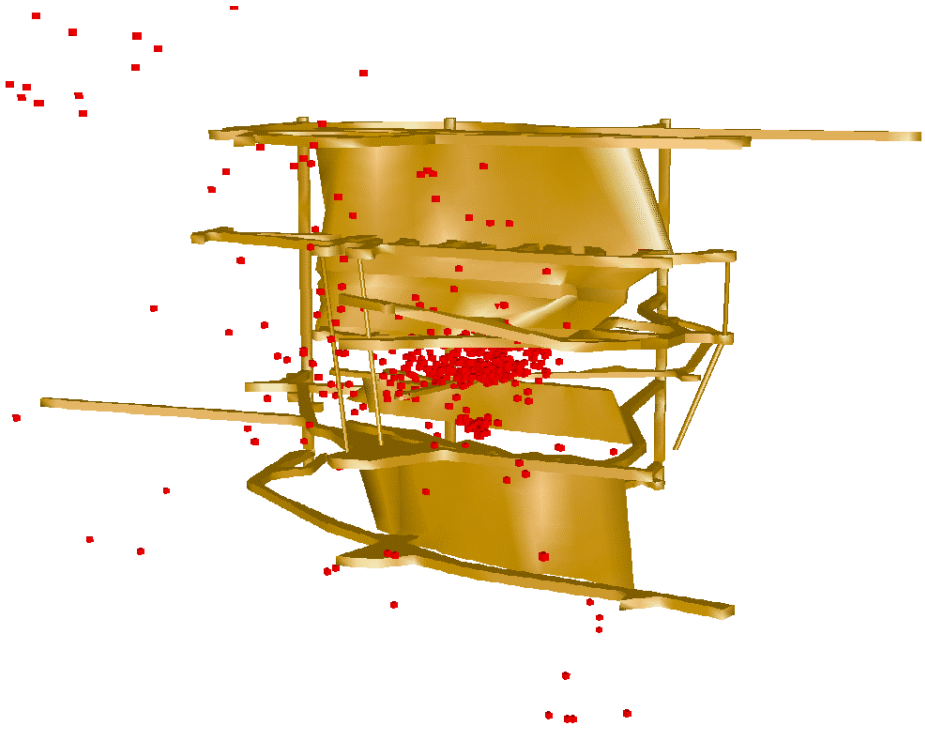

Figure 5.19 Microseismic event locations at the Falconbridge Lockerby mine

Figure 5.20 shows a few of the events which occurred during one stage in the excavation of the tunnel. The events are visualized as spheres whose color and size represent the relative magnitude of the seismic event. Notice the common pattern of a large event surrounded by a series of smaller magnitude

events. This concurrent display of event magnitude with event location can be used to gain information about the distribution of high energy seismic events.

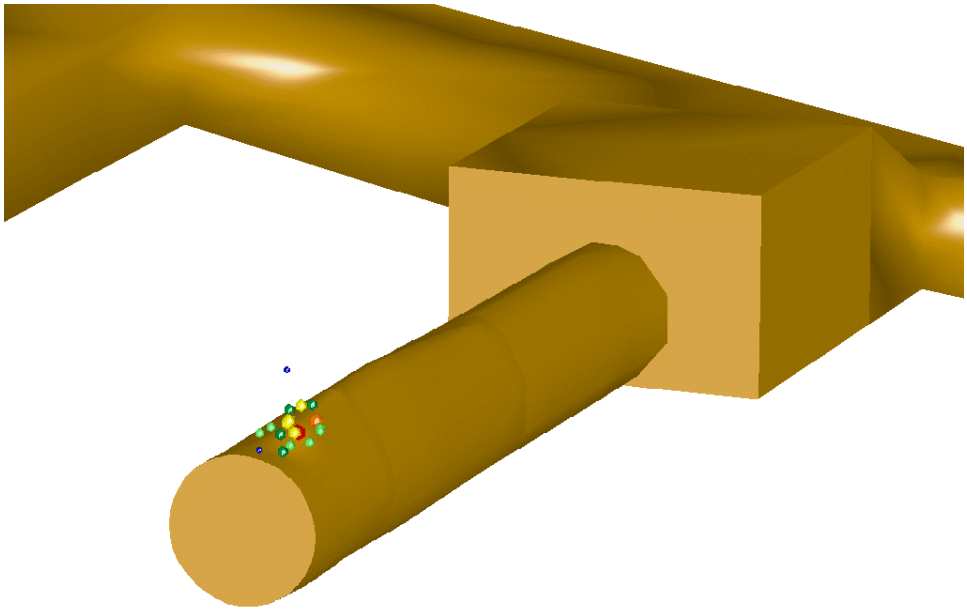

Figure 5.20 Microseismic event locations and magnitudes at the AECL URL

5.2.2 Event Density Data

The preceding section dealt with the display of discrete seismic events in conjunction with the mine geometry for the purpose of interpreting the spatial and temporal distribution of microseismicity. Although useful for qualitatively estimating zones of high seismicity, the quantitative assessment of the actual amount of microseismicity is not possible. Therefore, the display of event density is used to quantitatively assess the amount of seismicity in a volume of rock. To calculate event density, a regular grid is first superimposed over the event location data.

One method counts the number of events within a grid cell and divides this number by the grid cell volume, yielding the event density at the center of the cell. The counting method is computationally simple and faster, capturing high density regions better.

Another method calculates the relative location of an event within a grid cell and uses an inverse distance weighting function to distribute the event to the 8 vertices of the grid cell. After every event has been distributed, the resultant total at each cell vertex is divided by the cell volume to yield the density. This weighting method produces a smoother discrete approximation of the event density function and is thought to better represent the true nature of the data (Maxwell 1993). Although there are subtle differences in the data generated by both methods, when applied to the same problem, each seems to indicate the same trends in the data.

The computation of event density generates a scalar value of event density on every cell vertex of the superimposed regular grid. Thus, the same methods used for the display of scalar stress data can be used to display the event density. As an example, the main sill pillar at the Falconbridge Strathcona mine

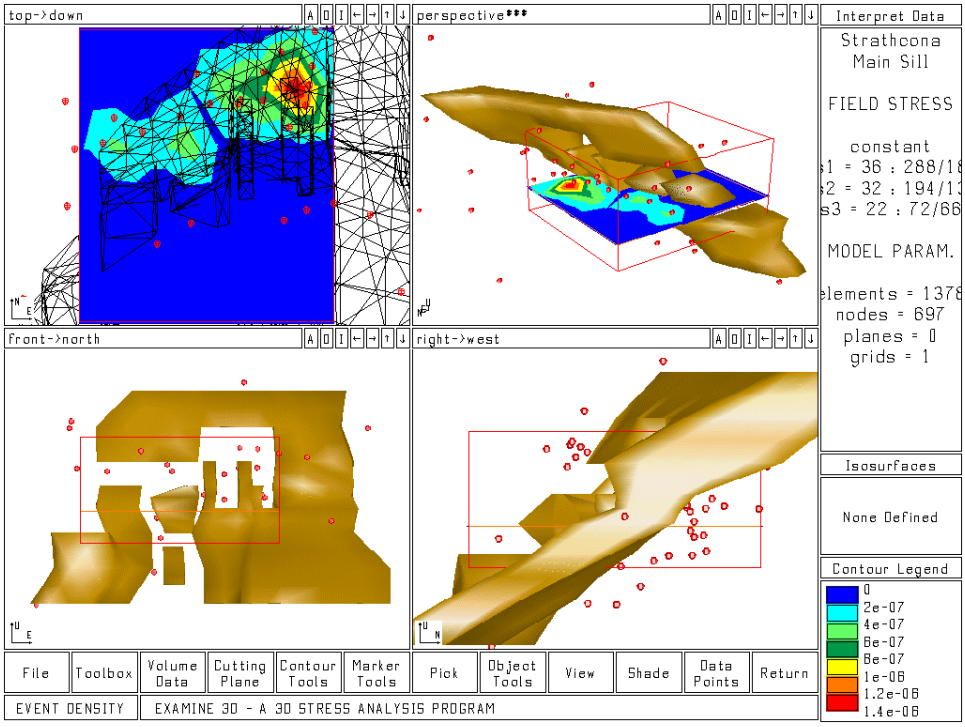

Figure 5.21 Event locations and density contours at the Falconbridge Strathcona mine

was being monitored for seismicity while mining was in progress. During attempted mining of the pillar, rockbursting started to occur, resulting in a shutdown of operations in the area. Figure 5.21 depicts the geometry of the main sill with the event locations and a contour plot of the event density in the region

surrounding the pillar. Figure 5.22 is a plot of the isosurface for an event density of 6e-7 events per cubic meter. The use of isosurfaces in this case works to quickly point out the volume of rock with high

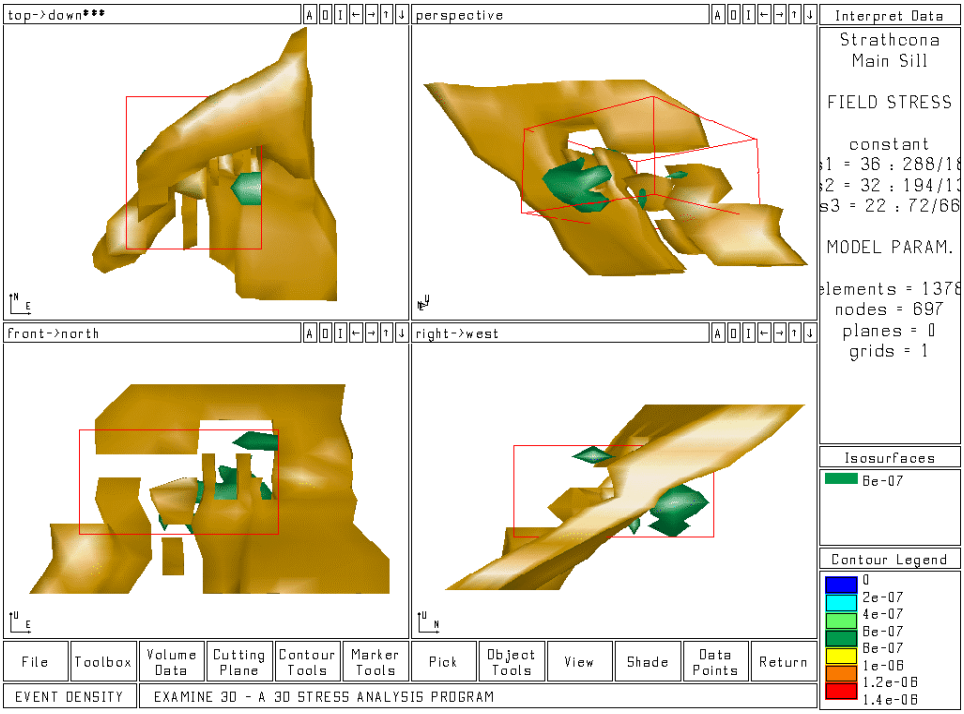

Figure 5.22 Isosurfaces of event density around the main sill pillar at Strathcona mine

event density.

The presentation of the seismic or stress analysis data by the rock mechanics engineer to those responsible for determining the logistics of where to mine, stoping patterns, etc. is extremely important. Although the use of three-dimensional visualization techniques such as isosurfaces and trajectory ribbons, and even to some extent the three-dimensional display of cutting planes, are very useful in interpreting mining data, experience has shown that the presentation and the conveyance of the data interpretation to other mining personnel is extremely problematic. In report form, static images of three-dimensional stope geometries and data are difficult to comprehend, even for the engineer doing the analysis. Without the use of the software to allow users to interactively manipulate and view the three-dimensional model, people may find these images confusing.

One method has proven successful in presenting results to people unfamiliar with the three-dimensional model. This method is to combine the three-dimensional images with those that overlay stress or seismic results on top of the mine's level plans for drifts and stopes. Since the mining engineers are very familiar with the two-dimensional geometry of drifts and stopes on a level within a mine, it is easy for them to spatially interpret any data presented in conjunction with these plans. The geometry for the level plans is generally stored in some digital form associated with the CAD system used at a particular mine. Facilities must therefore be incorporated into the visualization system for reading and displaying this level plan geometry in conjunction with the data.

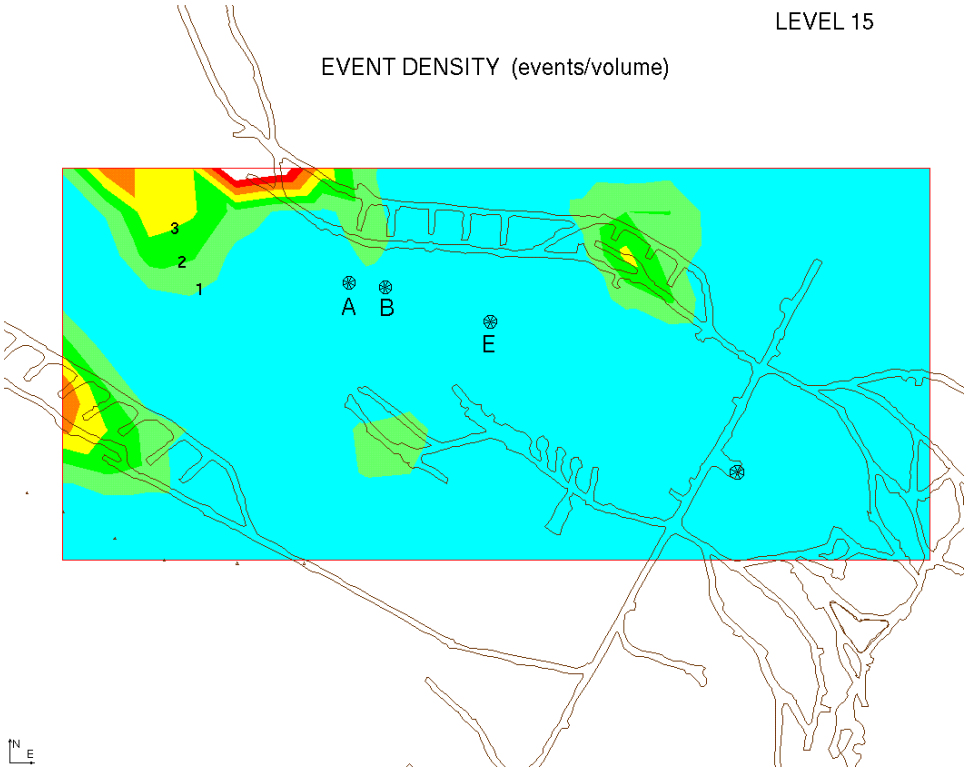

Figure 5.23 Event density distribution on Level 15 of the Placer Dome Campbell mine

Figure 5.23 is a plot of event density on level 15 (~1500 ft depth) of the Placer Dome Campbell mine in Red Lake, Ontario (Corkum and Grabinsky, 1995). The complete three-dimensional stope geometry can be seen in Figure 5.17 and Figure 5.18. Locations A, B, and E in Figure 5.23 are potential sites for a new access shaft. A stress analysis was done using the geometry in Figure 5.17, and the data

from the analysis was used in conjunction with the microseismic data to determine the optimal shaft location. During the course of the Campbell project, three-dimensional visualization techniques were used to quickly determine problem areas. Overlaying the results on the level plans, as discussed above, was used to present the analysis data to the engineers at the mine. This proved to be the optimal solution for both interpreting the data, and presenting the results.

5.2.3 Energy Density Data

Along with the source location for a seismic event, the magnitude of the event is also recorded. Being able to visualize the distribution of high energy seismic events is of importance to mining engineers, for obvious mine safety considerations.

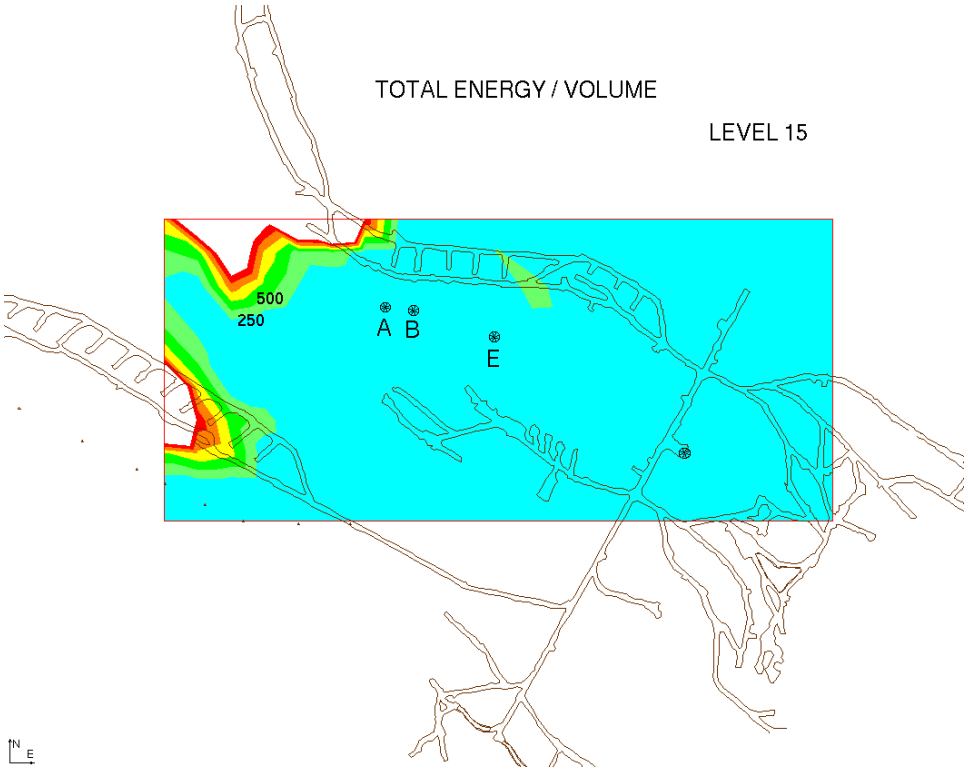

Figure 5.24 Energy density distribution (MJ) on Level 15 of the Campbell mine

As with event density, total energy density can be calculated within a volume of rock by first overlaying a three-dimensional discretized grid in the area of interest. Adding up the amount of energy

associated with each event within a grid cell and dividing by the grid cell volume yields the energy density.

Figure 5.24 is an illustration of the energy density on the 15th level of the Campbell mine. Notice that the data is presented in the same manner as the event density data in Figure 5.23, with contoured values overlying the level plans for easier location referencing by the mine personnel.

5.2.4 Velocity Data

Using active and passive geotomographic imaging techniques, seismologists can determine the P-wave velocity structure within a rock mass (Young and Maxwell, 1993-96). This velocity structure can then be used to delineate and characterize both anomalous rock mass quality and stress state ahead of mining. This information could further be used to modify mine design and minimize the risk of rockbursting. Correlation between stress analysis and velocity data can also be used to calibrate and validate the stress analysis results.

This validation helps to provide the confidence in the modeling of rock mass behavior due to future mining and possibly influence their design. Figure 5.25 shows the velocity distribution within the main sill pillar at the Falconbridge Strathcona mine. The reader may notice that the regions of high velocity map to the footwall of the orebody while the low velocity regions are in the hanging wall. Field observations in hanging wall drifts, which are close to the main sill pillar, have indicated a large volume of broken rock in this region. Since P-wave propagation is slower through broken rock and higher through highly stressed rock, the field observations seem to support the results of the geotomographic velocity image. It can also be seen in Figure 5.22 that seismic events are occurring predominantly in the footwall. Since seismic events can be associated with rock in a state of high stress, this also seems to indicate good correlation with the velocity image.

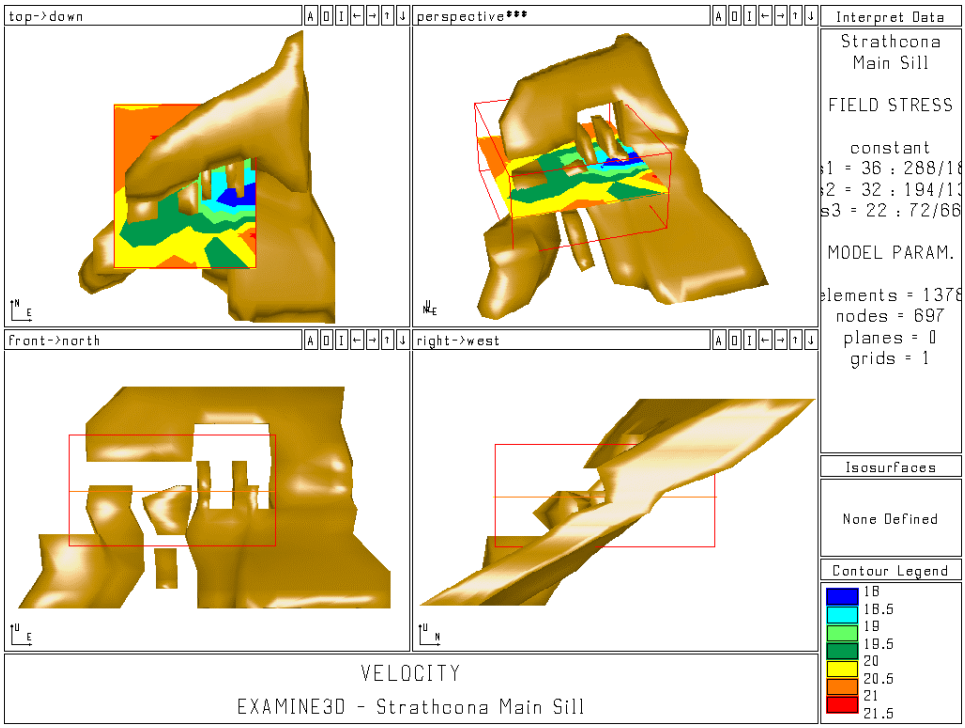

Figure 5.25 Velocity distribution (100m/s) in the Strathcona main sill pillar

To determine the velocity structure, data on event and sensor location is used and the assumption of a straight line P-wave propagation path and first arrival times of P-waves generated by the event, are assumed (Maxwell, 1993).

The velocities of a P-wave along each ray path are then mapped to a regular grid (Maxwell, 1993) and displayed using the same techniques and visualization system used for stress analysis data. However, it is essential that the visualization system be able to not only display the velocity data but also to be able to show the locations of the sensors and ray paths used in determining the tomographic data. This information is important in determining the coverage throughout the rockmass being imaged. The extent of coverage is very significant in determining the amount of confidence that the seismologist has in the geotomographic velocity data. Figure 5.26 shows a partial sensor and ray path distribution associated with the geotomographic imaging data presented in Figure 5.25. This figure shows good coverage in the area of interest in the main sill pillar.

The amount of coverage in a certain region of the rock mass, resulting in a certain level of confidence that the seismologist has in velocity data, can be quantified in terms of a confidence value at every grid point. When the ray path P-wave velocities are mapped to a singular value of velocity at each grid vertex, a confidence value based on the amount of local coverage by the seismic system can also be determined at this location. This confidence value usually ranges from zero to one, with zero indicating no confidence and one being full confidence in the velocity value.

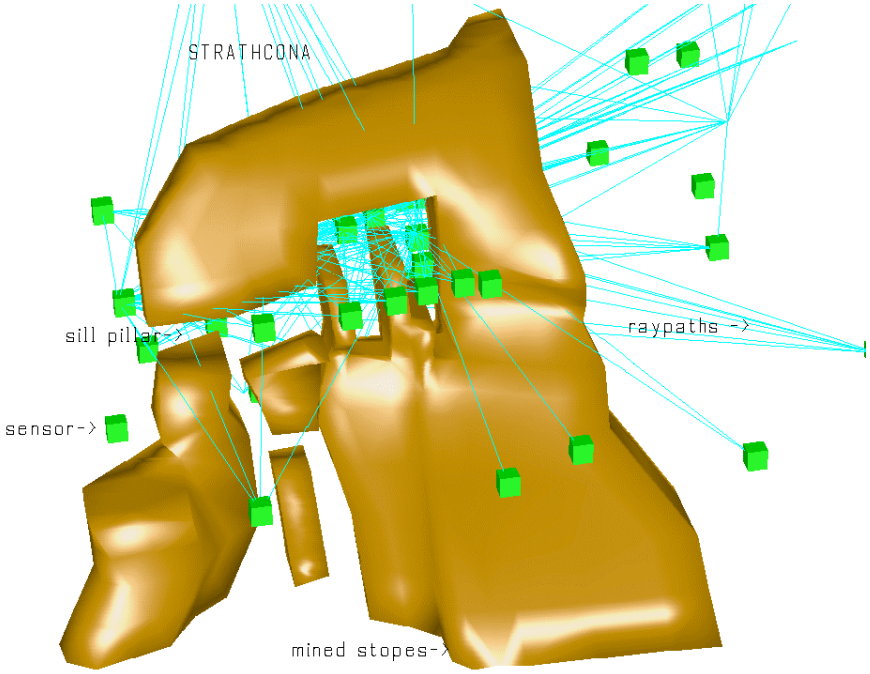

Figure 5.26 Event sensor and raypath locations around the Strathcona main sill pillar

One effective method for visualizing velocity and confidence data uses the six primary and secondary colors (red, green, blue, cyan, magenta, and yellow) for the contour range color bar. It then defines the color system based on the HSV (hue, saturation, and value) color model (Foley et al., 1990). Thus, when contouring the data, the value of velocity will be mapped to a color in the color bar and the value of confidence will determine the level of saturation that the color in the color bar will have. The value of saturation, like the value of confidence, also ranges from zero to one. Therefore, the six primary

and secondary range colors will vary from white to either red, green, blue, cyan, magenta, or yellow, depending on which contour range a value is being mapped to. The use of the primary and secondary colors guarantees that the intermediate colors will be a lighter, muted shade of the color being mapped. This fact alone ensures that the user will not be confused about which contour range a contour belongs to.

Therefore, when contouring a two-dimensional grid cell of a cutting plane, the level of saturation for the colored contours in that cell is based on the confidence values at the four corners of the cell. An average confidence value is first calculated by summing the confidence values at the four corners and dividing by four. The color saturation for the colors defining the contours in this grid cell is then set to this confidence value. Thus, regions of low confidence will be defined by contours of muted color and regions of high confidence will have more brilliant colored contours. Regions of zero confidence will be white without any contours, since zero saturation defines white for all the colors in the contour range.

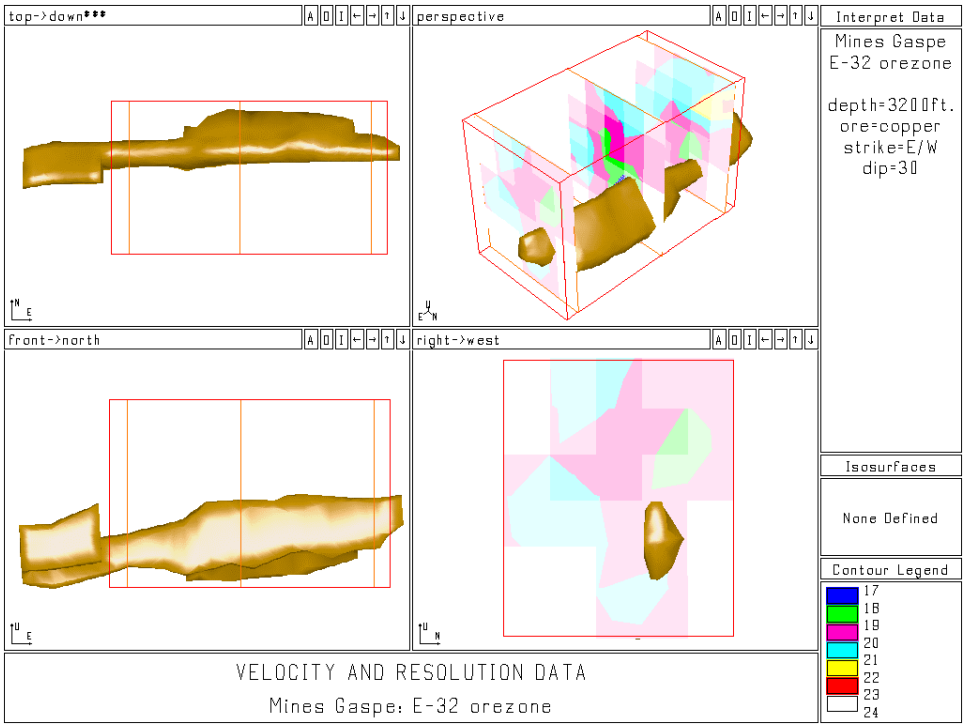

Figure 5.27 Combination of velocity and resolution data at the Mines Gaspe

Figure 5.27 is the visualization of velocity data in combination with resolution data around the E-32 stope at the Mines Gaspe in Quebec. Notice the regions of brilliant color definition, which are the regions of good coverage and high confidence in the data. The regions of high confidence are above the stope towards the center while regions of poor coverage are towards the ends and below the stope. This information is very useful when trying to correlate results from stress analysis, event density, and geotomographic data, since it allows the engineer to focus on areas of high confidence.

6. FUTURE RESEARCH

This thesis has provided the necessary groundwork for the definition of three-dimensional boundary element mesh geometry for underground openings. The most important area for future research is the advancement of the geometric modeling and meshing strategies presented in this thesis. The extrusion, skinning and facing algorithms for defining mesh geometry have been shown to be effective, but they are still quite crude. There is tremendous possibility for improvement by incorporating technology that would remove many of the restrictions associated with the initial polyline definition.

Currently, the skin polylines must have the same number of vertices and be ordered in the same direction. Future research should work at removing this restriction so that any set of arbitrary skin polylines could be managed. This is not an easy problem though, since the geometry of many mine openings is very complex, making the facilitation of a totally automatic and flexible technique quite a challenge. The facing algorithm also contains restrictions on the intersection of multiple face polylines. These intersection points must be associated with polyline vertices, making the initial definition of the skin polylines quite cumbersome. In the future, both the skinning and facing techniques should be made more general, allowing for greater flexibility in the initial geometry. This alone would greatly reduce the effort required to construct the mesh.

Another problem with defining the mesh geometry, using the current system, is in the incremental staging of future excavations. Currently, it is quite difficult to go back and intersect future new openings with a completed mesh without having to rebuild much of the geometry near the areas of intersection. The solution to this problem is a methodology for quickly, accurately and automatically defining the region of intersection and remeshing to create the geometry. This is a difficult problem without an obvious answer since the restrictions on the boundary element surface mesh require that the intersection geometry be composed of edge-connected somewhat equilateral triangles. One possible solution is to adopt solid modeling technology and/or remove the mesh definition from the geometry

definition. One would first create the model using boundary representation (B-REP) solid modeling, then create the mesh from this solid representation. Intersections could then be done automatically using the B-REP geometry. Remeshing with different mesh densities could also be fairly transparent as the underlying B-REP geometry is not changing. Although in theory this may work, the application to typical complex mine geometry might not be practical. Complex surface descriptions with multiple intersections and holes (representing rock pillars) through the geometry might be a formidable task for even the most state of the art solid modeling system. There should first be an extensive investigation into the applicability of solid modeling to mesh generation of underground excavations.

The visualization technology presented in this thesis has proven adequate for interpreting data around underground excavations. Although one could argue that incorporating the direct volume rendering technique for visualizing three-dimensional datasets would enhance the visualization process, the fact is that this would be so computationally expensive, it would be impractical for use in an interactive environment on today's personal computers. The data in this thesis is generally well-defined (not fuzzy) making the use of isosurfaces very effective in visualizing the correct behavior and negating the need for direct volume rendering.

Currently there are efforts to improve numerical analysis capabilities, incorporating joints and tabular orebodys using displacement discontinuities as well as multiple materials with plasticity using three-dimensional finite elements. These additions will result in a need to further enhance the visualization system to handle datasets produced by these analyses. Since joints produce a discontinuity in the stress and displacement field, facilities will have to be added to handle these features. In voxels that span joints, the continuous tri-linear interpolation technique will have to be modified to manage the discontinuity in stress and displacement where the joint intersects the voxel. The visualization of the geologic structure associated with a multi-material analysis will also prove to be a challenge, as the visualization system will have to have the facilities to show the different materials and their interaction with the stress field. The problem becomes more complex because, as with the joints, a discontinuity in

displacement occurs along the interfaces between different materials. The addition of three-dimensional finite elements will greatly alter the format in which the data enters the visualization system. Instead of the data being located on a regular grid, the data will be unstructured, composed of connected tetrahedrons or hexahedrons. A fundamental change in the data format will require changes in how visualization algorithms such as cutting planes, isosurface extraction and trajectory ribbons access and use the data. There is little doubt that the direction of future research into data visualization will change because of these new developments in the capabilities of the numerical stress analysis engines.

7. CONCLUSIONS

Until recently, three-dimensional stress analyses of underground structures were not carried out on a routine basis. The complexity and difficulty in accurately modeling the three-dimensional geometry of most underground structures and the large amount of work required to create the models has made the task impractical for most design situations. For models that have been built, simplifications made to the geometry have greatly compromised the results, influencing their ability to accurately predict the behavior. From an economic point of view, the amount of time that can be devoted to modeling is restricted, making three-dimensional analyses economically unjustifiable in the past.

The three-dimensional nature of the results of stress analyses of underground structures has often led to interpretation problems. Visualizing the stress and displacement distribution around three-dimensional models has long been cumbersome, leading to improper interpretation. The complexity of geometric modeling and visualization have been the two major reasons for the slow adoption of three-dimensional modeling as a design tool.

This thesis makes an organized attempt to solve both the geometric complexity issue and the data visualization problem. A methodology for allowing quick and accurate mesh generation for a three-dimensional boundary element stress analysis has been presented. Algorithms such as extrusion, skinning and facing are introduced as effective techniques for quickly and accurately creating three-dimensional meshes of underground structures.

The practical and effective use of these techniques by mining and civil engineering companies worldwide has led to the verification and validation of the modeling strategies presented in this thesis. Both mining and civil engineers can now routinely perform three-dimensional stress analyses of underground structures. This alone will lead to a better understanding of the three-dimensional stress state around underground excavations, leading to better designs of these types of structures.

Similar to creating the model, it is imperative that the design engineer be able to quickly and accurately visualize the results of the stress analysis. The design engineer should be able to view these

results in conjunction with other important three-dimensional datasets such as seismic event location and geotomography velocity imaging. It is also important that design engineers can validate the stress analysis results and the possible effect that these datasets can have on the design of future excavations.

This thesis has presented an assortment of algorithms and techniques used for the display of three-dimensional data around underground excavations. For the visualization of scalar stress and seismic data, cutting planes and isosurfaces are effective in accurately displaying the spatial distribution of these datasets. Isosurfaces have been shown to provide information on global stress distribution, making it possible to accurately visualize the mine-wide stress and seismicity distribution. Complimenting this important information, cutting planes, surface contouring and trajectory glyphs provide further information local to the area of interest.

Trajectory ribbons have been introduced as a convenient method for displaying the three-dimensional flow of stress around underground openings, providing useful insights into the effect that current and future openings will have on the distribution of stress. Computer graphics techniques such as transparency, shading and interactive rotation and movement of the model have been incorporated into the analysis tools so that the engineer can quickly visualize the three-dimensional nature of the geometry. These are important aspects in properly interpreting the spatial variability of three-dimensional mine datasets.

The increasing world-wide use of the modeling and visualization strategies presented in this thesis have led to the advancement of three-dimensional stress analysis modeling and data visualization as viable resources in the design of underground excavations in rock.

References

Agin, G.J. and Binford, T.O. (1977), Representation and description of curved objects, IEEE Trans. Comput., C-25, 439-449.

Bawden, W., and Tod, J. (1993), A linked microseismic-geomechanics-mine induced stress analysis of the 2151-6E sill pillar extraction, Report #QMD-CRL1. Geology and rock mass characterisation at Campbell Mine, Report to the Canadian Rockburst Research Program.

Binford, T.O. (1971), Visual perception by computer, invited paper, Proc. IEEE Conf. on Systems and Control, Miami, Fla., Dec. 1971.

Binford, T.O. and Agin, G.J. (1973), Computer description of curved objects, Proceedings of the Third International Conference on Artificial Intelligence, 629-40.

Brady, B. and Brown, E. (1985), Rock mechanics for underground mining, George Allen & Unwin, London.

Brebbia, C., and Dominguez, J. (1989), Boundary elements an introductory course, McGraw Hill, Toronto.

Brodlie, K., Carpenter, L., Earnshaw, R., Gallop, J., Hubbold, R., Mumford, A., Osland, C., Quarendon, P. (1992), Scientific visualization, techniques and applications, Springer-Verlag, New York.

Carlson, R. and Foley, T. (1990), The prameter R^2 and multiquadric interpolation, Technical Report, Lawrence Livermore National Laboratory.

Cavendish, J.C. (1974), Automatic triangulation of arbitrary planar domains for the finite element method, International Journal for Numerical Methods in Engineering, vol. 8, 679-696.

Cavendish, J.C., Field, D.A., Frey, W.H. (1985), An approach to automatic three-dimensional finite element mesh generation, International Journal for Numerical Methods in Engineering, vol. 21, 329-347.

Charles, R.D. (1989), Viewing velocity in flow fields, CIME Mechanical Engineering, August, 64-67.

Christiansen, H.N. and Sederberg, T.W. (1978), Conversion of complex contour line definitions into polygonal element mosaics, Compt. Graph., vol. 12, no. 2, 187-192.

Cline, H., Lorensen, W., Ludke, S., Crawford, C., and Teeter, B. (1988), Two algorithms for the three-dimensional reconstruction of tomograms, Medical Physics, vol. 15, no.3, May/June, 320-327.

Corkum, B. and Grabinsky, M. (1995), Numerical stress analysis of proposed shafts at Placer Dome Inc.'s Campbell Mine, Report to Placer Dome Inc., Dept. of Civil Engineering, University of Toronto, Toronto, Publication No. RG-95-07-31, 80 p.

Corkum, B., Grabinsky, M., Curran, J. (1994), Examine^{3D} - Energy balance utility, Report to The Mining Research Directorate, Canadian Rockburst Research Program, Dept. of Civil Engineering, University of Toronto, Toronto, Publication No. RG-94-04-30, 21 p.

Corkum, B., Grabinsky, M., Curran, J. (1993), Examine^{3D} - The EDEN2 event density utility, Report to The Mining Research Directorate, Canadian Rockburst Research Program, Dept. of Civil Engineering, University of Toronto, Toronto, Publication No. RG-94-09-23, 27 p.

Corkum, B., Curran, J. (1993), Examine^{3D} - Stiffness and energy utilities, Report to The Mining Research Directorate, Canadian Rockburst Research Program, Dept. of Civil Engineering, University of Toronto, Toronto, Publication No. RG-93-09-30, 20 p.

Corkum, B., Curran, J., Grabinsky, M. (1991), Examine3d - A three-dimensional data visualization tool for mine datasets, Proceedings of the 2nd Canadian Conference on Computer Applications in the Mineral Industry, Vancouver, British Columbia, Canada, vol.2.

Crouch, S. and Starfield, A. (1983), Boundary element methods in solid mechanics, GeorgeAllen & Unwin, London.

Curran, J., Grabinsky, M., Corkum, B. (1994), "Numerical analysis of the AECL Mine-by experiment (post construction phase) part 2a - triaxial strain cell results for a circular excavation", Dept. of Civil Engineering, University of Toronto, Toronto, Publication No. 94-01, 27 p.

Curran, J., Grabinsky, M., Corkum, B. (1994), "Numerical analysis of the AECL Mine-by experiment (post construction phase) part 2a - triaxial strain cell results for a circular excavation", Dept. of Civil Engineering, University of Toronto, Toronto, Publication No. 94-02, 27 p.

Delmarcelle, T. and Hesselink, L. (1992), Visualization of second-order tensor fields and matrix data, Proc. IEEE Visualization '92, Boston, 316-323.

Dickinson, R.R. and Bartels, R.H. (1988), Fast algorithms for tracking contours, streamlines, and tensor fields, Third International Conference on Computing in Civil Engineering, Vancouver, vol. 2, 495-502.

Drebin, R., Carpenter, L., Hanrahan, P. (1988), Volume rendering, Computer Graphics, vol. 22, no. 4, August, 65-74.

Duchon, J. (1975), Splines minimizing rotation-invariant semi-norms in Sobolev spaces, In Multivariate Approximation Theory, Schempp, W. and Zeller, K. (ed.), Birkhauser, Basel, 85-100.

Ekoule, A.B., Peyrin, F.C., Odet, C.L. (1991), A triangulation algorithm from arbitrary shaped multiple planar contours, ACM Transactions on Graphics, vol. 10, no. 2, 182-199.

Finnigan, P.M., Hathaway, A.F., Lorensen, W.E. (1990), CATFEM: Computer-Assisted tomography to finite element modeling, Proc. 1990 ASME International Computers in Engineering Conference, vol. 2, 153-160.

Finnigan, P.M., Hathaway, A.F., Lorensen, W.E. (1990), Merging CAT and FEM, CIME Mechanical Engineering, July, 32-38.

Foley, J., van Dam, A., Feiner, S., Hughes, J. (1990), Computer graphics: principles and practice, 2nd ed., Addison-Wesley, Toronto.

Foley, T. and Lane, D. (1990), Visualization of irregular multivariate data, IEEE Visualization 90 Conf. Proc., 247-254.

Fournier, A. and Montuno, D.Y. (1984), Triangulating simple polygons and equivalent problems, ACM Transactions on Graphics, vol. 3, no. 2, 153-174.

Franke, R. (1982), Smooth interpolation of scattered data by local thin plate splines, Comp. Math. Appls. 8, 273-281.

Franke, R. (1985), Thin plate splines with tension, Computer Aided Geometric Design, vol. 2, 87-95.

Franke, R. and Nielson, G. (1990), Scattered data interpolation and applications: A tutorial and survey, iIn geometric modelling: methods and their application, Hagen, H. and Roller, D. (ed.), Springer, Berlin, 131-160.

Frederick, D. and Chang, T.S. (1965), Continuum mechanics, Allyn and Bacon Inc., Boston.

Fuchs, H., Kedem, Z.M., Uselton, S.P. (1977), Optimal surface reconstruction from planar contours, Commun. ACM, vol. 20, no. 10, 693-702.

Gelberg, L., Kamins, D., Parker, D., Sacks, J. (1990), Visualization techniques for structured and unstructured scientific data, Siggraph'90 course notes: State of the art in data visualization, Dallas.

Globus, A., Levit, C., Lasinski, T. (1991), A tool for visualizing the topology of three-dimensional vector fields, Proc. IEEE Visualization '91, San Diego, 33-40.

Goodman, R. (1980), Introduction to rock mechanics, John Wiley & Sons, Toronto.

Grabinsky, M., Wilson, R., Zougas, A., Curran, J., Corkum B. (1995), Practical meshing considerations for finite element analyses of rock engineering problems, Proceedings of the 8th International Congress on Rock Mechanics, Tokyo, Japan, vol.3.

Grabinsky, M., Corkum, B., Curran, J. (1995), Energy considerations in geomechanical mine design, 3rd Canadian Conference on Computer Applications in the Mineral Industry, Montreal, Quebec, Canada.

Grabinsky, M., Corkum, B., Curran, J. (1994), The use of boundary element programs in calculating the energy release due to progressive mining, Report to The Mining Research Directorate, Canadian Rockburst Research Program, Dept. of Civil Engineering, University of Toronto, Toronto, Publication No. RG-94-08-31, 13 p.

Grabinsky, M. (1992), Quantifying rock stress and evaluating its significance in the geomechanical design of underground mines, PhD Thesis, Dept. Civil Eng., Univ. of Toronto.

Graichen, C.M., Hathaway, A.F., Finnigan, P.M., Kela, A., Schroeder, W.J. (1989), A 3-D fully automated geometry-based finite element meshing system, ASME Winter Annual Meeting, San Francisco.

Green, P.J. and Sibson, R. (1978), Computing Dirichlet tessalations in plane, Comp. J., vol. 21, 168-173.

Hardy, R. (1990), Theory and application of the multiquadric-biharmonic method, Comp. Math. Appls. 19, no. 8, 163-208.

Harris, L., Robb, G., Yuen, T., and Ritman, E. (1978), Non-invasive numerical dissection and display of anatomic structure using computerized x-ray tomography, Proceedings SPIE 152, 10-18.

Harder, R. and Desmarais, R. (1972), Interpolation using surface splines, Journal of Aircraft, vol. 9, 189-197.

Helman, J.L. and Hesselink, L. (1990), Surface representations of two- and three-dimensional fluid flow topology, Proc. IEEE Visualization ‘90, San Francisco, 6-13.

Herman, G., and Liu, H. (1979), Three-dimensional display of organs from computed tomograms, Computer Graphics and Image Processing, vol. 9, no. 1, 1-21.

Herrmann, L.R. (1976), Laplacian-isoparametric grid generation scheme, Journal of the Engineering Mechanics Division A.S.C.E., vol. 102, 749-756.

Hoek, E., Kaiser, P., Bawden, W. (1995), Support of underground excavations in hard rock, Balkema, Rotterdam.

Hoek, E. and Brown, E. (1980), Underground excavations in hard rock, The Institution of Mining and Metallurgy, London.

Hornbeck, R.W. (1975), Numercial methods, Prentice-Hall, Englewood Cliffs, New Jersey.

Hulquist, J.P.M. (1992), Constructing stream surfaces in steady 3D vector fields, Proc. IEEE Visualization ‘92, Boston, 171-178.

Hutchinson, D.J., and Grabinsky, M. (1992), Back analysis of stope stability at Ansil mine using instrumentation data and numerical modelling, Proceedings of the International Symposium on Rock Support, Sudbury, Ontario.

Jaeger, J. and Cook, N. (1969), Fundamentals of rock mechanics, Chapman and Hall, London.

Kazakidis, V. (1995), A numerical modelling analysis of the G-Zone of the Campbell Mine of Placer Dome Ltd., Report to the Canadian Rockburst Research Program.

Kazakidis, V., Punkkinen, A., Villeneuve, B.T. Corkum (1995), Use of seismic density analyses in burst-prone mines, 3rd Canadian Conference on Computer Applications in the Mineral Industry, Montreal, Quebec, Canada.

Kenwright, D.N. and Mallinson, G.D. (1992), A 3-D streamline tracking algorithm using dual stream functions, Proc. IEEE Visualization ‘92, Boston, 62-68.

Keppel, E. (1975), Approximating complex surfaces by triangulation of contour lines, IBM J. Res. Dev., vol. 19, 2-11.

Lang, P., Everitt, R., Ng, L., Thompson, P. (1986), Horizontal in-situ stresses versus depth in the Canadian shield at the Underground Research Laboratory, Proceedings of the International Symposium on Rock Stress and Rock Stress Measurements, Stockholm, Sweden.

Lawson, C.L. (1977), Sofware for C^1 surface interpolation, Mathematical Software III, ed. J.R. Rice, Academic Press.

Levoy, M. (1988), Display of surfaces from volume data, IEEE Computer Graphics and Applications, vol. 8, no. 3, May, 29-37.

Levoy, M. (1989), Design for a real-time high-quality volume rendering workstation, Proc. Chapel Hill Workshop on Volume Visualization, Dept. of Computer Science, University of North Carolina, 85-92.

Levoy, M. (1990a), Efficient ray tracing of volume data, ACM Transactions on Graphics, vol. 9, no. 3, July.

Levoy, M. (1990b), Volume rendering by adaptive refinement, The Visual Computer, vol. 6, no.1, Febuary, 2-7.

Levoy, M. (1990c), A hybrid ray tracer for rendering polygon and volume data, IEEE Computer Graphics and Applications, vol. 10, no. 2, March, 33-40.

Levoy, M. (1990d), A taxonomy of volume visualization algorithms, ACM Siggraph 1990 Course notes: Volume Visualization Algorithms and Architectures, Dallas, 6-9.

Lorenson, W., and Cline, H. (1987), Marching cubes: A high resolution 3D surface construction algorithm, Computer Graphics, vol. 21, no. 4, July, 163-169.

Lorenson, W. (1990), Creating surfaces from volumes using marching and dividing cubes, ACM Siggraph 1990 Course notes: Volume Visualization Algorithms and Architectures, Dallas, 13-24.

Martin, C.D. (1988), Shaft excavation response in a highly stressed rock mass, Proceedings of the OECD Workshop on Excavation Responses in Deep Radioactive Waste Repositories - Implications for Engineering Design and Safety Performance, Winnipeg, 331-340

Martin, C.D. (1989), Failure observations and in-situ stress domains at the Underground Research Laboratory, Proceedings of the International Symposium “Rock at Great Depth”, Pau, France, 28-31.

Maxwell, S. and Young, R.P. (1992), Sequential velocity imaging microseismic Monitoring of Mining-Induced Stress Change, Pure and Applied Geophysics, 139, 421-447.

Maxwell, S. (1993), Seismic P-Wave velocity imaging in underground mines: Observations on the relationship between velocity structure and mining-induced seismicity, Doctorate Dissertation, Department of Geological Sciences, Queen's University.

Maxwell, S. and Young, R.P. (1993), associations between temporal velocity changes and induced seismicity, Geophysical Research Letters, 20, 2929-2932.

Maxwell, S. and Young, R.P. (1993), Stress change monitoring using induced microseismicity for sequential passive velocity imaging, in Proc. 3rd International Symposium on Rockbursts and Seismicity in Mines.

Maxwell, S. and Young, R.P. (1994), An in-Situ investigation of the relationship between stress, velocity and induced seismicity, Geophysical Research Letters, 22, 1049-1052.

Maxwell, S. and Young, R.P. (1994), Application of seismic tomography for induced seismicity Investigations, in Proc. Eurock '94.

Maxwell, S. and Young, R.P. (1996), seismic imaging of rock mass response to excavation, International Journal of Rock Mechanics and Mining Science, in press.

Maxwell, S. and Young, R.P. (1996), velocity inversion from microseismic data, chapter in Seismic Monitoring In Mines, (A. Mendecki Ed), Balkema, Rotterdam, in press.

Meyers, D., Skinner, S., Sloan, K. (1992), Surfaces from contours, ACM Transactions on Graphics, vol. 11, no. 3, 228-258.

Nevatia, R. and Binford, T.O. (1977), Description and recognition of curved objects, Artificial Intelligence, 8(6).

Nielson, G. (1993), Scattered data modeling, IEEE CG&A, Vol. 13, No. 1, Jan., 60-70.

Pande, G., Beer, G., Williams, J. (1990), Numerical methods in rock mechanics, John Wiley & Sons, Toronto.

Press, W.H., Flannery, B.P., Teukolsky, S.A., Vetterling, W.T. (1989), Numerical recipes in C, Cambridge University Press, New York.

Ramakrishnan, C.V., Ramakrishnan, S., Kumar, A., Bhattacharya, M. (1992), An integrated approach for automated generation of two/three dimensional finite element grids using spatial occupancy enumeration and Delaunay triangulation, International Journal for Numerical Methods in Engineering, vol. 34, 1035-1050.

Read, R., Martino, J., Mitchell, J. (1993), Mine-by experimental data summary, Scientific Document Distribution Office, AECL Research, Chalk River, Ontario, TR-595.

Schroeder, W.J. and Sheppard, M.S. (1988), Geometry-based fully automatic mesh generation and the Delaunay triangulation, International Journal for Numerical Methods in Engineering, vol. 26, 2503-2515.

Shah, S. (1993), Practical implementation of the direct boundary element method for three-dimensional stress analysis of underground excavations, PhD Thesis, Dept. Civil Eng., Univ. of Toronto.

Shani, U. and Ballard, D.H. (1984), Splines as embeddings for generalized cylinders, Computer Vision, Graphics, and Image Processing, 27, 129-156.

Sibson, R. (1978), Locally equilateral triangulations, Comp. J., vol. 21, no. 3, 243-245.

Shepard, D. (1968), A two-dimensional interpolation function for irregularly spaced data, Proc. 23rd Nat. Conf. ACM, 517-524.

Siggraph'88 Course Notes: Algorithms for data representation graphics, Atlanta, 1988.

Siggraph'89 Course Notes: State of the art in data visualization, Boston, 1989.

Siggraph'90 Course Notes: State of the art in data visualization, Dallas, 1990.

Siggraph'90 Course Notes: Volume visualization algorithms and architectures, Dallas, 1990.

Simpson, R.B. (1979), A survey of two-dimensional finite element mesh generation, Proc. Ninth Manitoba Conference on Numerical Math. and Computing, 49-124.

Sutcliffe, D.C. (1988), Contouring over rectangular and skewed rectangular grids - an introduction, ACM Siggraph 1988 Course notes: Algorithms for Data Representation Graphics, Atlanta, 69-92.

Talebi, S. and Young, P. (1989), Failure mechanism of crack propagations induced by shaft excavation at the underground research laboratory, International Symposium "Rock at Great Depth", Pau, France, 28-31.

Upson, C., and Keeler, M. (1988), VBUFFER: Visible volume rendering, Computer Graphics, vol. 22, no. 4, August, 59-64.

Westover, L. (1989), Interactive volume rendering, Chapel Hill Workshop on Volume Visualization, Chapel Hill, North Carolina, 9-16.

Westover, L. (1990), Footprint evaluation for volume rendering, Computer Graphics, no. 8.

Wilhelms, J. and Van Gelder, A. (1990), Topological considerations in isosurface generation, Computer Graphics, vol. 24, no. 5, 79-86.

Wolff, R.S. and Yaeger, L. (1993), Visualization of natural phenomena, Springer-Verlag, New York.

Young, R., Talebi, S., Hutchins, D., Urbancic, T. (1989), Analysis of mining-induced microseismic events at Strathcona mine, Sudbury, Canada, Special Issue of Pure and Applied Geophysics on Seismicity in Mines, Vol. 129, Nos. 3/4.

Young, R.P., Maxwell, S., Urbancic, T., Feignier, B. (1992), Mining-induced microseismicity: Monitoring and applications of imaging and source mechanism techniques, Pure and Applied Geophysics, 139, 697-719.

Young, R.P. and Maxwell, S. (1994), Application of seismic tomography in rockburst investigations, in Proc. 1994 ISRM International Symposium (invited paper).

Zienkiewicz, O. and Taylor, R. (1989), The finite element method, McGraw Hill, Toronto.